Charles University

Faculty of Science

Study programme: Biology

Branch of study: Immunology

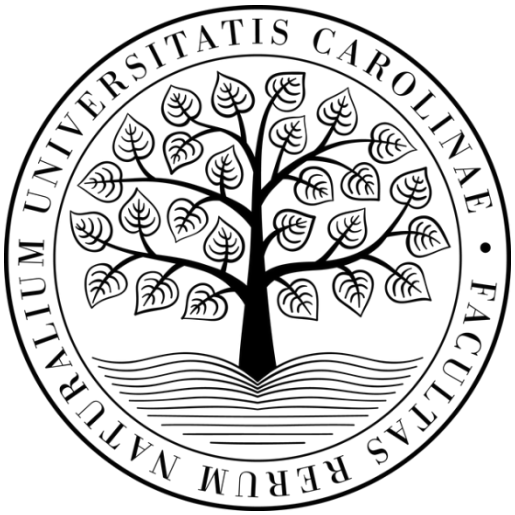

Bc. Liliana Tušková

MHC II-EGFP *knock-in* mouse model as a suitable tool for quantitative gut immunology under conventional and germ-free conditions

MHC II-EGFP *knock-in* myší model jako vhodný nástroj pro kvantitativní střevní imunologii za běžných podmínek a podmínek bez bakterií

Diploma thesis

Supervisor: prof. RNDr. Jan Černý, Ph.D.

Prague, 2021

Prehlásenie

Prehlasujem, že som záverečnú prácu spracovala samostatne a že som uviedla všetky použité informačné zdroje a literatúru. Táto práca ani jej podstatná časť nebola predložená k získaniu iného alebo rovnakého akademického titulu.

V Prahe, 11.8.2021

Bc. Liliana Tušková

Poďakovanie

Chcela by som predovšetkým poďakovať svojmu školiteľovi, prof. RNDr. Janovi Černému, PhD., za návrhy, rady a veľkú ústretovosť počas vypracovávania mojej diplomovej práce.
Taktiež ďakujem Mgr. Valérii Grobárovej, PhD. za ďalšie rady a podnety na zlepšenia počas písania a dokončovania práce. Poďakovanie patrí i Janovi Pačesovi a Karolíne Knížkovej, za zaučenie do techník prietokovej cytometrie a light sheet mikroskopie.

Abstract

Germ-free animals have been used to study the effects of microbiota for several decades. In that time, numbers of differences from specific-pathogen-free (SPF) animals have been reported, including differences in absolute numbers or percentages of various immune populations, enormously enlarged coecum and lack of germinal centers. However, many of the crucial information about structural and functional differences in their secondary lymphoid organs still remains uncovered. With novel microscopical approaches, such as light sheet fluorescent microscopy, enabling 3D visualization of whole samples without processing them to a series of slides, and multicolor cytometry, allowing the characterization of numbers of cellular populations within a matter of seconds and in a highly quantitative manner, the uncovering of fundamental differences finally seems to be within reach.

MHC II-EGFP *knock-in* mouse model brings the advantages of a fluorescent protein expressed in physiological histological contexts into both fields. Lymphoid and other tissues can be visualized microscopically without the need of staining (even *in vivo*). Information about the expression of both plasma membrane-localized and intracellular MHC II in various tissues could be acquired directly. Combining MHC II-EGFP *knock-in* mouse model with the gnotobiological approach makes it easy to visualize any kind of effect and quantify it, including the precise identification and preparation of the lymphoid organs.

In the current work, MHC II-EGFP *knock-in* mouse model was optimized for the use in both light sheet fluorescent microscopy as well as multiparametric flow cytometry. Precise tissue dissection allowed for the analysis of individual mesenteric lymph nodes and Peyer's patches in a sequential order. Secondary lymphoid organs were compared in specific-pathogen-free and germ-free animals using both microscopic and cytometric approaches, gaining both visual and quantitative information about the germ-free biology. Further work is needed to quantify the results from light sheet fluorescent microscopy with the help of neuronal network-based analysis. To avoid any subjective bias, unsupervised algorithms were adopted for the analysis of flow cytometric results. Reduced absolute cell numbers were found in Peyer's patches and coecal patch in germ-free animals compared to SPF. Also relative quanitity of γδT cells were decreased across all tissues sampled in germ-free mice. B cell frequencies were relatively increased in spleen and mesenteric lymph nodes, while helper and cytotoxic T lymphocyte frequencies were decreased. A significant increase of NK percentages was observed in coecal and colonic patches of germ-free animals. Other cell types were also differing significantly in germ-free animals and/or along the mesenteric of Peyer's patch gradient.

This work paves the path for the usage of MHC II-EGFP *knock-in* mouse model for investigating the entero-mammary pathway in great detail using gnotobiological monocolonized MHC II-EGFP mouse model.

Keywords:

MHC II, Peyer’s patch, mesenteric lymph node, multiparametric flow cytometry, light sheet microscopy

Abstrakt

Bezmikróbne organizmy sú používané k štúdiu vplyvov mikrobioty po niekoľko desaťročí. Počas tohto času bolo hlásených mnoho odlišností od tzv. specific-pathogen-free (SPF) zvierat (neobsahujúcich špecifické patogény), vrátane absolútnych počtov alebo percent rôznych imunitných populácií, obrovsky zväčšeného céka takmer žiadnych germinálnych centier. Avšak mnoho kľúčových informácií o štruktúrnych a funkčných rozdieloch v ich druhotných lymfatických orgánoch je stale neobjavených. Pomocou nových mikroskopických prístupov, ako light sheet fluorescenčná mikroskopia, umožňujúca 3D vizualizáciu celých vzoriek bez nutnosti ich spracovávania na sériu rezových preparátov, a mnohofarebnou cytometriou, umožňujúca vysoko kvantitatívnu charakterizáciu množstva bunkových populácii za niekoľko sekúnd, odkrytie podstatných rozdielov vyzerá byť konečne na dosah.

MHC II-EGFP *knock-in* myší model prináša výhodu fluorescenčného proteínu exprimovaného vo fyziologických historických kontextoch do oboch obstastí. Lymfatické a iné tkanivá môžu byť vizualizované mikroskopicky bez nutnosti farbenia (aj *in vivo*). Informácia o expresí MHC II na plazmatickej membráne i intracelulárne z rôznych tkanív môže byť okamžite získaná. Kombináciou MHC II-EGFP *knock-in* myšieho modelu s gnotobiologickým prístupom sa stáva vizualizácia akéhokoľvek vplyvu a jej kvantifikácia jednoduchá, vrátane precíznej identifikácie a prípravy lymfatických orgánov.

V tejto práci bol MHC II-EGFP *knock-in* myší model optimalizovaný na použitie v light sheet fluorescenčnej mikroskopii i v multiparametrickej prietokovej cytometrii. Detailná pitva rôznych tkanív umožnila analýzu jednotlivých mezenteriálnych uzlín a Peyerových plátov v poradí, ako za sebou postupujú. Sekundárne lymfatické orgány boli porovnané medzi specific-pathogen-free a bezmikróbnymi zvieratami s použitím mikroskopických i cytometrických prístupov, pričom sa získala vizuálna aj kvantitatívna informácia o biológii bezmikróbnych zvierat. Ďalšia práca bude potrebná na kvantifikáciu výsledkov z light sheet fluorescenčnej mikroskopie s pomocou analýzy na bázi neuronálnej siete. Za účelom vyhnutia sa akýmkoľvek subjektívnym chybám, nesupervizovaný algoritmus bol použitý na analýzu výsledkov z prietokovej cytometrie. Znížené absolútne počty buniek boli zistené v Peyerových plátoch, cékánom a kolickom pláte. Aj relatívne počty γδT lymfocytov boli u GF myši znížené vo všetkých pozorovaných tkanivách. Frekvenice B buniek boli relatívne zvýšené v slezine a mezenteriálnych lymfatických uzlinách, zatiaľčo frekvencie pomocných a cytotoxických T lymfocytov boli znížené. Signifikantný nárast percenta NK buniek bol pozorovaný u plátu z céka a kolon bezmirkóbnych zvierat. Ďalšie bunkové typy sa taktiež signifikantne líšili medzi bezmikróbnymi a klasickými zvieratami a/alebo pozdĺž mezenteriálneho gradientu alebo gradientu peyerových plátov.

Táto práca je prípravou na použitie MHC II-EGFP *knock-in* modelu na detailný výskum entero-mammárnej cesty prenosu baktérií s použitím gnotobiologického monokolonizovaného MHC II-EGFP myšieho modelu.

Kľúčové slová:

MHC II, Peyerov plát, mezenteriálna lymfatická uzlina, mnohoparametrica prietoková cytometria, light sheet mikroskopia

List of abbreviations

APC	antigen presenting cell
Breg	regulatory B cell
CD	cluster of differentiation
cDC	classical dendritic cell
CIITA	class II transactivator
CUBIC	Clear, Unobstructed Brain Imaging Cocktails and Computational analysis
DC	dendritic cell
EDTA	ethylenediaminetetraacetic acid
EGFP	enhanced green fluorescence protein
FBS	fetal bovine serum
FlowSOM	flow cytometry data analysis using self-organizing maps
FMO	fluorescence minus one
GALT	gut-associated lymphoid tissue
GF	germ-free
IBD	inflammatory bowel disease
IEC	intestinal epithelial cell
IFN	interferon
Ig	immunoglobulin
IL	interleukin
ILC	innate lymphoid cell
ILF	isolated lymphoid follicle
ISC	intestinal stromal cell
JAK	Janus kinase
LPS	lipopolysaccharide
LSFM	light sheet fluorescent microscopy
M cell	microfold cell
MHC II	major histocompatibility complex class II
MLN	mesenteric lymph nodes
PBS	phosphate buffered saline
pDC	plasmacytoid dendritic cell
PP	Peyer's patch
RPMI	Roswell Park Memorial Institute Medium
SCFA	short-chain fatty acid

SFB	segmented filamentous bacterium
SOM	self-organizing map
SPF	specific-pathogen-free
STAT	signal transducer and activator of transcription
t-SNE	t-distributed stochastic neighbor embedding
Tc cell	cytotoxic T cell
TCR	T cell receptor
Th cell	helper T cell
Treg cell (i/nTreg)	regulatory T cell (induced/natural)
UMAP	Uniform Manifold Approximation and Projection for Dimension Reduction
wt	wild type

Contents

1. Introduction 1

2. Theoretical backround 2

2.1. Microbiota and intestinal immunity 2

2.1.1. Metabolites 2

2.1.2. Gut dysbiosis 2

2.1.3. Gut organ axis 3

2.1.4. Microbiota and cancer 3

2.1.5. Microbiota versus host genetic backround 4

2.1.6. Specific bacterial strains and their effects 4

2.1.7. Microbiota establishment during ontogenesis 5

2.1.8. Approaches for studying microbial effects on the host 6

2.2. Secondary lymphoid organs 7

2.2.1. Peyer's Patches and solitary intestinal lymphoid tissues 7

2.2.2. Mesenteric lymph nodes 8

2.2.3. Spleen 10

2.3. Immune cell populations and their markers 10

2.3.1. B cells 11

2.3.2. T cells 12

2.3.3. NK cells 13

2.3.4. NKT cells 13

2.3.5. Innate lymphoid cells 14

2.3.6. Dendritic cells 14

2.3.7. Macrophages 15

2.3.8. Neutrophils 16

2.4. MHC II molecules and antigen presentation 17

2.5. MHC II-EGFP *knock-in* mouse model 19

2.6. Methods of quantitative histology – light sheet fluorescence microscopy 20

2.7. Multiparametric flow cytometry and data analysis 22

3. Aims 24
4. Materials and methods 25
4.1. Materials 25
4.1.1. Chemicals and solutions 25
4.1.2. Tissue clearing solutions 25
4.1.3. Antibodies 26
4.1.4. Expendable supplies 27
4.1.5. Instruments 27
4.1.6. Mice 28
4.1.7. Software for data acquisition and analysis 28
4.2. Methods 28
4.2.1. Organ sample preparation for flow cytometry 28
4.2.2. Light sheet microscopy 29
4.2.3. Data visualization 29
4.2.4. Flow cytometry 29
4.2.5. Data analysis 29
5. Results 30
5.1. Visualization of secondary lymphoid organs by stereomicroscopy 30
5.1.1. Mesenteric lymph nodes 30
5.1.2. Peyer patches 31
5.2. Visualisation of MLNs and PPs using light sheet microscopy 33
5.3. Flow cytometry 38
5.3.1. Optimalisation of the dissociation protocol 38
5.3.2. Flow cytometry panels troubleshooting 41
5.3.3. Data analysis with the help of unsupervised algorithms 44
5.3.4. C57BL/6 mouse vs. MHC II-EGFP *knock-in* mouse 53
5.3.5. SPF vs GF MHC II-EGFP *knock-in* mouse 56
5.3.6. SPF vs. GF – absolute numbers 66
5.3.7. Ly6C vs. CD3 72

6. Discussion 73
7. Conclusion 77
8. References 78
9. Supplementary figure 99

1. Introduction

Studies on microbiota are recently becoming increasingly popular across the world. A reason for this phenomenon is the previously unappreciated enormous impact of microbiota on our health and disease development that is just becoming clear. The effects of microbiota do not end on the mucosal surfaces, but rather spread across the whole body.

Gnothobiological approaches were developed to study the effects of (the absence of) microbiota in the sterile environment. They involve keeping the animal either completely germ-free or introdung a defined microbial strain or strains of bateria to study. Alternatively, a cheaper alternative is the antibiotic treatment (usually by a combination of antibiotics) designed to keep the mice free from bacteria.

MHC II-EGFP *knock-in* mouse model is an excellent tool to study the secondary lymphoid organs, as they emit fluorescene when excited by a blue laser. This allows for more accurate dissection of lymphoid organs under stereomicroscope. Combining the gnothobiological approach with the MHC II-EGFP *knock-in* mouse model, as used in this work, enables easy visualization of potential effects the germ-free mouse exerts. One of the main aims of this work is to compare the standard, speficic pathogen free, mice and germ-free mice with the focus on morphology as well as the composition of secondary lymphoid organs, more specifically Peyer's patches, mesenteric lymph nodes, and spleen.

2. Theoretical backround

2.1. Microbiota and intestinal immunity

In recent years, an increasing focus has been set on the effects of microbiota on organisation as well as function of the immune system. There is also a rising evidence of the involvement of microbiota and changes in proportions of individual bacterial strains on pathophysiological mechanisms of disease development, such as inflammatory bowel diseases (IBDs)[1]. The significance of microbiota is most often perceived in relation to gut homeostasis, although recent research confirms its role in other organ systems, such as brain[2].

2.1.1. Metabolites

Microbiota interacts with the intestinal layer by releasing number of metabolites. These can be classified into two main groups: diet-independent microbial products, such as lipopolysaccharide (LPS), ATP or polysaccharide A, and diet-dependent microbial products[3]. The latter group can be further divided into metabolites originating from the host and secondary modified by bacteria (secondary bile acids and taurine) and metabolites originating from ingested food[4]. Of the directly diet-dependent microbial products, the most widely understood are short-chain fatty acids (SCFAs), particularly acetate, propionate, and butyrate, that help to maintain the anti-inflammatory immune state by epigenetic mechanisms[5]. Other microbial metabolites originating from dietary compounds that facilitate the microbiota-host crosstalk include tryptophan metabolites (indole derivatives), polyamines, and more[4,6]. They help to maintain epithelial barrier function, antimicrobial peptides production, protection against colitis, innate lymphoid cell function, T helper (Th) and regulatory T (Treg) cells differentiation and proliferation or immunoglobulin class A (IgA) production[3,7,8]. For instance, long-term antibiotically treated mice were shown to have systemically lowered proliferation and numbers of Th cells as well as locally diminished numbers of Treg cells in Peyer's patches (PPs) and in mesenteric lymph nodes (MLNs), demonstrating a complex relationship between microbiota and the host[9].

SCFAs and other anti-inflammatory microbial metabolites are mainly produced by obligatory anaerobic bacterial strains, while many of the facultative anaerobic ones are associated with gut dysbiosis (i.e. elevated relative or absolute numbers of pathogenic bacteria, a decrease in the abundance of commensal microbiota or changes in bacterial metabolism or spatial distribution of microbiota in the gut) and pro-inflammatory state.

2.1.2. Gut dysbiosis

Gut dysbiosis is associated with a rising number of documented pathological conditions resulting from immune dysregulation, such as autoinflammatory and autoimmune diseases (e.g. systemic lupus erythematodes, type 1 diabetes mellitus, rheumatoid arthritis and more), diabetes mellitus type 2, cardiovascular diseases, obesity, cancer, infectious diseases, and others (discussed in [4,5,10–14]).

The prototype disease cluster known to be associated with dysbiosis is IBDs. There is an ongoing research of the interplay between genetic polymorphisms/mutations (most notably polymorphisms in the nucleotide-binding oligomerization domain-containing protein 2 gene – *NOD2*), immune response dysregulation and the effect of microbiota and other environmental factors on the pathogenesis of IBDs[1]. The exact bacteria-induced pathophysiological trigger, as well as a single causative strain for the disease is unknown. However, there is a clear correlation between susceptibility genes, bacterial dysbiosis and abnormal immune reaction to microbes leading to inflammation, possibly generating a vicious cycle that results in worsening conditons of IBD patients[1,15]. To enlighten the potential causative role of microbiota for the disease development, several mouse colitis models were established, with impressive results. Colitis-susceptible mouse strains, for instance TRUC mice, developed colitis (or developed more severe symptoms) only in the presence of microbiota[16]. After microbiota transfer from mice with colitis to germ-free mice or even specific pathogen-free (SPF) wild-type (wt) mice, the recipients also developed colitis symptoms[16]. Analogous results were achieved in clinical trials of ulcerous colitis patients, when experimental fecal transplants were used that resulted in clinical remission when "healthy" microbiota was used (e.g. several strains of *Clostridium* and *Ruminococcus*)[17]. Similar evidence of the obligatory microbial presence and/or dysbiosis for the disease development were demonstrated for other diseases, such as rheumatoid arthritis[18,19].

2.1.3. Gut organ axis

One of the recent most striking findng in the field of microbiota is the vivid bidirectional connection between the gut microbiota and other organs of the host – the gut-organ axis, often mediated by immune system[2]. Examples include the gut-adipose axis, gut-bone axis, gut-heart axis, gut-kidney axis, gut-liver axis, gut-skin axis, and perhaps the most surprising connection found was the gut-brain axis, with important functional consequences in both health and disease[2]. Immunological, hormonal, metabolical and neuronal connections are all part of the network connecting gut microbiota to the function of the brain and vice versa[2]. Recently, the effect of microbiota was proven in numerous neurological conditions, most notably Alzheimer's disease, multiple sclerosis, autism spectrum disorder, depression or others[20,21]. Comparative studies of patients with respective neurological disorders and control individuals revealed significant abundance shifts for various bacterial strains[21]. It was also demonstrated that SCFAs from gut bacteria affect the development and function of microglia throughout the life of an individual, providing further links between gut-brain axis as well as the microbiota-immune system interface[22].

2.1.4. Microbiota and cancer

Another rapidly emerging topic in the field of microbiota is its relation to cancer. On one hand, specific bacterial strains can promote tumorigenesis, the classic example being the development of gastric cancer as a result of *Helicobacter pylori* infection[23]. On the other hand, gut microbiota can influence not only the pathogenesis of cancer, but also the outcome of cancer therapy, such as the effectivity of

immunotherapy, its adverse effects, such as graft-versus-host disease after hematopoietic stem cell transplantation, of influencing the tumor microenvironment[23–26]. For instance, the microbiota was demonstrated to be essential for the success of checkpoint inhibitor therapy[26–28]. In the future, tailoring the microbiota for the respective treatment (or vice versa) could therefore be an important strategy to highly improve disease outcome.

2.1.5. Microbiota versus host genetic backround

Despite the unique outer environment of every individual, resulting in importantly unique microbiota composition, we should not omit the genetic factor that comes to play as a response to bacterial colonization. This variation can be demonstrated on distinct mouse strains kept under the same living conditions, that shows differing levels of IgA production[29]. This finding highlights the influence of genetic backround on microbiota diversity and composition from within. It can also be a warning for experimental design as many procedures may lead to dissimilar results once different mouse strain is used. In addition, it may put a limit to the extent fecal microbial transpants or the use of probiotics may have on long-term changes in microbiota composition needed for therapeutical success.

2.1.6. Specific bacterial strains and their effects

So far, the general concept of metabolites, changes and diseases associated with variations in microbiota was discussed. However, there are also specific bacterial strains with unique effects on the host, that generally cannot be achieved by other strains, or only to a lesser extent. Two famous examples are segmented filamentous bacteria (SFB) and specific strains of *Clostridium*. Segmented filamentous bacteria were documented to induce Th17 response within the individual, that includes the production of interleukin 17 (IL-17) by group 3 innate lymphoid cells (ILC3) and Th cells[30,31]. For adequate Th17 response, bacterial sensing has to be mediated by dendritic cells (DCs) and generally occurs in Peyer's Patches[32].

On the other hand, several strains of *Clostridium*, mainly *Clostridium leptum* and *coccoides* groups, were found to have anti-inflammatory effects by boosting the differentiation as well as the activation of induced Treg cells (iTregs) in colonic lamina propria[33]. They were also shown to be able to lessen colitis symptoms upon oral introduction[34]. Similar effect on the activation of Tregs, although not necessarily on boosting their cell numbers, was observed after the colonization of germ-free (GF) mice with *Bacteroides fragilis*[35]. Monocolonisation of GF mice with *B. fragilis* was also able to balance the Th1/Th2 balance within host (normally skewed towards Th2 in GF animals) and ensure normal development of lymphoid organs in the gut[36]. These functions were attributed to bacterial polysaccharide of *B. fragilis*[36].

Recently, a study showed that upon monocolonisation, nearly all bacteria are able to massively colonize a murine gastrointestinal system, and that *de facto* all bacteria had some kind of effect on immune cell population counts or their functions[37]. Surprisingly, these seemed to be independent of the bacterial phylum, as there was no shared effect among strains within any of the bacterial phylla used,

and conversely, there were many shared effects between strains from different phylla[37]. Therefore, in conventionally colonized individuals, the complex effects on the host likely result from the sum of the individual effects of all bacterial strains weighted by respective strain abundances.

However, a recent study showed that (at least in some aspects) colonization by a single bacterial strain may be sufficient for normal development of murine pups. *Lactobacillus plantarum* was able to fully revert the changes seen in the maturation of young mice kept under GF conditions, such as lower weight gain and shorter body size[38]. These findings indicate that monocolonisation with *L. plantarum* has a systemic effect on the development of juvenile mice into adulthood and that it may provide a simplified but well-defined system for comparing the effects of microbiota between germ-free and conventional breeding conditions.

2.1.7. Microbiota establishment during ontogenesis

There is still and ongoing debate on how and when the microbiota enters the bodies of newborn individuals, and which factors affect its composition. Evidence suggests that there happens to be a limited time window ("window of development") in the ontogenesis of an individual during which a distinct pro- or anti-inflammatory "imprinting" pattern is established according to the presence of microbiota that is then carried on later in life, leading to a differing susceptibility to various inflammatory conditions (e.g. colitis) for an individual[39]. This time period is usually attributed to the newborn period, from birth until weaning, although another – fetal time period – is also increasingly discussed as evidence suggests that dysbiosis or antibiotic treatment during pregnancy has a profound impact on the newborn[39,40]. Placenta may also contain some bacteria, metabolites of which may shape the early immune system of the fetus, although the findings are still controversial and often even contradictory[41,42]. Nonetheless, researchers agree that while some effects may not be imprinted and can be normalized when "healthy" microbiota is induced later in life, some, such as higher chances of developing food allergy, appear to be rather permanent once the weaning period ends[43]. There is therefore a critical time for an individual to be introduced to microbiota during delivery and lactation for their healthy development.

The delivery mode was found to influence the microbiota composition of the newborn child, at least for the early childhood[44]. The microbiota enriched in the ceasarean section in comparison to vaginal delivery contained more potentially pathogenic taxa, which may put infants born via ceasarean section into greater risk of developing respiratory tract infections, at least during their first year of life[44]. The group born via vaginal delivery showed greater abundance of *Bifidobacterium* species, beneficial for overall health[44]. The consequences of delivery mode on microbiota composition were independent from the outcome of lactation[44].

Understanding how lactation and maternal microbiota influence the microbiota composition in offspring is still under investigation. It was determined that breast tissue microbiota differs with the geographical location and is also not identical to the skin tissue of the breast, with the possibility that

some bacteria present in breast tissue may be originating in the gut[45,46]. The same is true for milk ingested by the newborn, with the mixture of skin microbiota and some phylla with much higher abundance in the gut, such as *Firmicutes*[47,48]. The bacteria in the breast tissue could therefore be transferred to the newborn by lactation, as the breast tissue microbiota and the newborn gut microbiota share some similar bacterial phylla[45]. Although not all bacterial phylla found in milk may stably colonize the newborn, lactation obviously affects the newborn fecal microbiota, the biggest effect being an increased abundance of *Bifidobacterium* species in comparison to formula-fed infants[49,50]. With the knowledge that parts of the bacteria or even whole alive bacteria may be transferred by DCs from the gut (mostly from Peyer's Patches) through mesenteric lymph nodes and lymph or blood up to the breast tissue and milk and that this translocation is strengthened during pregnancy and lactation led to the formulation of entero-mammary pathway hypothesis[51–53]. Changes to the maternal body during pregnancy could help enabling increased translocation of bacteria and various observed immune cells from the gut to the breast, supporting the hypothesis[54,55]. Despite this evidence, the existence of entero-mammary pathway remains controversial and is yet to be fully proven an accepted with the help of novel methodological approaches.

2.1.8. Approaches for studying microbial effects on the host

Last but not least, two most common approaches for studying microbiota and its effects on development and homeostasis in general will be discussed and compared briefly. Antibiotic treatment, offering cheap and fast results without the need of special equipment or manipulation, is much less standardized than GF approach, partially due to numerous treatment regimens and different antibiotic combinations[56]. Off-target drug effects should also be taken into consideration and results should be ideally verified with another approach[56]. Resistance to antibiotics and colonization with other parts of microbes, such as viruses and fungi both present difficult challenges to resolve, sometimes leading to the addition of antimycotics to the mixture of antibiotics[56,57]. Bacterial colonization is also still present on the skin (and to some extent in other sites as well) of treated animals[56]. GF conditions on the other side, despite generally more expensive, harder and more time consuming to establish, offer stable and standardized approach with the ability to colonize the animal with specific microbiota (gnothobiologic approach)[56]. However, each strain and each genotype has to be established into GF conditions *de novo* and with the special handling options, some experiment types are limited[56]. Another difference between the two approaches is that while GF organisms never interact with microbiota unless colonized, antibiotic treatment is generally introduced to adult/adolescent animals after a normal development (although antibiotic treatment of pregnant and lactating animals may simulate the GF approach for the pups), which can be both advantageous and disadvantageous depending on specific research topic[56]. Antibiotic treatment and GF approach can therefore produce identical or differing results, and some results are still often inconsistent or controversial depending on the conditions (such as antibiotic treatment regimen or mouse strain used)[56]. Using both these approaches, numerous morphological, numeric and/or functional

differences (both local and systemic) from SPF mice were found (topic extensively reviewed in [56]). A few examples include reduced numbers of B and T cells in small intestine, reduced colonic Th cell numbers, or systemic reduction of memory and effector T cells and Tregs[58]. Many myeloid cell types, such as macrophages, neutrophils and monocytes were also decreased in numbers systemically[59]. It was also established that to the development of isolated lymphoid follicles (ILFs), bacterial signals (such as peptidoglycan from gram-negative bacteria or lymphotoxin) were essential[60,61]. Despite clear advancements in recent years, there is still space for uncovering unknown instances about the impact of microbiota on development and function of organisms. There is also an increasing amount of dated information regarding GF animal morphology that is ofen widely accepted and passed on, with the need of data reviewing and validation with newer approaches and methods[62]. There is also a need for quantitative approaches since rates and abundances of the immune cells/particular microbiota species could greatly help to understand the overall complexity of the above-mentioned concepts.

2.2. Secondary lymphoid organs

Secondary lymphoid organs consist of spleen, lymph nodes, tonsils, and mucosa-associated lymphoid tissues. Gut-associated lymphoid tissue (GALT) is the biggest and most studied mucosal lymphoid structure, especially in relation to microbiota. There are two parts of GALT: organized GALT, which will be discussed further, is composed of MLNs, PPs in the small intestine (and coecal and colonic patches), and solitary intestinal lymphoid tissues (SILTs) – cryptopatches and their mature counterparts ILFs[63–65]. Diffuse GALT contains mostly effector immune cells in lamina propria and intraepithelial lymphocytes[65]. GALT encompasses a variety of innate and adaptive immune cells, most abundant being B and T lymphocytes (cytotoxic, helper and regulatory), dendritic cells, macrophages, and innate lymphoid cells[13]. The formation and function of GALT structures is under a great influence of microbiota[13,66].

Most often, in the analyses of these structures, only relative abundance changes are discussed, without the emphasis on absolute numbers. Data on quantification of cells and cell types among these compartments is relatively scarce and often comes from estimates from histological slides in pre-cytometric era and data from various sources often differ significantly[62]. Yet even minor abundacne shifts could have a great impact on the health or physiological status. Therefore, it is important to confront the “universal truths”, quite often as part of the “scientific mythology”, with the quantitative data obtained using up to date approaches.

2.2.1. Peyer’s Patches and solitary intestinal lymphoid tissues

Peyer’s Patches are the largest (1-2mm in diameter in mouse) and the only macroscopically visible lymphatic structures within the gut[67]. From the luminal side, they are lined by M (microfold) cells transporting antigens and bacteria to the subepithelial dome for antigen presentation and T cell priming by DCs[65]. The bulk mass of Peyer’s patches consists of B cell lymphoid follicles with germinal centres,

surrounded by smaller interfollicular T cell zones[65,68]. Germinal centers first appear during the weaning period and GF mice were reported to lack germinal centers within lymphoid follicles[69,70]. The number of Peyer's patches slightly varies with different strains of mouse, gender as well as from animal to animal. For C57BL/6J female mice, the average number of Peyer's patches per mouse was 6,5 varying from 5 to 9[71]. Gender also affected the number of cells in PPs, for females being slightly lower than for males, at about 8.19×10^5 cells per PP[71,72]. For BALB/c female mice, the number of PPs per mouse was 6-8, with the pooled cell number of 8×10^6 per mouse[73].

Cryptopatches and ILFs differ in size and cellular content. While cryptopatches are about 100μm in diameter and are composed mainly of precursor *c-kit*$^+$IL-7R$^+$ cells LTi ILC3s and CD11c$^+$ DCs, ILFs are about 2-5 times bigger in diameter and contain a B cell germinal centre, surrounded by a small T- and DC-rich area[74,75]. ILFs are also lined by M cells on the luminal side and have analogous cellular content to PPs, including nearly identical ratios of immune cells in addition to analogous spatial organisation of B, T and dendritic cells, bearing further similarity to them[75]. However, in GF animals, composition of ILFs is changed drastically, as B cells are present in minority and scarce germinal centers are found while a substantial increase in *c-kit*$^+$ cells is observed, mimicking the „less-differentiated, cryptopatch-like" phenotype[75]. While conventional SPF mice has around 100-200 relatively regularly interspersed ILFs along the antimesenteric side of the gut, only cryptopatches are detected in lymphotoxin $\alpha^{-/-}$ mice, supporting the hypothesis that ILF may develop from cryptopatches as a form of their maturation[61,75]. This hypothesis is further supported by a finding that mouse cryptopatches may give rise to human GALT in a chimeric mouse model and are critical for GALT formation[74]. While PP development starts prenatally, SILT development and maturation into ILFs is initiated after birth and is dependent on microbiota[60,75]. Nonetheless, while PPs are present in GF mice, the PPs are still influenced by microbiota introduction, as the absolute numbers of cells in PPs as well as B to T lymphocyte ratio both increase during the weaning period[76].

2.2.2. Mesenteric lymph nodes

Mesenteric lymph nodes in mice, together with duodenopancreatic lymph nodes and caudal lymph node, drain lymph from the small and large intestine and coecum, in an anatomical location-based manner analogous to humans (see)[65]. There is also a lymph-draining gradient present within MLNs, resulting in slightly different composition (e.g. differing relative numbers of DC subsets and presence of food antigens in upper MLNs – draining small intestine)[77]. Murine MLNs are part of an encapsulated string-like complex within the fatty tissue, placed parallel to the superior mesenteric artery. Usually, the complex is analysed as a whole, due to the challenging task of differentiating between individual nodes within the fatty capsule[78].

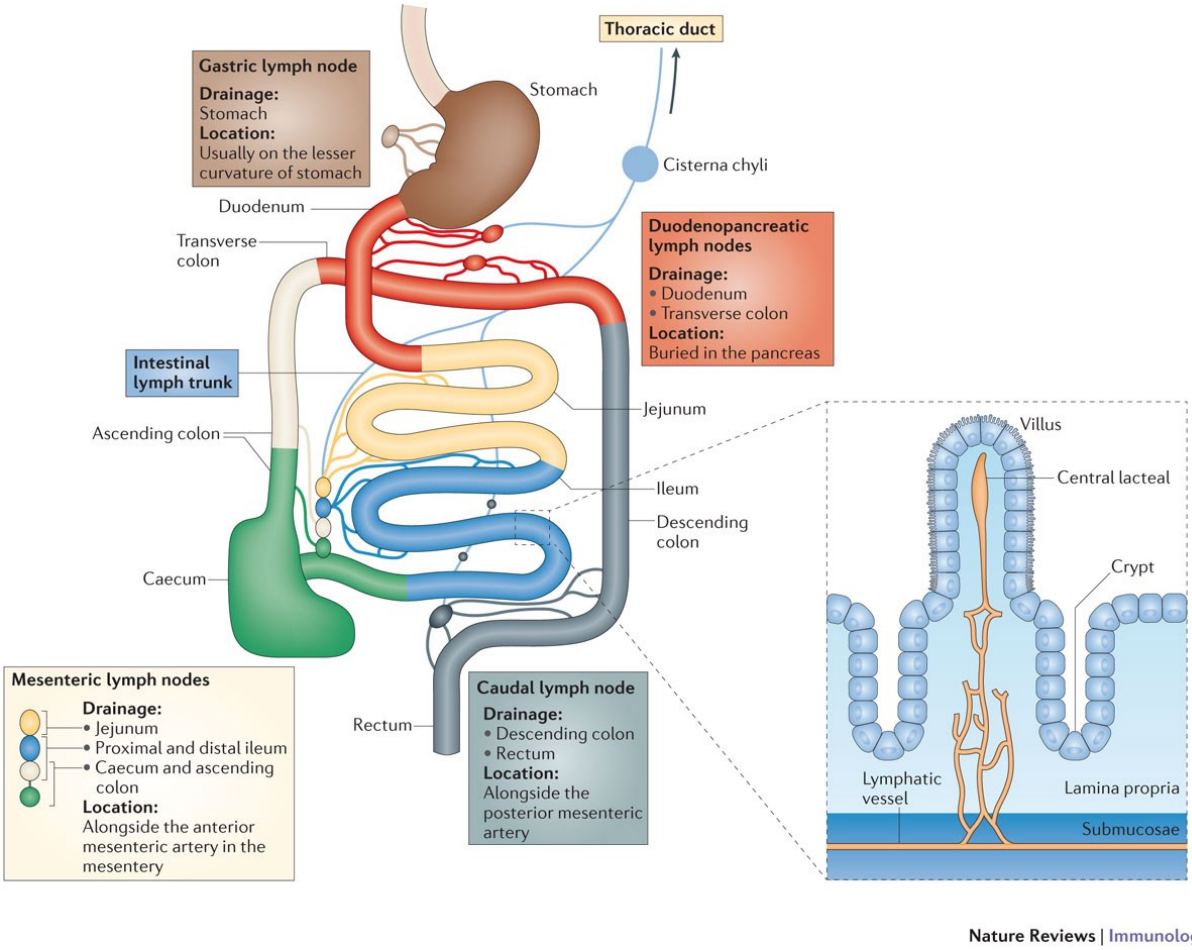

Figure 1: Schematic representation of the lymph drainage system from the gastrointestinal tract in mouse. Sites drained by respective lymph nodes is color-coded. Schematic drainage system inside the intestinal vilus is depicted on the right. Figure reprinted from Mowat and Agace[65].

The structure of the individual MLNs is that of classical lymph nodes: the B cell-rich cortex with germinal centers, the T cell-rich paracortex where DC:T cell immunological synapse takes place, and medulla, containing blood vessels, medullary sinuses and medullary cords rich in macrophages and plasma cells[79]. Under physiological conditions, the number of cells in the MLN complex is reported as nearly 13 million for C57BL/6 mice and increases significantly during infection[80]. Still, data on MLN cellularity for different mouse strains differ significantly, up to 60 million for BALB/c strain[81]. However, the overal cellularity ratio remains roughly the same among different studies, with over 2:1 T:B cell ratio in normal conditions and shifting towards B cells during infection[80,81]. On the other hand, germ-free animals are reported to have slightly reduced size of MLNs, which lack germinal centers (or have highly diminished numbers) and show reduced numbers of IgG-producing plasma cells within the lymph node[62].

A unique but critical function of MLNs on top of lymph filtration includes initiation and maintainance of oral tolerance, this task being performed by DCs migrating to MLNs from the gut and PPs[82,83]. In fact, more food antigen presentation was reported to take place in MLNs than in PPs[84]. Aside from the antigens and fatty molecules from the diet, live bacteria are also transported from the gut to the

MLNs, the transport being mediated by $CD11c^+$ DCs again[85]. The presence of MLNs hinders bacteria from reaching systemic circulation and allows for antigen presentation in the MLNs[85]. CCR7 chemokine has a crucial role in the migration of DCs from the gut wall into MLNs[83,86].

2.2.3. Spleen

Spleen is a secondary lymphoid organ with an increasing evidence of its importance in recent years, for example for controlling sepsis[87]. It reflects systemic changes in the immune system state and function, which is the reason why it is often explored or serves as a control or reference for other sites in numerous immunological studies[88]. It consists of red pulp, which is the place for blood filtration from pathogens, old cells and smaller bodies by macrophages, and white pulp, with B and T lymphocyte zones and outer marginal zone rich in B cells and macrophages that enter the inner follicles once activated[89]. Nevertheless, the main functions of spleen include blood filtration and iron salvage, antibody production and immune response to foreign or pathogenic cues in general, and, conversely, the induction and conservation of antigen tolerance[88–90].

In mice, spleen consists of about 1.19×10^8 cells in mice, most predominant being B cells followed by T cells[71,90,91]. Spleen also hosts various other immune cell types, such as various DC subsets, NK cells, monocytes, ILCs, NKT cells, γδ T lymphocytes and other[90]. No differences in overall cell numbers between strains (C57BL/6J and BALB/c) were observed in steady state[91]. In GF mice, germinal centers in B cell zones are very rare, similarly to the lymph nodes[62]. However, this finding reflects the activation status of B cells but not necessarily significantly affected their numbers, although some studies describe a decrease in cell numbers of the spleen in GF animals and/or changes in their ratio[56,92]. From above mentioned is obvious that despite the recent focus on interaction between microbiome and host immune system, more studies are necessary to reflect the whole spectrum of changes in cellular content in systemic as well as local immunity, particularly with the power of GF or gnotobiological mouse models.

2.3. Immune cell populations and their markers

Immune cell populations *sensu stricto* (almost all cell types could be involved in the immune reactions) are all of the hematopoietic origin (both myeloid and lymphoid) and therefore share some common traits and cell surface markers, while significant differences are also present between each population. Every common immune cell population, such as B and T lymphocytes, macrophages, or DCs, has a spectrum of subpopulations, defined by a unique set of markers (sometimes unique markers are not yet well defined)[93]. Many of them vary among different species, such as human and mouse, although some are shared[93]. Respective subpopulations differ not only in their expression profile, but also in abundancies and distributions among different tissues and the blood, in their functions and sometimes even in their morphology. This chapter is not trying to be and exhausting list of all the different subtypes of all immune cell populations and their markers in mouse by any means, but rather a highlight of the most

important core information relevant for this work. Hence, some cell types, such as eosinophils, basophils or mast cells will be omitted from this overview.

Being of the hematopoietic origin, all immune cells are CD45 positive (with a wide range of surface abundance, glycosylation patterns and, importantly, several splicing variants). CD45 is a multiple-isoform transmembrane protein tyrosine phosphatase present on all hematopoietic cells except mature erythrocytes and platelets[94,95]. Therefore, CD45 is a suitable pan-immune cell marker to differentiate between immune cells and other cells in tissues/blood that may have similar morphology to avoid numerological bias[96]. CD45 is responsible for inducing or attenuating Src kinase family activity in lymphocytes depending on dephosphorylation of respective tyrosines, according to various circumstances[95]. Janus kinases (JAK) and some other proteins have also been reported to be substrates for CD45, widening the horizon of CD45 function to other signalling pathways, such as terminating the JAK/STAT (signal transducer and activator of transcription) pathway in cytokine signalling[95,97]. In conclusion, as CD45 is a crucial molecule in various immunological signalling pathways and is common to all immune cells, its positivity as a marker should always be accounted for in addition to specific cell markers for respective immune cell types.

2.3.1. B cells

B cells are an abundant subset of lymphocytes bearing the B cell receptor (BCR), whose main goal in naïve B cells is to recognize a specific native antigen and internalize it for digestion and antigen presentation on MHC II molecules to T cells. Upon costimulation from follicular helper T cell (Tfh), activation, proliferation, and affinity maturation of the antigen-recognizing B cell is induced, producing memory cells and plasma cells. During maturation, B cells form germinal centers within lymphoid follicles in B-cell rich areas of secondary lymphoid organs where the encounter with foreign antigen took place, the antigen being scaffolded on follicular dendritic cells[98]. Thoughout the maturation process in the periphery, just as during the development of B cells in the bone marrow, each developmental stage is characteristic of its unique set of cellular markers.

A non-specific pan-B cell marker (not expressed in plasma cells), present on all antigen presenting cells (APCs), is CD40[99]. It is a critical costimulatory protein for B cell activation by Tfh, germinal center formation and maturation of B cells[99]. However, typical and most widely used B cell-specific markers in flow cytometry, immunohistochemistry, and therapy, are CD19 and CD20. While CD19 is a pan-B cell marker and acts as a co-receptor in BCR signalling by signal amplification from src family kinases, CD20 is a mature B cell marker functioning as a calcium channel[100,101]. In mouse, B220, an isoform of CD45 – CD45R, is also a pan-B cell marker, positive from the pre-pro B cell stage on. Howerver, unlike CD19, B220 expression is not restricted for B cells, rather it can be found on some activated T cells or plasmacytoid dendritic cells[102–105]. B220 expression lowers during the B cell maturation into plasma cells[106]. Instead, CD138 marker is a typical cellular marker for plasma cells, playing a role in their pro-survival signalling[106,107].

Above mentioned information mostly holds true for conventional follicular B-2 cells. Other subpopulations of B cells, however, may not share all the specifications and, rather, express some unique markers. For example, B-1 cell, marginal zone B cells and plasma cells share the expression of CD9[108]. B-1 cells further express CD11b, a myeloid cell integrin marker, and are differentially segregated into B-1a and B-1b cells according to the expression of CD5 (positive and negative, respectively)[109]. A broad category of regulatory B cells (Bregs), *sensu lato* also including marginal zone B cells or plasma cells, is rather defined functionally by the production of anti-inflammatory cytokines[110]. Its subpopulations have some defined unique markers, such as $CD19^{+}CD21^{+}CD23^{-}$ for marginal zone B cells or $CD5^{+}CD1d^{hi}$ for B10 cells, both found in spleen[111,112]. However, cellular markers are not yet known for every subpopulation in human/mouse (such as B regulatory 1 cells in mouse) and the origin and required conditions for development of different populations are still under investigation[110].

A newly described but still highly controversial lymphocyte species is "lymphocyte X" – a cellular cross in between B and T lymphocyte, bearing both BCR and T cell receptor (TCR)[113]. It was first reported only relatively recently in diabetes mellitus type 1 patients and was highly discussed and questioned immediately[114,115]. However, the appearing coexpression of B and T cellular markers is a long-known phenomenon in flow cytometry, reported by numerous studies[116–118]. Nevertheless, double positivity of B and T cell markes is usually accounted for cellular dublets, other preparation artifacts, or, in most cases, not adressed at all[115,119,120]. For these reasons, further research will have to be concluded to confirm these findings for them to be widely accepted in immunological community.

2.3.2. T cells

T lymphocytes, TCR-containing CD3-positive cells, are a population of immune cells encompassing a great variety of subpopulations with different functions. From αβ $CD4^{+}$ Th cells, further subdivided into three main branches of effector T cells – Th1, Th2 and Th17 and other smaller populations; Tregs, other regulatory T cell subsets, and Tfh cells; through αβ $CD8^{+}$ Tc cells, to a population of γδ T cells with TCR of limited variability. CD3 is a protein co-receptor of TCR, responsible for signal transmission into the cell, as well as CD4 and CD8, recognizing MHC II and MHC I molecule, respectively. However, as evidence suggests, some αβ cells may physiologically remain CD4 and CD8 double negative outside of the thymus, which was previously attributed only to lymphoproliferative diseases[121]. Similar is also true for double positive cells, which could in physiological circumstances have anti-viral or regulatory effects[122,123]. While extracellular marks of respective Th (and Tc) subpopulations exist (mostly in the form of chemokine receptors or lectins), intracellular transcription factor markers (such as T-bet, GATA3 and IRF4, RORγT and Foxp3 for Th1, Th2, Th17 and Treg, respectively) and cytokine secretion signatures are generally used more frequently[124]. Of extracellular markers, CD25 (which is a IL-2 receptor alpha chain) and CTLA4 (a checkpoint inhibitor), both markers of Tregs (and Bregs and activated B and T cells in case of CD25) are best characterized[124,125]. Regarding γδ T cells, they are

usually recognized by γδTCR and CD3, although about 30% can also bear CD8 co-receptor[126,127]. Some of γδ T cells are also MHC II positive and can effectively serve as APCs[128].

To uncover the memory phenotype T cells, which is linked to altered expression profile after their activation takes place, several other markers are available. While there is still controversy about the developmental origin, several T cell memory phenotypes are known[129,130]. First, two memory compartments – central and effector memory T cells (T_{CM} and T_{EM}) – were uncovered in peripheral blood, differing in their expression of CCR7 (positive and negative, respectively), meaning preferential homing of T_{CM} into secondary lymphoid organs and T_{EM} into peripheral, especially inflamed, tissues[131]. Lymphocyte antigen 6C (Ly6C) was also reported to enhance the homing capacity of T_{CM} into lymph nodes in mice[132]. Residing in peripheral tissues even in homeostatic conditions are the tissue-resident memory cells, usually CD69 positive (unlike circulating memory T cells)[133]. However, their expression profiles vary according to the respective organ[134]. Another discovered memory T cell population with stem cell properties, named stem cell memory T cells, is characterised by the expression of CCR7, CD45RA, and CD95 (Fas), among others[135]. On the other hand, a terminally differentiated population with the re-expression of CD45RA (characteristic of the naïve and stem cell memory T cells) was found and named TEMRA. This population has varied cell numbers as well as phenotypes, ranging from one similar to T_{EM} to the expression of cytotoxic signature, such as the expression of perforin, granzyme B, and many others[136]. Finally, perhaps the most peculliar population of memory T cells is the virtual memory T cell population with memory-like phenotype of high expression of CD44, which is able to react rapidly on the first encounter with an antigen and present even in GF mice[137].

2.3.3. NK cells

NK cells, often perceived as innate counterparts of Tc cells, are cytotoxic innate lymphocytes classified into group 1 ILCs[138]. As for all ILC groups, for NK cells is distinctive the absence of both BCR and TCR (and their co-receptors). For NK cell markers, typical is the presence of NKp46 (natural cytotoxicity receptor), and CD56 (neural cell adhesion molecule) in humans and NK1.1 in mice[139–141]. Other receptors, such as NKG2D and various species-specific molecules, regulate the activation status of NK cells[142]. While human NK cell repertoire is formed by the combinatorics of KIR family (Killer Ig-like receptors) receptors, murine NK cell receptors are of Ly49 family (lectin-like)[143]. Some NK cells also express CD11b and/or CD27 and are further divided into four developmental categories regarding the expression of these markers, with different abundance among tissues as well as their functional capacity[144].

2.3.4. NKT cells

NKT cells share both T-cell and NK-cell markers – they express both TCR, with its co-receptor CD3, as well as CD56 and NK1.1[145]. However, NK1.1 is not expressed in BALB/c mouse strain, as well as many others, leading to difficulties in identification of NKT cells in some mouse strains, as NKT cells also do not express NKp46[146,147]. It was also reported that the NK1.1 expression is not completely

universal among NKT cells[148]. TCR of NKT cells has a limited variability and recognizes lipidic molecules in the complex with CD1d. According to their TCR, NKT cells can be further divided into two types: type 1 is the invariant NKT cell subset (with TCR containing Vα14-Jα18 rearrangement in mouse or Vα24-Jα18 in humans) recognizing primarily α-galactosylceramide, and type 2, diverse NKT cells, recognize various other glycolipids[149,150]. In the sense of CD4 and CD8 molecules expression, NKT cell can be either double negative or express CD4 in mice, and further subsets, expressing Th1-, Th2-, Th17- or Treg-like cytokines have been reported for iNKT cells[151–154]. In humans, CD8 expression is also possible[155]. The importance of studying NKT cells and their functions became clear after an anti-tumorigenic activity was proposed in type 1 NKT cells and the opposite was reported in type 2 NKT cells, leading to various therapeutic trials[156]. Asthma and autoimmune disorders are among other diseases NKT cells were identified to play an important role in[157,158].

2.3.5. Innate lymphoid cells

Innate lymphoid cells, a lymphoid population characterized by the absence of both BCR and TCR, is especially abundant at mucosal surfaces. Three main groups of ILCs are described according to cytokine production – the first group consists of the aforementioned NK cells, and ILC1, innate counterparts of Th1 cells. The only known representant of the second group are ILC2, resembling Th2 cells. The third group is composed of ILC3, mirroring Th17 (and Th22 cells), and lymphoid tissue inducer cells (LTi) of fetal origin, which antenatally regulate lymph node and Peyer's patch development[159,160]. In addition to the three groups, ILCreg, a Treg-like cell population, was recently described[161]. Innate lymphoid cells mostly lack specific cellular markers and are distinguished by their transcription factor expression (analogous to T cells) and their cytokine production profiles (IFN-γ; IL-5, IL-9, IL-13; and IL-17 and IL-22 for ILC1, ILC2, ILC3, respectively)[162]. Regarding cell surface markers, ILC1 are, like NK cells, NK1.1 and NKp46, as well as CD122 positive[163,164]. However, unlike NK cells, ILC1 express TRAIL cytotoxic molecule but do not express perforins (or only in small quantities)[163]. Murine ILC2 express CD44 as well as CD127 (IL-7Ra) and CD25[163,164]. ILC3 can be further subdivided into NK cell receptor positive (with the development dependent on microbiota) and negative subpopulations according to the expression of NKp46 (and some even NK1.1), and, together with LTi cells, are CD254 (RANKL), as well as IL-1R and IL-23R positive[163,165,166]. However, ILC3 differ from LTi by the absence of CCR6 and CD4 (most subsets) expression and by the lower expression of CD127[163,164,167]. Both ILC2 and ILC3 subsets were demonstrated to express MHC II and are capable of antigen presentation[168,169]. Nonetheless, the phenotype of all ILC subtypes, especially ILC1, is highly tissue-specific and positivity or negativity of many markers must be accounted for in respect to the concrete tissue[170]. To sum up, there is still much to be uncovered about ILC subpopulations, their potential markers and plasticity.

2.3.6. Dendritic cells

Dendritic cells are the main antigen-presenting cell type in the body. They internalize antigens by numerous processes, partially digest them and present them on MHC II (or MHC I by cross-

presentation) to T cells after migration to lymph nodes in a chemiokine gradient. However, DCs do not form a single uniform population, and are in fact categorized into several groups and subgroups with unique cellular markers and sometimes even form tissue-specific populations.

Two main groups of dendritic cells are established – conventional (classical) DCs (cDCs) and plasmacytoid dendritic cells (pDCs). cDCs can be further subdivided into two subgroups, cDC1 and cDC2[171]. cDC1 are a usually less abundant than cDC2 (with the exception of thymus), but the degree varies across different tissues[172]. They are mainly endowed with cross-presenting capabilities, enabling them to prime primarilly CD8+ Tc cells[173]. Typical cellular markers separating them from cDC2 subset are CD8 in lymphoid tissues and CD103 (an integrin) in other tissues, XCR1 (a chemokine receptor), IRF8 (a transcription factor) and low to no levels of CD11b[171–175]. On the other hand, CD4+ Th cell-priming cDC2 express high levels of CD11b, IRF4, CD172a (SIRPα, an inhibitory „don't eat me" signal receptor) and vary in the expression of CD4 and F4/80 (an adhesion-G protein-coupled receptor)[171–173,175]. In the intestine, an additional CD103+ CD11b+ population was reported[173,176,177]. Both cDC types express typical cDC markers, such as CD26 (a costimulatory molecule), CD11c, CCR7 and a wide rande of toll-like receptors (TLRs), the most famous pattern-recognition receptors[173,178]. However, murine CD11c cell surface expression lowers once cDCs are activated[179].

pDCs are a subset od DCs with unique morphology and function[180]. While the main function of cDCs is to capture antigens by various cellular processes and prime T cells, pDCs resemble plasma cells and excel in their ability to produce type I and III interferons (IFNs) as a response to viral infection[180]. This is reflected in their distinct expression of cDC-specific cellular markers, such as lower levels of MHC II and CD11c expression[173]. pDCs also bear a unique set of markers compared to cDCs, including Bst2 (a lipid raft associated protein), Ly6C, Siglec-H (a lectin binding sialic acid) and B-cell marker B220[172,173,180]. Typical for pDCs is also the expression of TLR7 and 9[173,180]. Similarly to cDCs, pDCs also express CD26[172,173]. CD172a expression and CD4 expression are markers pDCs share with some cDC2s, while some pDC subsets (especially in the gut) can also express CD8, similarly to cDC1s[172,173]. pDCs also express high levels of IRF8 and only low to intermediate levels of IRF4 transcription factor[172,173,180].

2.3.7. Macrophages

Macrophages, functioning as professional phagocytes and APCs residing in all peripheral tissues, are descendants of embryonal macrophages and of monocytes after their extravasation from the blood[181]. Monocytes, CD11b+F4/80+CD115+ cells in mice, can be further divided into two subsets. The classical, Ly6C+ subset, patrols extravascular tissues in addition to blood and gives rise to tissue macrophages and even special subset of monocyte-derived DCs, especially in inflammatory conditions, whereas non-classical Ly6C- subset (originating from Ly6C+ monocytes) patrols blood only, not giving rise to macrophages[182]. Just as monocytes, macrophages are also known to express CD11b, F4/80 along with CD14, TLR 2 and 4, and Fc gamma receptors (CD64, CD32, CD16)[183]. Additionally, some of them,

such as dermal, alveolar or intestinal macrophages, can also express CD11c, hindering the easy separation from DCs[184,185]. Macrophages are also known to have high autofluorescence, further complicating the problem with cell analysis[172].

Macrophages form several subpopulation according to their activation status, anatomical distribution, and corresponding cellular marker expression. The basic dichotomy of activated macrophages are M1 („classical“) and M2 („alternative“) subsets, with a pro-inflammatory and anti-inflammatory (reparative) phenotypes, respectively. For their diferentiation, several unique cellular markers were found, such as CD38 for the M1 and Egr2 for the M2 population[186]. Regarding organ-specific populations, a few examples will be provided. Peritoneal macrophages, an abundant, easily obtainable and frequently analysed population, can be further subdivided into large and small peritoneal macrophage subset[187]. Large peritoneal macrophages are more abundant in steady state and are characteristic of high levels of F4/80 and CD11b expression, along with the CD11c expression, and low MHC II expression, whereas the small peritoneal macrophage subpopulation expresses only lower levels of F4/80 and CD11b and is negative for CD11c[187,188]. However, the expression of MHC II is higher in small peritoneal macrophages and they are the prevalent population in inflammatory conditions[187,188]. In lymph nodes, three distinct subsets of macrophages were found – subcapsular sinus macrophages (CD169+ CD11b+ F4/80-), medullary sinus macrophages (CD169+ CD11b+ F4/80+) and medullary zone macrophages (CD169- CD11b+ F4/80+)[189]. In spleen, four macrophage subpopulations were reported – white pulp macrophages, red pulp macrophages, marginal zone macrophages and marginal zone metallophilic macrophages, differing in levels of the expression of CD11b, F4/80 and Tim4[190]. In Peyer’s patches, monocyte-derived macrophages express CD4, and, together with monocyte-derived DCs, pDC marker Bst2 (although lower levels than pDCs)[191]. These examples clearly demonstrate that macrophage identification is not straightforward and is very tissue- and subpopulation-dependent, and various measures to clearly differentiate macrophages from other immune cell populations should always be taken.

2.3.8. Neutrophils

Neutrophils, the most abundant granulocytes in the peripheral blood, are myeloid polymorphonuclear cells. They migrate to the infection site from blood via diapedesis and fight pathogens either via phagocytosis and release of intracellular granules, or via netosis, releasing of neutrophil extracellular traps based on cellular chromatin[192]. Typical cellular markers of murine neutrophils include CD11b and Ly6G[193,194]. Together with numerous other cell types, neutrophils also express Ly6C[195]. Recently several subpopulations were uncovered, both in circulation and tissues[196]. In the blood, neutrophils are separated into fresh and aged fractions, with an increase in CXCR4 chemokine receptor, CD11b, CD11c, CD49d and others (possibly promoting entering the tissues) expression and decrease in Ly6G, CD62L and their size and number of granules during aging[196–198]. Tissue-specific neutrophils can be found in many organs including spleen (CD62L^{low} CD11b^{hi} ICAM-1^{hi}) or lymph nodes (CCR7-positive)[196,199,200]. Other forms

of neutrophils with unique functions include granulocytic myeloid-derived suppressor cells (expressing markers of classical neutrophils), low density neutrophils (CD15+ CD33+ CD66b+ $CD16^{low}$ in humans), or tumor-associated neutrophils, all with a significance in cancer[196,201]. Alteration of neutrophil phenotype was also reported to be achieved by microbial metabolites, enhancing antimicrobial properties and lifespan and influencing ageing of neutrophils[196,197,202,203].

2.4. MHC II molecules and antigen presentation

Major histocompatibility complex (MHC) molecules are highly variable polygenic and polyallelic transmembrane glycoproteins encoded on chromosome 17 in mice and on chromosome 6 in humans (here termed HLA - human leukocyte antigen). Functionally, MHC molecules are responsible for presentation of peptides on the cell surface, either of (mostly) self antigens in the case of MHC I, or of non-self, ingested antigens for MHC II. The peptides for antigen presentation fit into grooves on MHC molecules (8-10 amino acid residues for MHC I and 15-35 for MHC II), which are their most variable 3D loci, ensuring a varying binding specificity for different peptides. Almost every individual has a unique combination of MHC alleles and is therefore capable of presenting different combinations of peptides. This diversity functions as a guarding mechanism against vast variability of pathogens (and their appropriate antigenic patterns) so that the population as a whole can survive the infection, as well as shaping the susceptibility to various diseases on an individual level[204].

MHC II is a dimeric molecule composed of two transmembrane chains (α and β), each containing two extracellular immunoglobulin domains in addition to the transmembrane segment. Its assembly starts in the endoplasmatic reticulum by the dimerization of α and β subunits. The groove is covered with a trimeric invariant chain molecule (Ii) until the complex travels through the Golgi network into the late lysosome (more specifically MVB or MHC II-loading compartment, where the Ii gets cleaved, leaving a small residue called the class II-associated invariant chain peptide (CLIP) in the groove for peptide binding. Later, based on the activation of APCs and reorganization of the vesicular structure of MVB involving the non-classical MHC II variants) an exogenous peptide replaces the CLIP in the groove the and mature MHC-II molecule travels to the cell surface[205].

MHC II is expressed mostly on „classical“ or „professional“ APCs (DCs, macrophages and B cells, with DCs having the best presenting capability), and is especially upregulated upon their activation. The expression of MHC II is regulated mostly through transcription by the master regulator, CIITA (Class II Transactivator)[206]. CIITA has three different functional promoters, each used by a different subset of cells and responsive to different cues. MHC II production in DCs is mostly under the control of promoter I, whereas other hematopoietic cells utilize mostly promoter III[207]. Promoter IV is inducible, especially by IFN-γ[208]. This promoter plays a major role in macrophages as well as in non-hematopoietic cells[207].

As implicated, other, non-professional antigen-presenting cell types, able to express MHC II and successfully prime naïve T cells (with the highest threshold for activation), have been reported in

the past several decades. At first, inflamed tissues across the body, via an infection or an autoinflammation diseases were identified as positive[209,210]. This way, critical roles for the presentation of antigens with similar sequences to microbial antigens (molecular mimicry) and antigens typically outside of the reach of the immune system (such as behind the hematoencephalic barrier or inside highly specialized cells such as endocrine cells) in the development of autoimmune conditions were uncovered. In the inflammatory microenvironment, a multitude of cell types (including astrocytes, thyroid cells, pancreatic islet endothelial cells, neutrophils, and many others) express detectable levels of MHC II and often also costimulatory molecules, crucial for succesful priming of naïve T cells and avoiding their death or anergy[211–214].

However, later it was uncovered that MHC II expression on non-professional APCs can occur even during homeostasis and serve unique functions. For example, studies have found the basal MHC II molecule expression in intestinal epithelial cells (IECs), with an increasing gradient from the crypt to the villus, in steady-state conditions[215]. Both IEC and ILC3 MHC II expression was demonstrated to help prevent pro-inflammatory conditions development in the gut in the steady state when MHC II expression was not accompanied by costimulatory molecule expression[216,217]. Nonetheless, the amount of MHC II and costimulatory molecules expression increases in (auto)inflammatory and immune-mediated conditions, such as IBDs or coeliac disease, or during infection[218,219]. This goes hand in hand with a relatively recent finding of MHC II expression on intestinal stem cells (ISCs), with novel functional contexts atop of the role of a non-professional APC. MHC II function in ISCs during homeostasis and inflammation is linked to their self-renewal capacity as well as a differentiation bias to either Paneth (Th1 microenvironment) of tuft (Th2 microenvironment) cells, though the exact mechanism remains unknown[220]. In lymph nodes, multiple subtypes of lymph node stromal cells can also express MHC II molecules, though usually with a tolerogenic outcome[221]. Yet another function of MHC II expression in mice and various other animals is its role in fertilization, particularly in the recognition between a sperm and an egg[222].

Nonetheless, the most prevalent function of MHC II is classical antigen presentation. After a boom in identifying numerous cell types with cell surface-localized MHC II and therefore potential antigen presenters, it was also uncovered that the surface levels of MHC II do not always correlate with mRNA levels or even MHC II protein content inside the cells. To enlighten this phenomenon, several known mechanisms of cell-to-cell molecule transfer were proposed and later validated, such as exosomes (small extracellular vesicles), trogocytosis (exchange of small cell membrane patches during a close cellular contact, e.g. immunological synapse) or tunneling nanotubes[223–225]. This means that not all cells surface-positive for MHC II have the capability to endogenously produce MHC II, but rather that they may have acquired it from a nearby APC. An important example of this phenomenon are basophils, which were first identified as MHC II positive in a stimulatory environment but later the results were compromised when a lack of endogenous MHC II expression was shown[226–228]. Research has demonstrated that the surface molecules of MHC II were obtained by trogocytosis from DCs[229].

Interestingly, exosomes-containing MHC II molecules produced by IECs were identified to stand behind the presentation of microbial antigens on DCs (at least to some extent), with both pro- or anti-inflammatory outcomes possible[230–232]. Alternatively, MHC II molecules together with costimulatory molecules were detected on the surface of murine T cells, which normally do not express MHC II, after an interaction with a DC[233]. In conclusion, a finding of surface-bound MHC II (or other molecules) does not imply the origin of the molecule and alternative ways should be considered, especially if a discrepancy between surface and intracellular levels (or mRNA expression) of MHC II is observed. Another thing to consider is the presence of costimulatory molecules (CD80, CD86, CD40) on the cell surface, severely impacting the outcome of (non-professional) APC:T cell interaction. Nonetheless, MHC II cell surface positivity can be a good indicator of the involvement of a cell type in immune reactions, at least under specific conditions.

2.5. MHC II-EGFP *knock-in* mouse model

The discovery and isolation of GFP (green fluorescent protein) from the original host, the jellyfish *Aequorea Victoria*, has revolutionized the approaches to protein localization in living organisms in the last several decades so enormously that it was awarded a Nobel prize in 2008[234]. Since its discovery, several variants of GFP (or different fluorescent genes derived from invertebrates) were established with shifts in their excitation or emission spectra, such as YFP (yellow fluorescent protein) or CFP (cyan fluorescent protein), providing a way to study several proteins at once, and many more[235]. EGFP (enhanced green fluorescent protein) is a protein developed from the original GFP by two point mutations, resulting in the 35-fold increase of the fluorescence intensity[236]. This highly enhances the detection and therefore opens up the door for more precise measurements in the region of interest. Many hybrid genes with (E)GFP (or other fluorescent protein variants) inserted as *knock-ins* were engineered since, enabling the direct in vivo localization of protein of interest, and even quantification of their expression[237].

MHC II-EGFP *knock-in* mouse model was developed by replacing the original *MHC II* gene with *MHC II-EGFP* transgene in 129/Sv; H-2^b murine embryonic stem cells[238]. After the demonstration of the lack of functional difference compared to wt mice, the model was first used as a unique visualization tool for the DC:T cell immunological synapse and DC late endosomal compartment directional tubulation[238]. Since then, the model was crossbred with C57BL/6 mouse, generating MHC II-EGFP C57BL/6 mice. This model, while being functionally indistinguishable from wt mice, enables direct visualization of MHC II-expressing cells and MHC II-rich organs. In comparison to using fluorescent antibodies, the visualization can be done *in vivo* or right upon dissection, without the need of any additional time-consuming steps that may lead to many artifacts while handling or staining tissues and cells. Compared to traditional antibodies it is also possible to visualize intracellular expression of MHC II without the need of any permeabilization, and, by combining both endogenous and antibody MHC II detection, it is also possible to obtain relative ratios of intracellular vs. surface MHC II

expression. Therefore, this model is suitable for both flow cytometry analysis as well as advanced microscopy options. 3D visualization techniques, such as light sheet microscopy, are especially advantageous in this model, as all MHC II positive cells are emitting green fluorescence, whereas traditional staining techniques are severely limited in the size of the sample by the maximum effective dye diffusion into the tissue. This way, even whole organs (organisms) could sometimes be visualized without the need of additional dissection, so that the 3D picture can give us better representation of the actual tissue structure inside the body. On top of that, this model enables much more detailed tissue dissection of MHC II positive tissues in the body, as well as the observation of otherwise invisible tissue architecture, such as structural patterns composed of small accumulations of MHC II positive cells in the tissue, with possible functional relevance. To sum up, this model is an excellent immunological tool suitable for numbers of various microscopic and cytometry techniques, with the possibility to obtain multi-dimensional, quantitative data closely reflecting the conditions in living organisms. It enables the search for novel phenomena in the field of professional and non-professional APCs and for other, yet unknown functions of MHC II molecule.

2.6. Methods of quantitative histology – light sheet fluorescence microscopy

The goal of quantitative histology is to count cells or other structures within a sample, usually within a microscopic slide or a set of slides, and then extrapolate the number to a larger structure, such as the organ or a whole organism. Choosing a representative sample is critical and corrections are needed to account for any unintentional artifacts or biases. This is the reason why, when regarding for example the cellular content of a whole organ (such as the intestine) or an organism, often a difference of several orders of magnitude is observed between various estimates. To overcome this highly biased two-dimensional view, 3D visualization techniques, including light sheet fluorescent microscopy (LSFM), were developed. Since LSFM was the method used in this work, the following chapter will be solely focused on this technique, highlighting the strengths and weaknesses of LSFM compared to other methods, such as confocal microscopy.

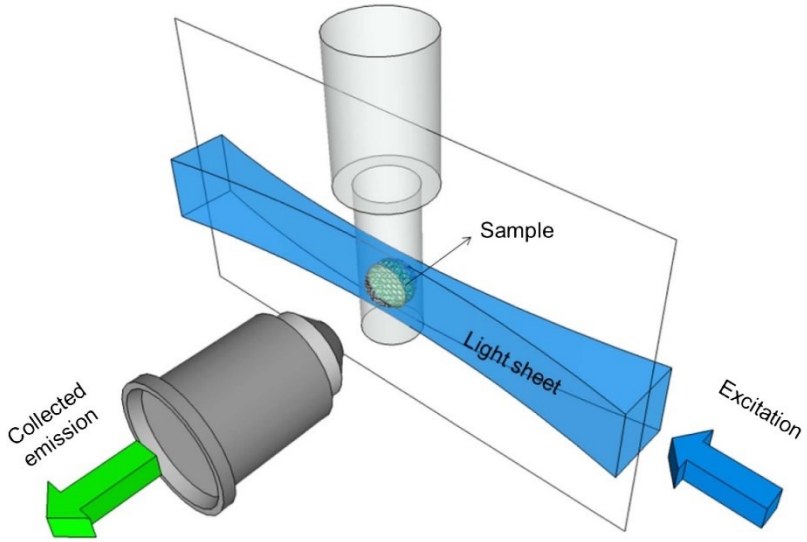

Figure 2: The basic scheme of the light sheet microscope. The excitation light (blue) is focused onto a sigle plane within the sample. The emitted fluorescence is then detected by an orthogonal camera (green). Figure reprinted from Olarte et al. [273].

LSFM is a unique approach to studying 3D samples. Unlike most microscopical methods including confocal microscopy, the cylindrical lens focuses the light into a thin sheet (hence the name light sheet microscopy), rather than illuminating the whole sample, which creates virtual "slide" within the sample and minimizes photobleaching and phototoxicity in the rest of the sample. The signal from the single plane is then collected by an orthogonally positioned camera (see *Figure 2*)[239]. However, the maximum sample size was limited by light scattering and absorption within the sample, which could not be quite resolved by rotating the sample. Therefore, the basic premise was later upgraded with a second source of light located on the opposite side of the sample. The two sources would create a single, more focused plane by computationally combining both signals[240].

The resolution of light sheet microscopy of larger samples is generally lower than that of confocal microscopy, especially in the *z* dimension, unless special acquisition techniques and deconvolution are used[241–244]. This is due to the light scattering as it travels through the sample. These special approaches, such as isotropic multiview light sheet microscopy, are therefore able to increase the penetration depth and visualize bigger samples more thoroughly[245]. With proper optimalization, sample size of more than 1 cm can be achieved. However, except for the newly available commercial light sheet systems, the tailor-made systems are poorly standardized accross laboratories.

The acquisition speed of the wide-field camera is also one of the great advantages of LSFM. Combined with minimum photobleaching, it offers real-time imaging over the course of minutes, hours, or days, which is the reason why long-term dynamic processes are often studied by LSFM. Unsurprisingly, one of the biggest branches of current applications of LSFM is developmental biology, producing 4D (temporal) time-lapses, from a single cell to the whole embryo, or imaging a detailed development of a particular organ[246–248]. Other emerging uses for LSFM are immunology, enabling scanning of whole organs for immune cells during inflammation or in the search for disperse and

unevenly distributed mucosa-associated lymphoid tissue; or clinical medicine, by quick and easy 3D tumor assesment instead of traditional histological slides[249–252].

In general, LSFM enables *in vivo* imaging of organisms, providing unique information about complex functional histological contexts. However, this applies to a limited number of species, such as zebrafish, as few organisms are transparent, which is essential for light to travel through the sample. To enable visualization of other species, special clearing protocols (generally speaking removing lipids from the sample), such as CUBIC (Clear, Unobstructed Brain Imaging Cocktails and Computational analysis) needed to be developed[253]. However, these often include harsh chemicals and are therefore not suitable for living organisms. Still, LSFM offers imaging of these samples with *in situ* morphology with minimum amount of artifacts compared to other microscopy techniques.

The limitation of light sheet microscopy is the optical nature of samples (or their parts) with different refractive index than the scanning solution used, as light sheet gets scattered at their interface. These could include air, crystals, or fat. Only very limited improvement can be achieved with clearing in the latter case, as in most protocols the fat is incompletely penetrable for most chemicals and sample preparation time needs to be adjusted, which brings the risk of lowering the signal/increasing the noise in the case of fluorescent samples. Another limitation is the generation of terrabytes of data in the matter of seconds, which brings out problems with their storage as well as handling and further analysis[254]. This is a huge problem of modern-day imaging technologies that will need to be tackled effectively in the future.

2.7. Multiparametric flow cytometry and data analysis

Classical flow cytometry is semi-routinely capable of measuring up to 20 parameters at once (with rising number). Recent advancements, such as spectral flow cytometry, which minimizes the problems with spectral overlap and compensation, expands the multiparametricity even further[255,256]. On top of that, rapidly evolving mass cytometry is theoretically almost unlimited in the number of parameters[257]. However, it is not trivial to envision this 20- or more-dimensional space on a 2D screen at once (or in a human brain accustomed to thinking in a 3D space) for further analysis. Therefore, multiple challenges are arising in an effort to analyze such data. For example it is problematical to manually develop a gating strategy for all possible combinations of markers and a failure to detect some populations is probable, as well as introducing bias into gated populations depending on a gating strategy and its hierarchical configuration. The exact gates are also highly unstandardized and nearly irreproducible, and manual control of larger datasets is extremely timely[255].

Therefore, several dimensionality reduction algorithms, such as t-SNE (t-distributed stochastic neighbor embedding) or UMAP (Uniform Manifold Approximation and Projection for Dimension Reduction), were developed[258,259]. Both of these methods are able to comprise the information from a number of dimensions into a 2D (or 3D) space, creating clusters of similar objects. While small distances (especially within a cluster or for nearby clusters) in multi-dimensional space get clustered together by

t-SNE, closeness in 2D does not mean closeness in multi-dimensional space, and large distances (such as between various clusters) have no informative value[255]. Contrarily, UMAP is a faster algorithm where the distances between clusters better represent the degree of alikeness between different populations and the visual output varies less across the samples (although the latter is still a highly discussed topic)[260–263]. The data from both algorhitms can be easily visualized, and clusters can then be gated and identified according to their expression pattern. The dimensionality reduction and clustering itself is unsupervised, however for further work, manual or automated gating of clusters is needed, bringing the risk of subjective bias.

Another approach for data analysis is the unsupervised clustering, such as generating SOMs (self-organizing maps), including algorithms such as FlowSOM (included in the FlowJo software package) or EmbedSOM (with a new graphical interface – ShinySOM), and many others[264–266]. These algorithms are usually very fast and can directly transform data from a multi-dimensional space into clusters and then group them into (manually defined) number of populations (metaclusters). The clustering is fully unsupervised, and the analyzing subject only identifies respective (meta)clusters by their expression patterns, usually visualized in a grid or a heatmap. With new algorithms for population identification emerging, even this next step may soon be routinely automated[255].

It is possible and may be even beneficial to combine the aforementioned two main approaches (dimensionality reduction or unsupervised clustering) as means of better visualization of automatically clustered data[267]. Dimensionality reduction algorithms may provide information about the similarity between neighboring clusters and therefore help with the categorization of less pronounced cluster phenotypes, while unsupervised clustering uses a fast and standardized algorithm to cluster different populations, and is less likely to be influenced by biases, such as spreading errors or backround noise as t-SNE, which may generate artificial accessory clusters[268]. With t-SNE, the “clustering” on a 2D plane generates a different output with every run (as the algorithm is stochastic), so different samples cannot be directly compared[255]. t-SNE also proves ineffective as a differentiating tool for multiple subpopulations, differing by levels of expression of few parameters[269]. On the other hand, tSNE is better at accounting for differential expression of cellular markers, as within a (meta)cluster using SOMs, a mean fluorescence intensity value is represented and the information about expression variance is lost[255]. It is also often used as a “trial-and-error” pathway, identifying the desired number of metaclusters, as lower numbers, although better reflecting the expected number of “rational” populations and easier to analyze, may not lead to separation of some desired populations[267].

It is important to highlight the fact, that each unsupervised analysis should be preceded by manual or automated quality control check, to ensure uniformness and meaningfulness of inserted data. Pre-gating of living singlet cells is also advised to remove possible problems with clustering and cluster identification. Last but not least, downsampling for some more time-consuming algorithms (t-SNE) helps to operate with more manageable running times[255].

3. Aims

- Establishment of the combinatonal methodological toolbox (fluorescent macroscopy, LSM (light sheet microscopy), and flow cytometry) to study microbiota transfer (entero-mammary pathway) in detail using MHC II-EGFP *knock-in* mouse model and unsupervised data analysis.
- Quantitative and qualitative characterization of the gut lymphoid tissue putatively involved in entero-mammary microbiota transfer.
- Description of the effect of microbiota on Peyer's patches and mesenteric lymph node cellular composition and function – comparison of the SPF and GF mouce models.

4. Materials and methods

4.1. Materials

4.1.1. Chemicals and solutions

BSA (Sigma-Aldrich) – 1% PBS

Collagenase IV (Roche) - 1 mg/ml in HBSS (-/-)

Dispase (Gibco) – 1 mg/ml in HBSS (-/-)

dH_2O

DRAQ5 (Invitrogen)

EDTA (Sigma-Aldrich) – 2mM

FBS (Life Technologies) – 3-5% solution in RPMI medium

Formaldehyde (Sigma-Aldrich) – 3,8% in H_2O

Gelatin (Sigma-Aldrich)

N-TEA (Sigma-Aldrich)

PBS (pH 7,3; 0,79% NaCl (Lachner), 0,29% $Na_2HPO_4.12H_2O$ (Lachner), 0,011%KCl (Penta), 0,031%KH_2PO_4 (Lachema)

PBS with gelatin – 0,02% gelatin (Sigma-Aldrich) + 0,01% sodium azide (Sigma-Aldrich)

RPMI (Gibco)

Sodium azide (Sigma-Aldrich) – 0,01% in PBS

Sucrose (Penta) – 30% in PBS

Sytox blue (Invitrogen) – 20 000x

TEA (Sigma-Aldrich)

Triton X-100 (Sigma-Aldrich) – 0,5% in PBS

True-Stain Monocyte Blocker™ (BioLegend) – 20x

Urea (Lachema)

VersaComp Antibody Capture Bead Kit (Beckman Coulter)

4.1.2. Tissue clearing solutions

Adapted CUBIC protocol[270]:

Tissue clearing solution CUBIC 1: 175 ml dH_2O, 125 g Urea (25 wt%), 124 ml N-TEA (25 wt%), 70 ml Triton X-100 (15 wt%)

Wash: 500 ml PBS, 2,5 g 0,5% BSA, 500 µl 0,01% Sodium azide (0,01%), 500 µl Triton X-100 (0,1%)

Tissue clearing solution CUBIC 2: 130 ml dH_2O, 125 g Urea (22,5 %), 44,5 ml TEA (9 %), 250 sucrose (45%), Triton X-100 (0,1 %)

4.1.3. Antibodies

Flow cytometry:

Two flow cytometry antibody panels were used – myeloid and lymphoid. Myeloid panel construction was inspired by the panel used in The Czech Centre for Phenogenomics, Biocev, Vestec. Both panels were later adjusted because some of the antibodies did not stain properly in the experiment conditions. Both original and final versions are included. Please note that in addition to fluorescent antibody conjugates, there is also MHC II-EGFP fluorescence included (when using MHC II-EGFP mouse model), fluorescent in FITC, and dead cell staining by Sytox Blue.

Marker	Fluorophore	Dilution	Origin	Producer
Ly6G	BV421	300x	rat	BD Biosciences
Bst2	BV605	400x	rat	BioLegend
F4/80	PE-Dazzle 594	300x	rat	BioLegend
CD19	APC	40x	rat	BioLegend
CD11b	PerCP-Cy5.5	200x	rat	BioLegend
Ly6C	BV711	200x	rat	Biolegend
CD45	A-700	100x	rat	Invitrogen
CD11c	PC7	150x	hamster	BD Biosciences
MHC II	APC-Cy7	1000x	rat	BioLegend

Table 1: Original Myeloid panel

Marker	Fluorophore	Dilution	Origin	Producer
Ly6G	BV421	300x	rat	BD Biosciences
Bst2	PE	300x	rat	Invitrogen
CD19	APC	40x	rat	BioLegend
CD11b	PerCP-Cy5.5	200x	rat	BioLegend
Ly6C	BV711	200x	rat	BioLegend
CD45	A-700	100x	rat	Invitrogen
CD11c	PC7	150x	hamster	BD Biosciences
MHC II	APC-Cy7	1000x	rat	BioLegend

Table 2: Final myeloid Panel

Marker	Fluorophore	Dilution	Origin	Producer
TER-119	PacBl	1000x	rat	BioLegend
CD4	PE	1000x	rat	exbio
γδ TCR	BV605	100x	Armenian hamster	BioLegend
CD8	PE-Dazzle 594	1000x	rat	BioLegend

CD19	APC	40x	rat	BioLegend
CD25	PE/Cy7	40x	rat	BioLegend
NK1.1	BV785	100x	mouse	BioLegend
CD3	APC-Cy7	100x	Armenian hamster	BioLegend

Table 3: Original lymphoid panel

Marker	Fluorophore	Dilution	Origin	Producer
TER-119	PacBl	200x	rat	BioLegend
CD4	PE	1000x	rat	exbio
γδ TCR	APC	150x	Armenian hamster	BioLegend
CD8	PE-Dazzle 594	1000x	rat	BioLegend
CD3	PerCP-Cy5.5	20x	Armenian hamster	BioLegend
CD25	PE/Cy7	40x	rat	BioLegend
NK1.1	BV785	100x	mouse	BioLegend
CD19	APC-Cy7	150x	rat	BioLegend

Table 4: Final lymphoid panel

Marker	Name	Dilution	Origin	Producer
CD16/32	TruStain FcX™ PLUS	1000x	rat	BioLegend

Table 5:Other antibodies used in flow cytometry

True-Stain Monocyte Blocker™ was added to each staining mix (20x dilution).

4.1.4. Expendable supplies

96-well plate (Costar)

Cell strainer 50µm (Corning)

Centrifuge tubes – 15ml, 50ml (Eppendorf)

Eppendorf tubes – 0,5ml, 1,5ml, 2ml (Eppendorf)

Petri dishes (Nunc)

4.1.5. Instruments

Centrifuge mini spin plus (Eppendorf)

Centrifuge Universal 16 R (Hettich)

Flow cytometer BD LSR II (BD Biosciences)

Laboratory scales (Schoeller instruments)

Light sheet fluorescent microscope (Zeiss Lightsheet Z.1)

Stereomicroscope (Carl Zeiss SteREO Lumar.V12)

Thermoblock (Eppendorf Thermomixer comfort)

4.1.6. Mice

Two mouse models were used: wtC57BL/6 and C57BL/6 MHC II-EFGP *knock-in* mouse model[238]. The latter was bred in two distinct environments: SPF and germ-free. SPF mice were bred in Center for Experimental Biomodels, 1st Faculty of Medicine, Charles University. Germ-free mice were prepared and bred in Laboratory of Gnothobiology, Institute of Microbiology of the CAS, v. v. i., Nový Hrádek. All mice were kept under standard conditions (12hr day/night regimen, 22°C, 55% relative humidity, ST1 diet (Velaz) *ad libitum*). All procedures were approved by the Czech Animal Care and Use Committee and The Institutional Committee for Ethics of Animal Experiments. Any animal handling was done under the supervision of Valéria Grobárová or Jan Pačes.

4.1.7. Software for data acquisition and analysis

FlowJo™ v10.7.1, BD Biosciences
ImageJ
R and R studio
FlowSOM plugin
Zeiss ZEN
Arrivis

4.2. Methods

4.2.1. Organ sample preparation for flow cytometry

The mouse was executed by cervical dislocation. Under the stereomicroscope, MLN complex of MHC II-EGFP mouse was carefully excised and transferred into the small Petri dish with PBS. MLNs were separated and put into 1,5ml Eppendorf tubes with 450 µl of 3% FBS in RPMI (*). In BL mice or control pooled sample of MHC-II EGFP, the whole complex was put into 1,5ml Eppendorf tubes with 900 µl of 3% FBS in RPMI. Spleen was localized and put into 1,5ml Eppendorf tubes with 900 µl of 3% FBS in RPMI. Next, the whole intestine was transferred to a large Petri dish and PPs were sequentially harvested into 1,5ml Eppendorf tubes with 270 µl of 3% FBS in RPMI. The collagenase was added to a concentration of 0,1 mg/ml to each tube and samples were incubated for 40 minutes in 37 °C (*) in Thermoblock. Next, the samples were always handled on ice. EDTA was added to each sample (250x) and the samples were pipetted through a cell strainer to a clean tube Spleen was resuspended to 20 ml in a 50 ml centrifugation tube and 100µl were stained per sample. After centrifugation (5 min, 300G), and discarding the supernatant, the samples were resuspended in 100 µl of TruStain FcX™ PLUS (250x) and transferred to a 96-well split into two for each sample (2 panels). After the centrifugation (5 min, 300G), the samples were stained by the myeloid and lymphoid panel mixtures for 30 minutes (20 µl per

cell for PPs and 50 µl for MLNs and spleen) and then washed with PBS with gelatin twice. 200 µl of PBS with gelatin were then pipetted to each sample, along with Sytox Blue (20 000x).

- When using dispase, PBS was used instead of RPMI with FBSand the digestion took 10 minutes. FBS was added along with EDTA to a finl concentration 3%)

4.2.2. Light sheet microscopy

During the whole process, the samples were kept in dark. Harvested samples (as in previous section) were transferred to a 1,5ml Eppendorf tube with formaldehyde for one hour. Next, the samples were transferred to a CUBIC 1 solution for 1-2 days at 37 °C, depending on the size of the tissue, until they were cleared. Samples were then transferred to a WASH solution and were kept in a fridge for 1 hour. Next, 1ml of 10000x (MLNs) or 20000x (PPs) diluted DRAQ5 solution in PBS was added to clean 1,5ml Eppendorf tube and samples were incubated in the cold chamber for 4-5 days. The data were then transferred to CUBIC2 solution and were kept in 37 °C until the image acquisition using Light sheet fluorescent microscope (Zeiss Lightsheet Z.1) and ZEN software. Throuhout the whole process of sample preparation, I was assisted by Karolína Knížková.

4.2.3. Data visualization

Stereomicroscopical images were visualized using Fiji software.
Lightsheet data were visualized by ZEN and Arrivis softwares.

4.2.4. Flow cytometry

Flow cytometry data were aquired from HTS, using 160 µl out of 200 µl of the sample, speed 1,5. The acquisition was done using application settings for each panel.

4.2.5. Data analysis

Data were analysed using FlowJo™ v10.7.1. with the use of FlowSOM plugin (based on R). Statistical evaluation was done using ANOVA testing in R.

5. Results

To establish MHC II-EGFP mouse model as a tool for studying the entero-mammary pathway hypothesis, a detailed anatomy and histology of the relevant organs – especially MLNs and PPs (with the help of microscopical techniques) as well relative and absolute cell numbers of immune cells in studied organs under physiological conditions had to be described. Optimalization of sample preparation for light sheet microscopy and multicolor flow cytometry had to be carried out and fine-tuned to allow for capturing even minute differences in the composition of lymphoid organs caused by bacteria. GF mouse served as a way to capture possible differences compared to SPF (conventional microbiota state) conditions. MHC II-EGFP mouse model was used as a tool for detailed secondary lymphoid organ dissection and further analysis by both microscopical and flow cytometric approaches. By a combination of both methods the structural as well as the quantitative (numerical) perspective on the composition of MLNs and PPs could be applied.

5.1. Visualization of secondary lymphoid organs by stereomicroscopy

5.1.1. Mesenteric lymph nodes

The first step in both microscopic and cytometric experiments was sample acquisition. Mesenteric lymph nodes were retrieved from the peritoneal fatty tissue and split into single lymph nodes. The number, size and 3D pattern varied significantly in both SPF and GF mice (n=4-11, including the colonic lymph node, see Figure 4 and Figure 3). MLNs were then assigned a number according to the oral gradient (the last lymph node being the colonic lymph node) and lightsheet or flow cytometric samples were prepared. No remarkable differences between SPF and GF mice MLN morphology were observed (compare Figure 4 and Figure 3).

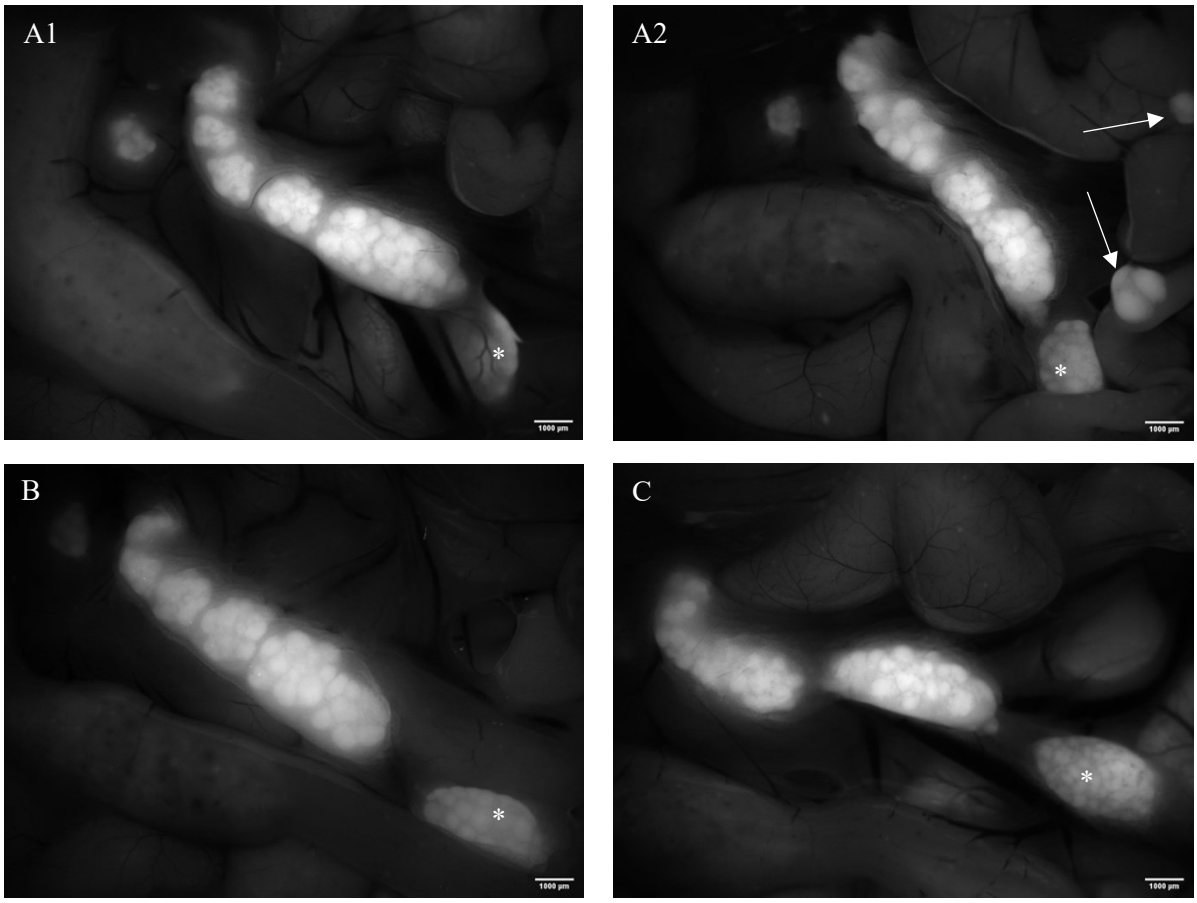

Figure 4: Stereomicroscopic images of MLNs in 3 SPF MHC II-EGFP mouse. The last lymph node (colonic, lower right, asterisks) is significantnly separated from the pack of other MLNs that usually only separate with dissection. A varying number, configuration and size of MLNs can be seen. Arrows on A2 indicate Peyer patches on the nearby small intestine. Scale bars: 1000 µm.

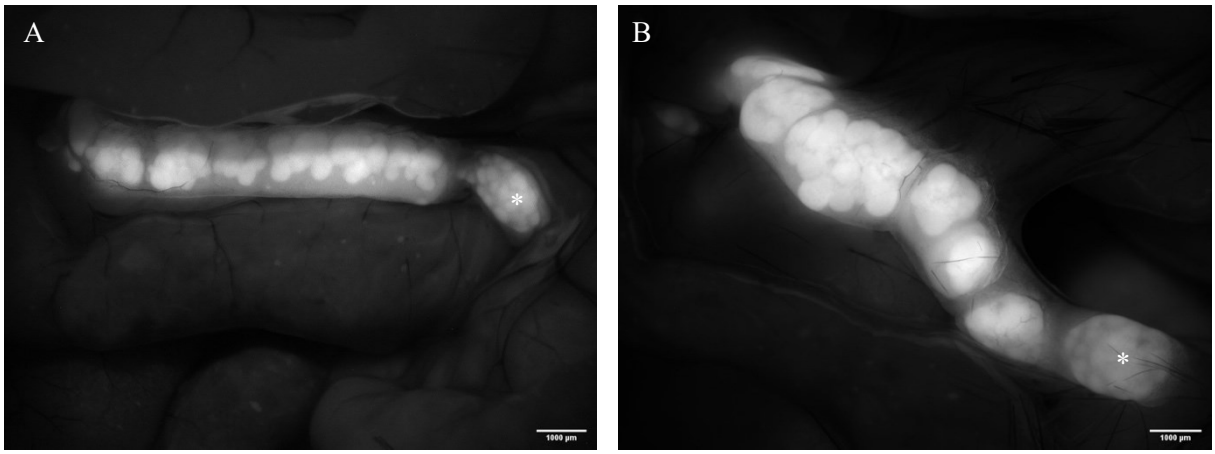

Figure 3: Stereomicroscopic images of MLNs in GF mice. Varying number of nodes as well as a "degree of cohesiveness" can be observed. Separated colonic lymph node is indicatd by asterisks. Scale bars: 1000 µm.

5.1.2. Peyer patches

After the extirpation of MLNs, the whole intestines were extracted and examined for PPs in a sequential order, from duodenum to the colon. This was performed not to lose the vital information about the intestinal gradient in PPs, which could enable a direct comparison to the MLN gradient. Again, the

numbers of PPs in the small intestine varied across both SPF and GF animals (n=5-10), as well as the size of PPs, that could be consisting of 1-7 “follicles” (see Figure 5A, B and C). The major difference was observed in the morphology of coecal patch. In SPF mouse the morphology of coecal patch is usually a single bulky unit – splitting into of 2 patches in a small distance from each other was also observed (compare Figure 5A and B) and resembles the PPs in the small intestine. On the contrary, in GF mice the coecal patch usually did not hold a compact structure and was rather dispersed to several small units throughout the enlarged coecum (see Figure 5D). The colon contained 1-3 small patches usually within a small area, which were analysed as a whole due to their small cellular numbers and lower survival rate (see the Flow cytometry – Optimalisation of dissociation protocol section).

Figure 5: Stereomicroscopic images of small intestinal PPs, coecal and colonic patches. (A) PPs and coecal patch with typical pattern from SPF mouse. Image captured by Jan Černý. (B) Coecal patch variant in SPF mouse – coecal patch made up of 2 separate units. (C) Small intestine of GF mouse with a single PP compposed of 4 individual "follicles". Small "dots" along the gut stand for putative "micropatches", a structure visible using the MHC II-EGFP mouse model (partially attributable to cryptopatches or dispersed lyphoid tissue). (D) Dispersed coecal patch in GF mouse. (E) Image of the whole intestine in SPF mouse, from duodenum (left) to the colon (right). The intestines contain seven small intestinal PPs, coecal patch (arrow) and colonic patch. Image captured by Valéria Grobárová and Ondřej Šebesta. Scale bars: 1000 µm.

5.2. Visualisation of MLNs and PPs using light sheet microscopy

In MHC II-EGFP mouse model overall structural composition in 3D of MLNs and PPs using MHC II-EGFP mouse model, the samples for lightsheet microscopy were cleared via the adapted CUBIC protocol (see Methods section) and the nuclei were stained with DRAQ5, for easier subsequent analysis and potential cell number determination. The concentration of DRAQ5 had to be optimalised for each analysed organ separately. The tested dilutions were 5000x (MLNs), 7500x, 10000x and 20000x (PPs),

with the final dilution of 10000x for MLNs and 20000x for PPs. The pilot experiment was composed of two sets of MLNs from GF mice (Figure 7, only one set is shown here), one set of MLNs from SPF mice (Figure 6), and one set of PPs from the small intestine (Figure 8). MLNs needed to be carefully liberated from the fatty capsule, because DRAQ5 could bind to the fatty droplets effectively, resulting in an extremely high backround in the sample. Particullar PPs and the whole MLN complex from the wtC57BL/6 mouse were used as a control for autofluorescence (Figure 9). 3D acquisitions were performed using the light sheet microscope Zeiss Lightsheet Z.1 (20x objective lens and 488 nm – GFP, 561 nm – autofluorescence, and 638 nm – DRAQ5 lasers). The sample preparation and measurement were performed with the assistance of Karolína Knížková. The figures used for representative demonstration depict a single plane from the acquisition. Despite the same dilution of DRAQ5 used, PP2 sample exhibited (from unknown reason) a much higher intensity of DRAQ5 fluorescence, causing the signal from the nuclei fuse together. Therefore, this picture needed to be adjusted manually for presentation purposes. All other images are set to the same threshold ratios.

The imaging datasets were acquired with the future perspective of counting all the cells (including MHC II-positive cells) in the whole MLN/PP (or at least the scannable part of the sample with the posibility to extrapolate to the whole volume). This has not yet been entirely successful due to the small-sized, densely packed lymphocytes with hardly visible cellular borders (compare MLNs and PPs (in the former less than 50% of cells are MHC II-positive according the flow cytometrical evaluation, while in the latter it is the case for over 90% of cells) despite deconvolution and several algorithms used. However, the images of all lymphoid organs imaged seem comparable andobviously contain a high protoption of MHC II-positive cells), which make up the vast majority of cells in both MLNs and PPs as quantified by Flow cytometry (see next chapter). To tackle this problem, new or modified algorithms will likely need to be exerted in the future (including the artificial intelligence-based neural networks, which are already used in the laboratory to quantify the levels of microchimersim in LSM datasets).

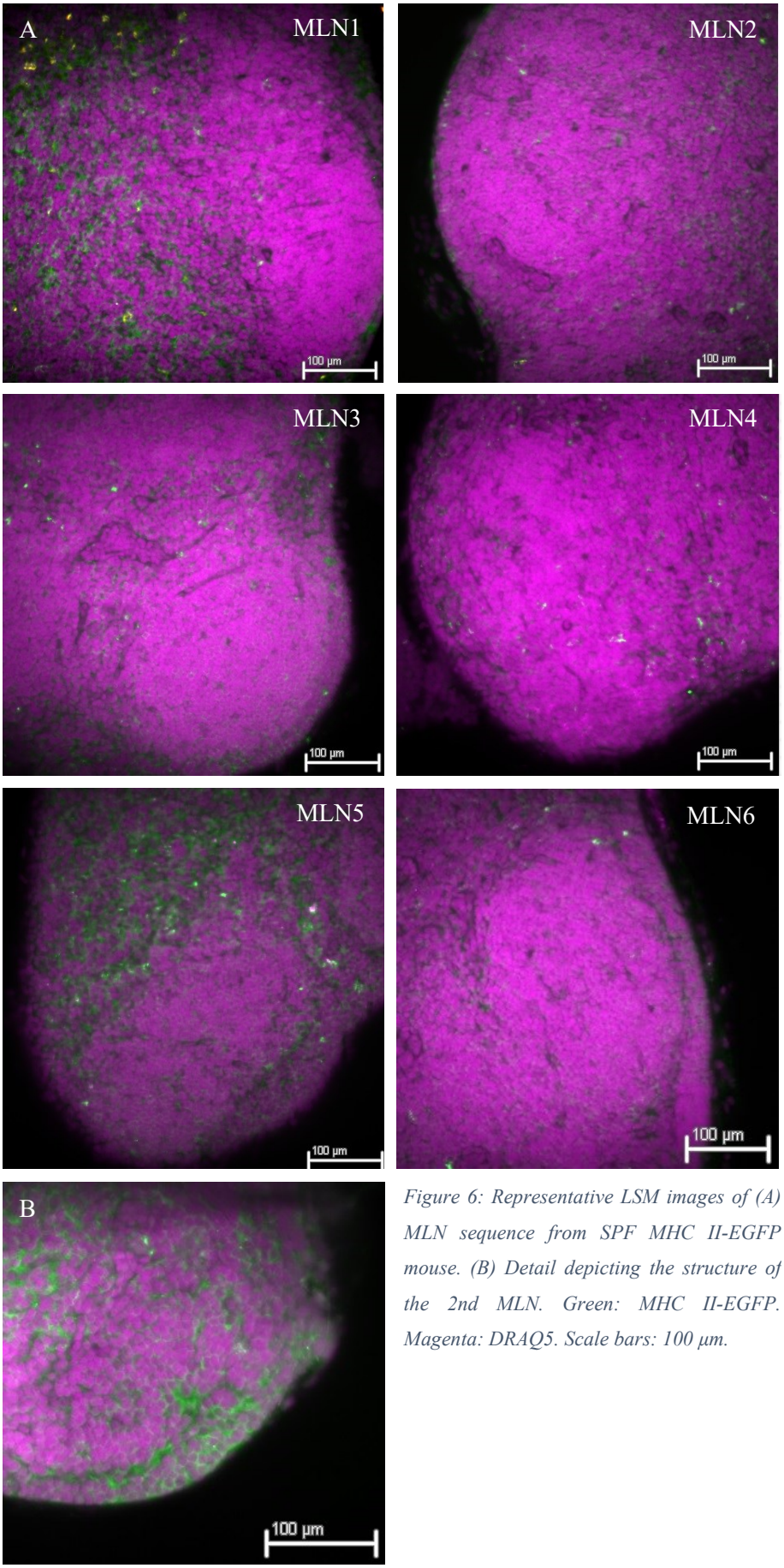

Figure 6: Representative LSM images of (A) MLN sequence from SPF MHC II-EGFP mouse. (B) Detail depicting the structure of the 2nd MLN. Green: MHC II-EGFP. Magenta: DRAQ5. Scale bars: 100 µm.

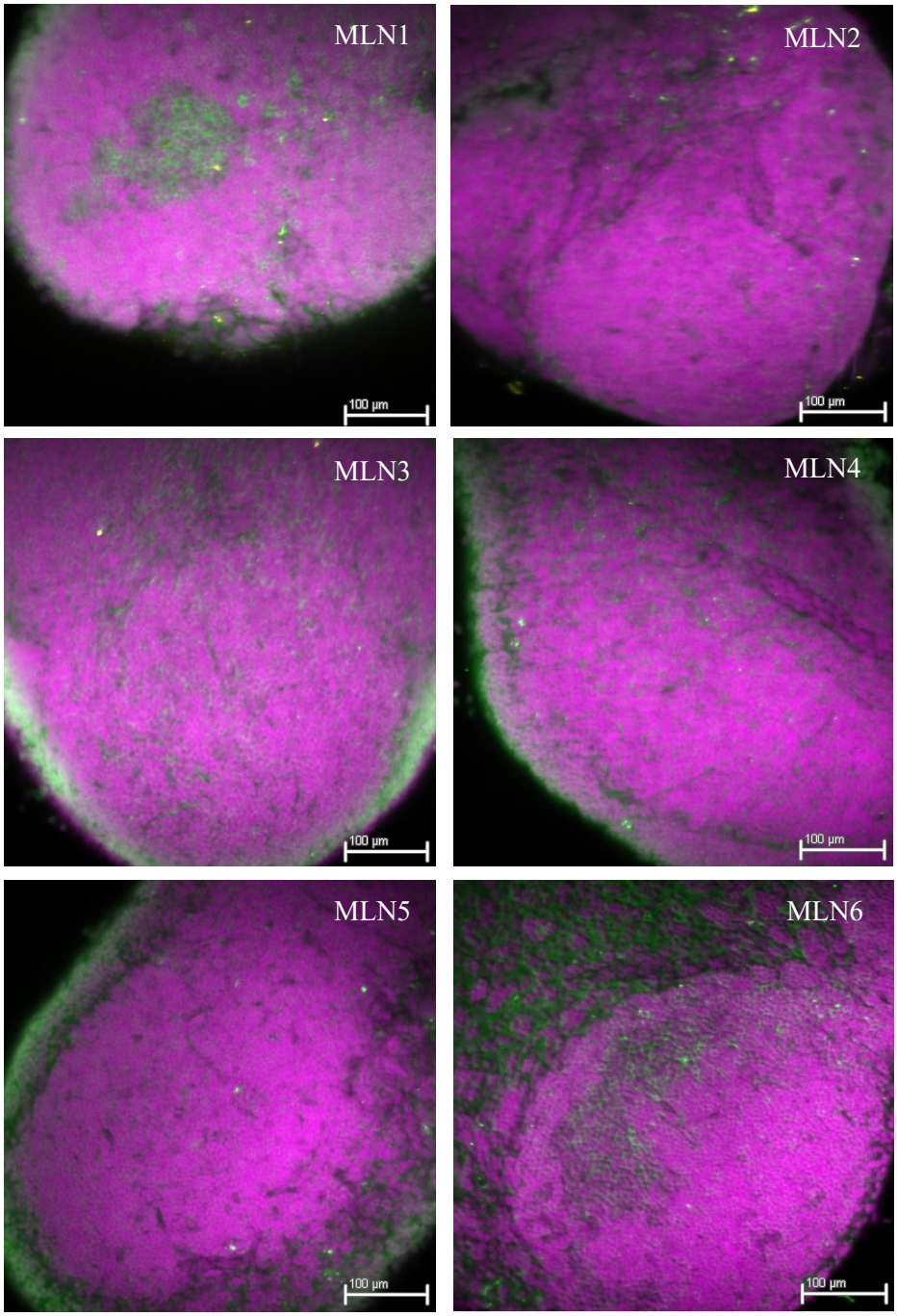

Figure 7: Representative LSM images of the MLN sequence in GF mouse. Green: MHC II-EGFP. Magenta: DRAQ5. Scale bars: 100 µm.

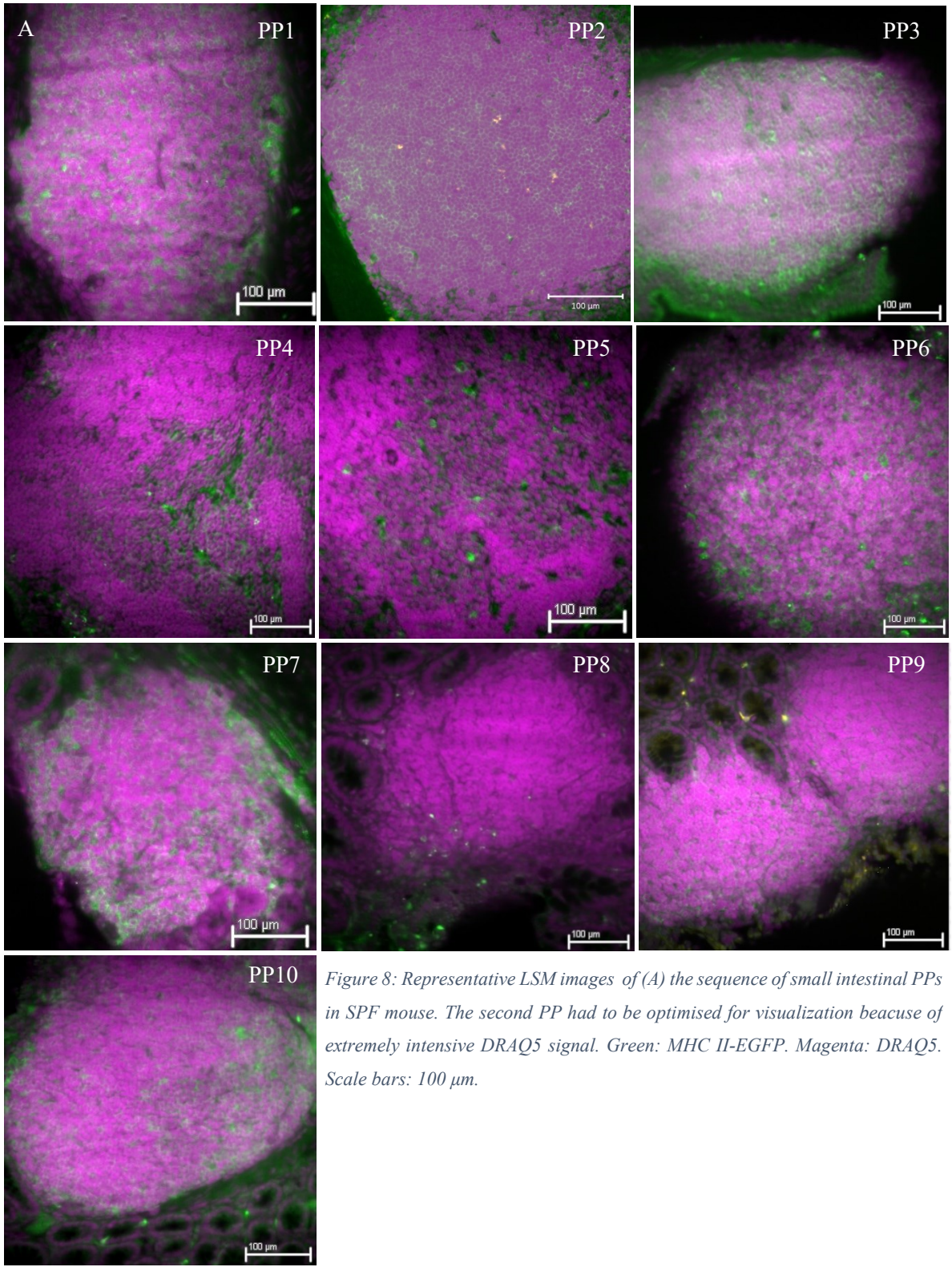

Figure 8: Representative LSM images of (A) the sequence of small intestinal PPs in SPF mouse. The second PP had to be optimised for visualization beacuse of extremely intensive DRAQ5 signal. Green: MHC II-EGFP. Magenta: DRAQ5. Scale bars: 100 µm.

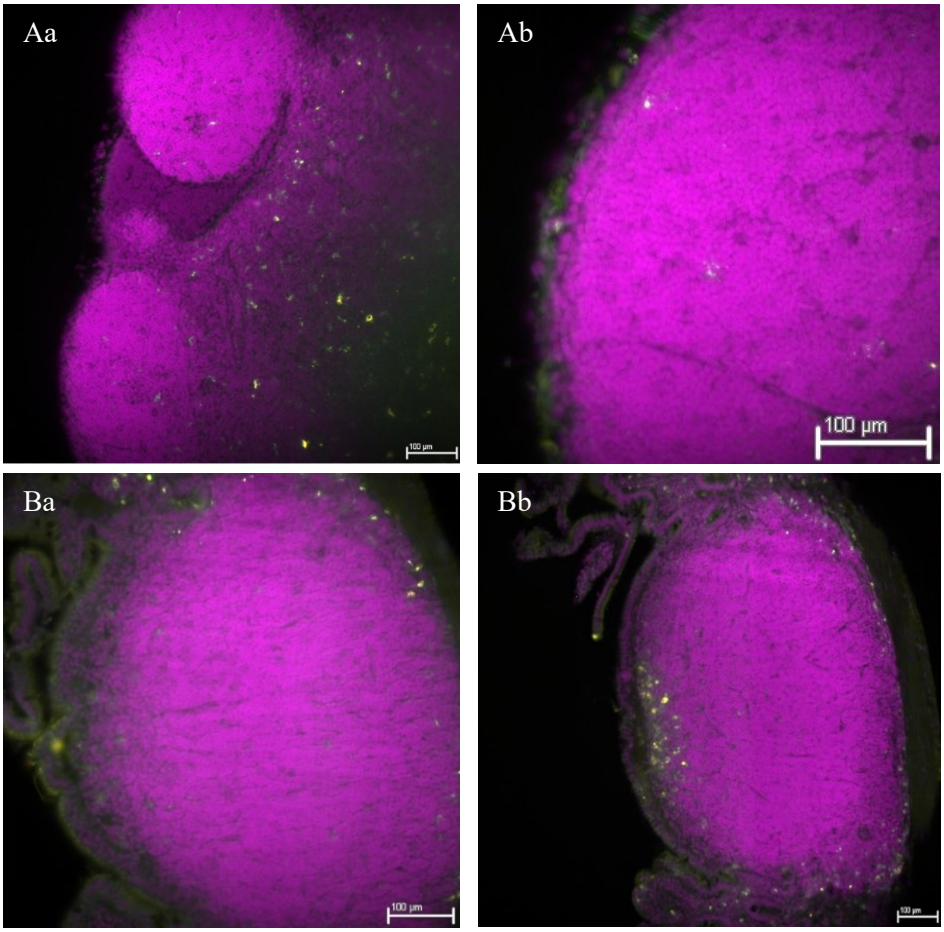

Figure 9: Representative LSM images of (Aa and Ab) MLN structure and (Ba and Bb) PPs in a C57BL/6 mouse capturing "follicle" surrounded by intestinal villi.. Green: autofluorescence. Magenta: DRAQ5. Scale bars: 100 µm.

5.3. Flow cytometry

Multicolor flow cytometry requires careful optimalization of each step in order to provide desired results. Here, the parallel usage of two cytometry panels, myeloid and lymphoid (see Materials and methods) was performed on the set of separate or pooled MLNs, PPs and spleen, to determine absolute and relative numbers of cells in each category. Shown is the optimalization process as well as surprising findings and limitations of methods and panels used in this setup.

5.3.1. Optimalisation of the dissociation protocol

Firstly, both MLNs and spleen (used as a “control” secondary lymphoid organ depicting the systemic immunity) were processed through a cell strainer and PPs were digested by dispase and then filtered through a cell strainer to obtain single cell suspension. However, the yield of myeloid cells was extremely low using just a cell strainer without the enzyme and the number and percentage of living cells in PPs varied multifoldly within a single mouse. Therefore, after a consultation with Jan Dobeš, (Laboratory of Microbial Immunology, Department of Cell Biology, Faculty of Science, Charles University), the collagenase dissociation was introduced. To determine the effectivity and robustness of

collagenase vs. dispase, both treatments were performed 3 times on a whole set of separated PPs from a mouse. The results are presented in Figure 10. Digestion by collagenase provided a higher yield of live cells and preserved the percentages of MHC II-positive cells (that could be skewed by different dying rates of various cell types) better than dispase. Therefore, collagenase was used as an enzyme of choice for all subsequent experiments, both for PPs as well as MLNs and spleen.

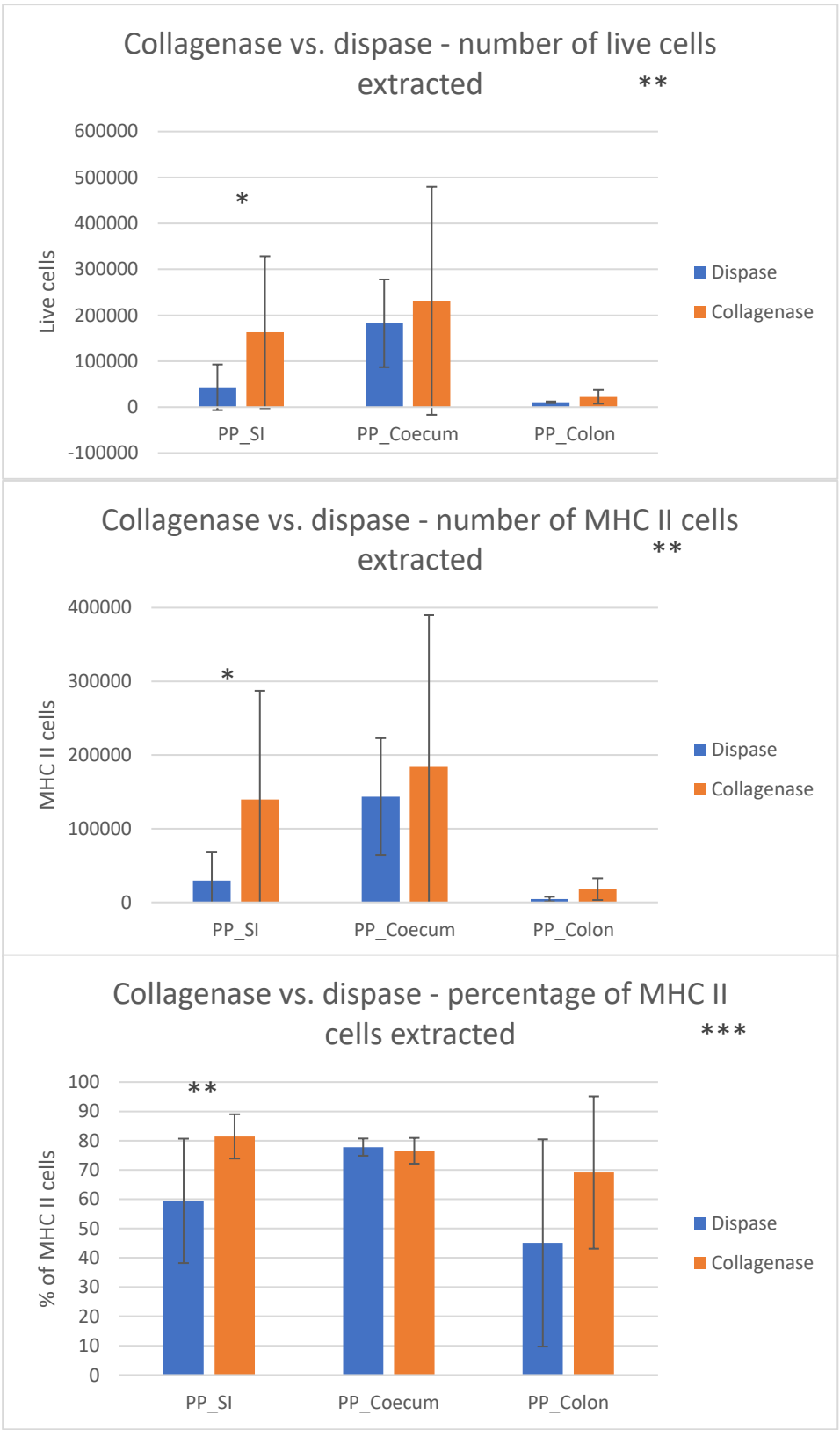

Figure 10: Comparison of dispase and collagenase enzyme treatment on the yields of living cells, MHC II-EGFP-positive cells and percentages of MHC II-EGFP-positive cells in Peyer patches from the small intestine (PP_SI), coecal patch (PP_Coecum) and colonic patch (PP_Colon).

5.3.2. Flow cytometry panels troubleshooting

Before the cellular composition of selected secondary lymphoid organs could be determined, a compensation matrix had to be calculated for both lymphoid and myeloid panel. The composition of the panels was inspired by the panels used in The Czech Centre for Phenogenomics, Biocev, Vestec. Especially the myeloid panel compensation proved challenging, as very low positivity percentages of several markers were observed at the beginning in each of the studied organs. Therefore, single stain controls for some markers, such as CD11b and F4/80, were performed on tissues with higher abundancy of positive cells, in this case peritoneal cells (abundant in peritoneal macrophages), and for others, such as Bst2, VersaComp Antibody Capture Beads were used. After the compensation was made by my colleagues, it was applied to the mix-stained MLNs and spleen. However, as is demonstrated on Figure 11, while peritoneal macrophages stain highly positively for both F4/80 and CD11b, no significant double positivity could be observed in the studied organs. Therefore, after several unsuccessful compensation attempts, F4/80 antibody was removed out from the panel.

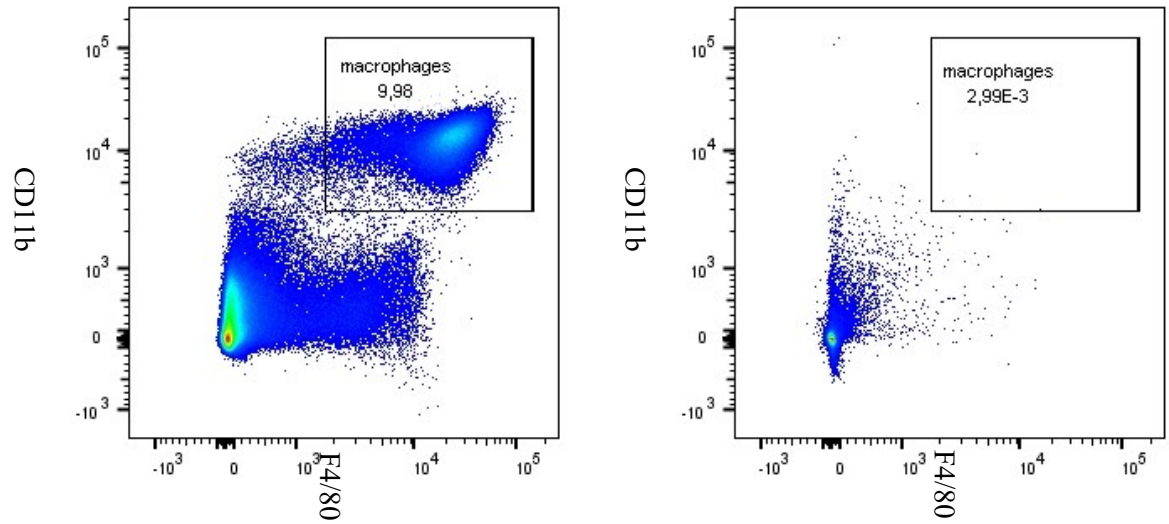

Figure 11: F4/80 and CD11b staining of peritoneal cells (left) vs. MLN (right) of SPF MHC II-EGFP mouse. No reliable signal could be determined for F4/80 outside of peritoneal macrophages.

In the case of Bst2, while the positivity could be determined by the staining beads, it could not be observed after compensation on the studied cells (see Figure 12). Therefore, after F4/80 was skipped from the myeloid panel, a new Bst2 antibody with different fluorophore conjugate was introduced instead of the original. After that, compensation matrix was successfully optimized by my colleague Jan Pačes and FMO (fluorescence minus one) controls on MLNs were performed by me for some markers to clearly differentiate between positive and negative populations for gating purposes (FMO controls attached in supplements).

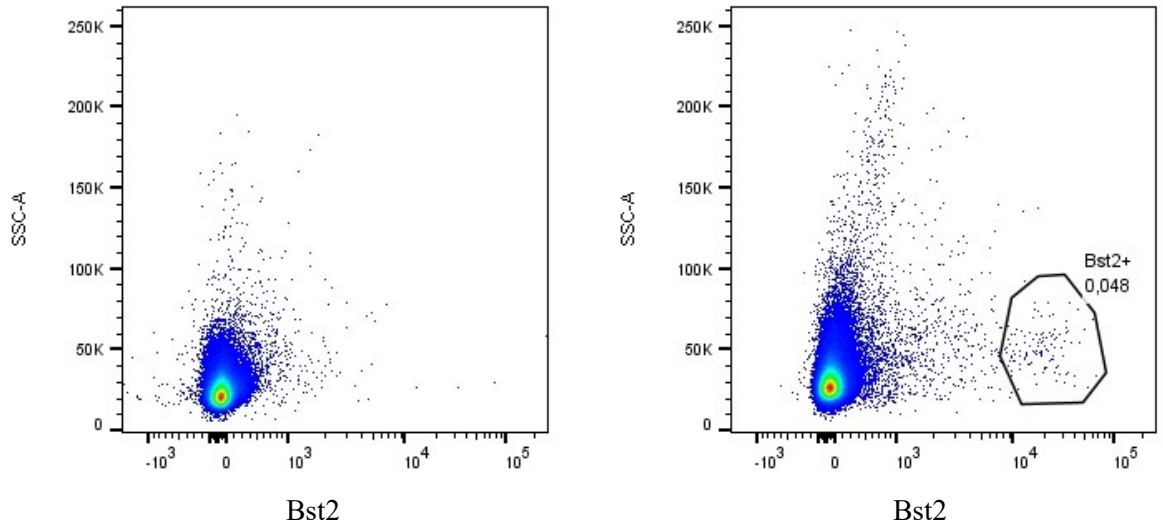

Figure 12:Staining of MLNs by original Bst2 – BV605 fluorochrome (left) vs. new Bst2 – PE fluorochrome (right) used in the final version of myeloid panel.

For lymphoid panel, most of the markers have clear, almost binary expression in the studied organs. Therefore, less optimalisation was needed for the most part. However, in the original panel, CD19 (APC) and CD3 (APC-Cy7) antibody fluorescence was acquired by R1 and R3 detectors, respectively, with relatively big spillover between these two channels. This proved to be problematic in the course of time, as some days, the relationship between these two markers appeared to be not compensated enough and "diagonal" instead of orthogonal relationship was observed. In addition, γδTCR signal was poorly distinguishable. To overcome these problems, CD19, CD3 and γδTCR antibodies were switched as described in Materials and methods and new compensation matrix was created by my colleague Valéria Grobárová (FMO controls of γδTCR and CD25 antibodies can be found in supplements section, along with gating strategies for both panels and each organ studied).

However, as can be seen, the usage of the combination of R1 and R3 lasers was not restricted to the lymphoid panel. The very same problem with the diagonal formation (clearly demonstrated in Figure 13) could be observed in lymphoid panel between MHC II and CD19 markers. This is the reason a separate analysis needed to be performed for 3 groups of myeloid results – without any diagonal, with a slight diagonal and with a (sub)-complete diagonal.

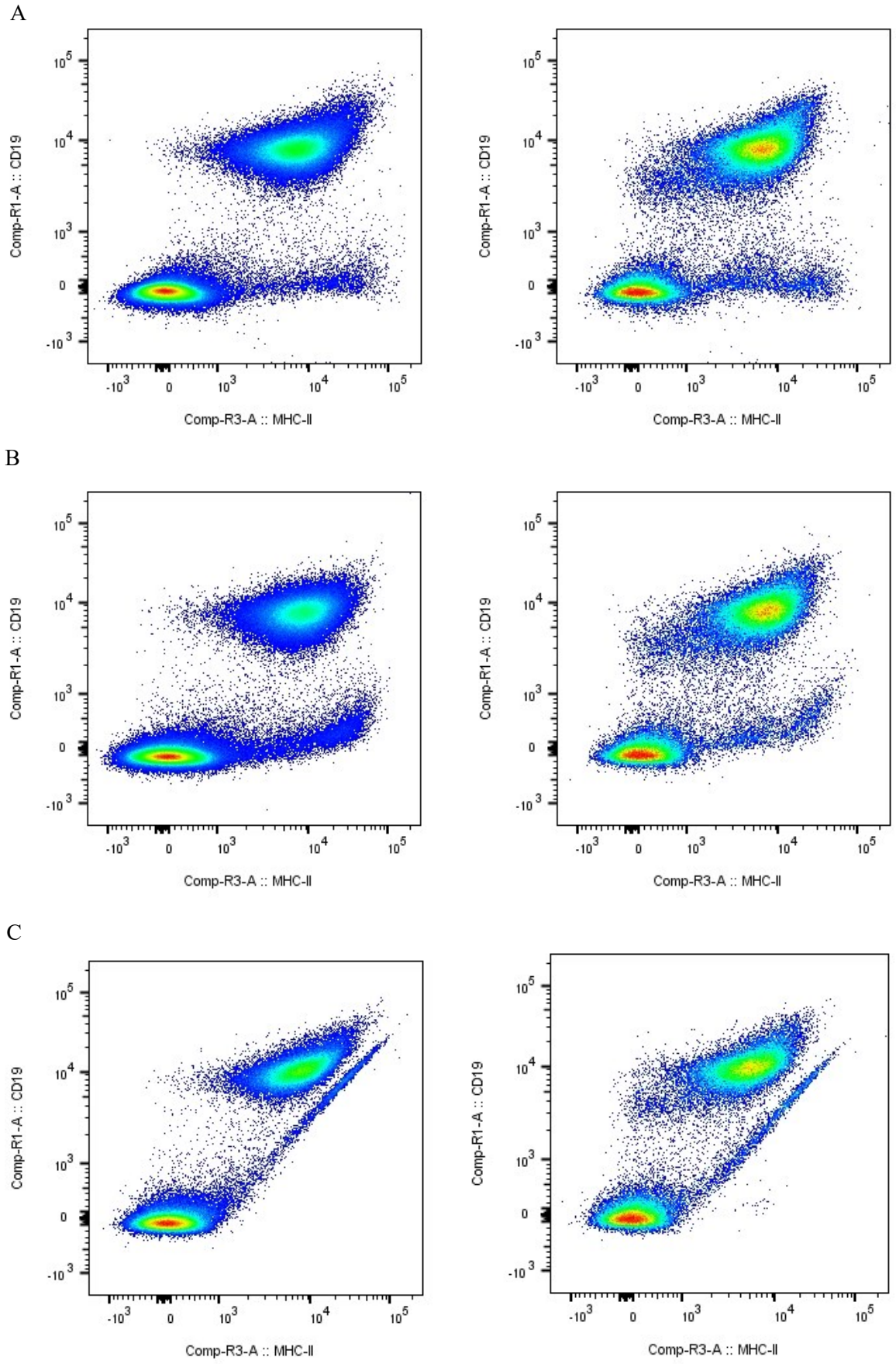

Figure 13: Demostration of orthogonal MHC-II:CD19 setup (top), slightly diagonalized setup (middle) and fully diagonal (bottom) of MLNs (left) and spleen (right). The data were acuired on consecutive days by the same method method using saved application settings during FACS measurement and the same compensation was used.

5.3.3. Data analysis with the help of unsupervised algorithms

Reflecting the great variety of possible combinations of markers on different cell types, as described in the theoretical section of this work, and relatively large panels used, the decision of not relying on manual gating was made in order to capture rare populations. Before any algorithm was run, the data were pre-gated to get CD45-positive cells (myeloid panel) or erythrocyte-free fraction (lymphoid panel) by conventional gating (see supplements) and manual quality control was performed. After that, the data or their downsampled fractions (to get under the 2 million event limit in a concatenated sample) were concatenated and FlowSOM analysis was performed with 25 desired metaclusters and 10 by 10 grid size for both panels and all organs (and in the case of myeloid panel for each diagonal status). C57BL/6 mouse organ analysis was performed separately. The resulting FlowSOM map was then applied to each sample within a group. The relatively high number of metaclusters was the result of optimalization to capture rare populations that were not otherwise separated (such as "Treg cells" – CD3+CD4+CD25+ cells). Despite that, some populations, such as neutrophils were not separated in all organs and diagonal status analyses (MLNs and PPs) due to their low number and could therefore not be quantified across all samples. To capture "Treg cells", the number of metaclusters in PPs needed to be further optimized to 26 with a grid size of 13 by 13. Representative FlowSOM heatmaps for each organ can be observed in Figure 14. Only the "no diagonal" variant is shown for the myeloid panel. From the FlowSOM output, each population was verified by manual control (whether it formed single population in the expected region in FSC-A/SSC-A dotplot and whether it formed a single population with uniform expression of markers rather than a spectrum), annotated according to its phenotype and "meaningful" populations (with marker combinations characteristic of a known immune cell population) were chosen for further analysis. For simplification, some populations, such as B cells or "memory T cells" (further explored in the chapter Ly6C vs. CD3, were analysed as pooled samples of several FlowSOM-made populations (they were split into several populations by their differential marker positivity expression – MHC II for B cells (pooled low, medium and high MHC II-expressing populations of CD19 cells – e.g. populations 4, 5 and 9 for MLNs in myeloid panel (see Figure 14A - left)) and Ly6C for memory T cells (low/medium and high expression – e.g. populations 21 and 23 in MLNs – low levels of positivity in Ly6G were not taken into consideration because of the known issue with Ly6G false positivity using current compensation). pDCs (population 15 in Figure 14A - left) were assigned to a population with high levels of Bst2 and Ly6C and low levels of MHC II and CD11c. cDC1 and cDC2 (populations 10, and 11 and 13 in Figure 14A – left, respectively) were characterized by high expression of CD11c and MHC II and differed in their expression of CD11b (low vs. high, respectively). Neutrophils (forming a separate population only in spleen – population 5 in Figure 14B – left) were characterized as CD11b high, Ly6G high and Ly6C high cells, with higher FSC and SSC). Because F4/80 needed to be omitted, macrophage populations could not be reliably identified

Lymphoid cells were assigned as follows: B cells (CD19+MHC II-EGFP+ - population 3 in Figure 14A – right), Th cells (CD3+CD4+ - population 15), Tc cells (CD3+CD8+, population 0), "Treg

cells" (CD3+CD4+CD25+, population 21) γδT cells (CD3+γδTCR+ - population 7), NK cells (NK1.1+ cells, population 13), NKT cells (CD3+NK1.1+ cells, population 12), "Breg cells" (CD19+MHC II-EGFP+CD25+, population 24) and "X" lymphocyte (CD19+CD3+, sometimes with CD4 or CD8 expression). These populations were then used for quantitative analysis.

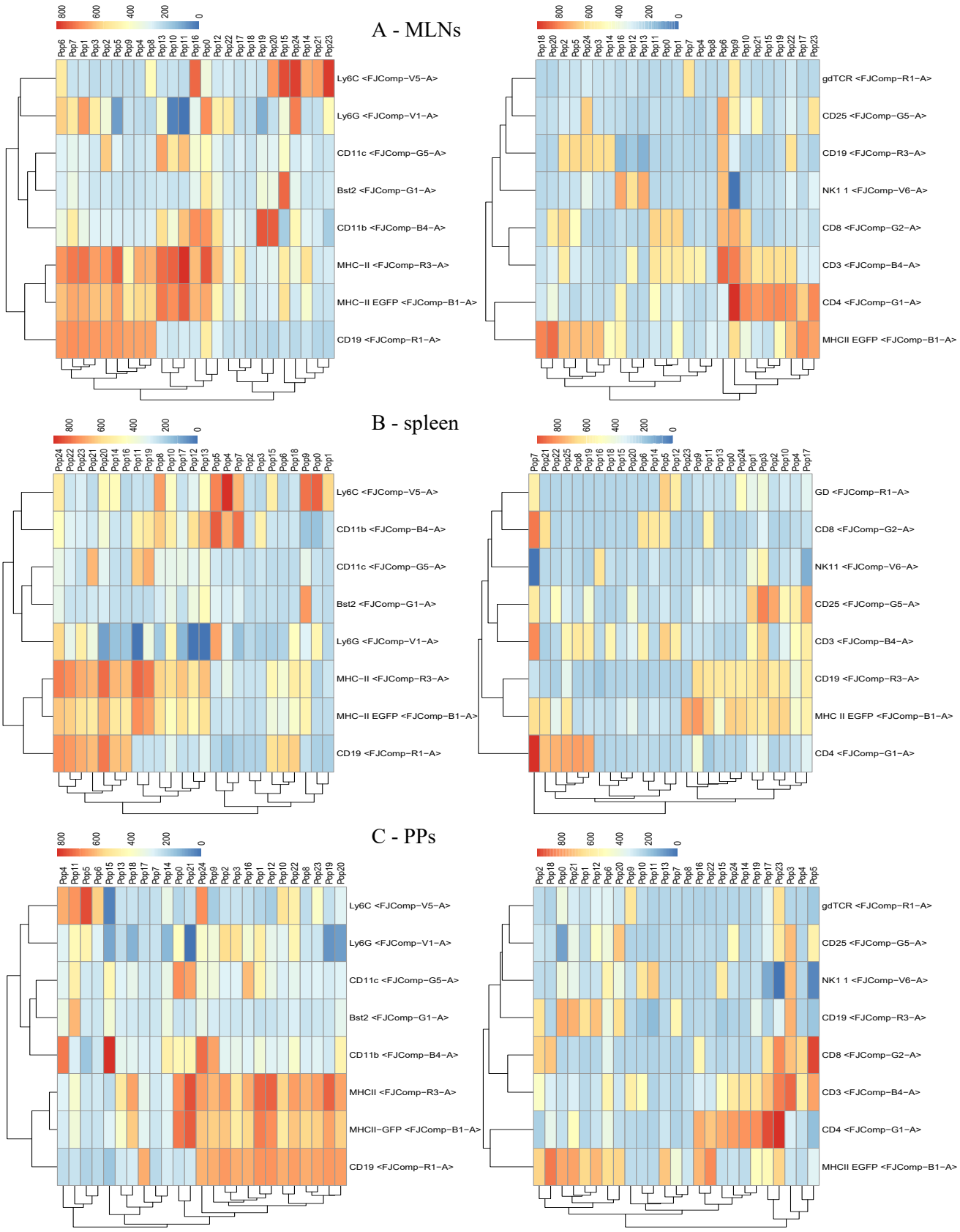

Figure 14: Heatmaps of FlowSOM populations from (A) MLNs, (B) spleen and PPs (C). Left - myeloid panel, right - lymphoid panel.

To better visualize and verify the FlowSOM output, tSNE analysis for some samples was performed (bigger samples were first downsampled to 100 000 events). In the following figures the representative tSNE outputs for all organs and panels ("no diagonal" variant for myeloid panel was used) are visualized with denoted marker expression as well as visual correlation with FlowSOM analysis.

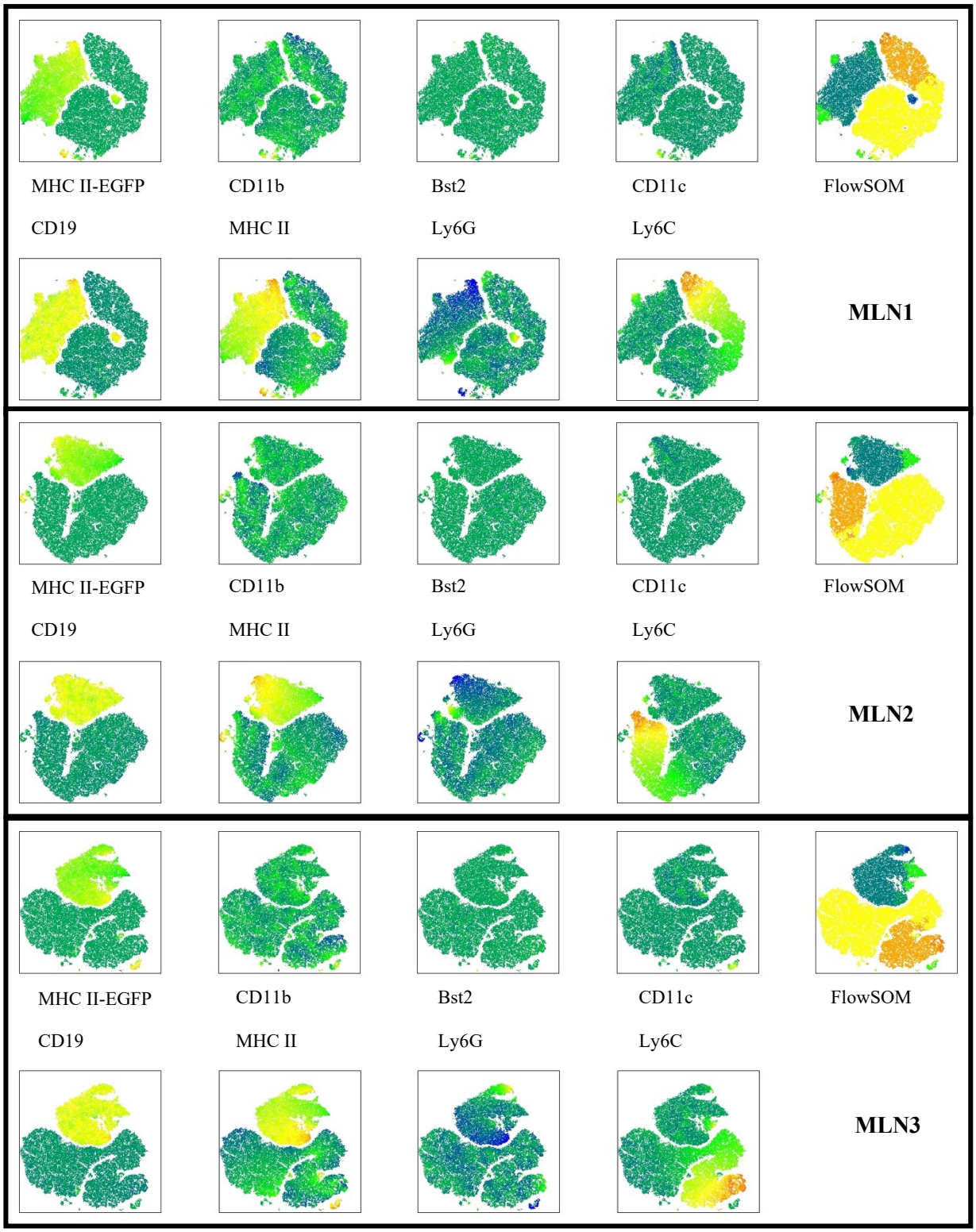

Figure 15: The first 3 out of 7 MLNs visualized by tSNE algorithm – myeloid panel.

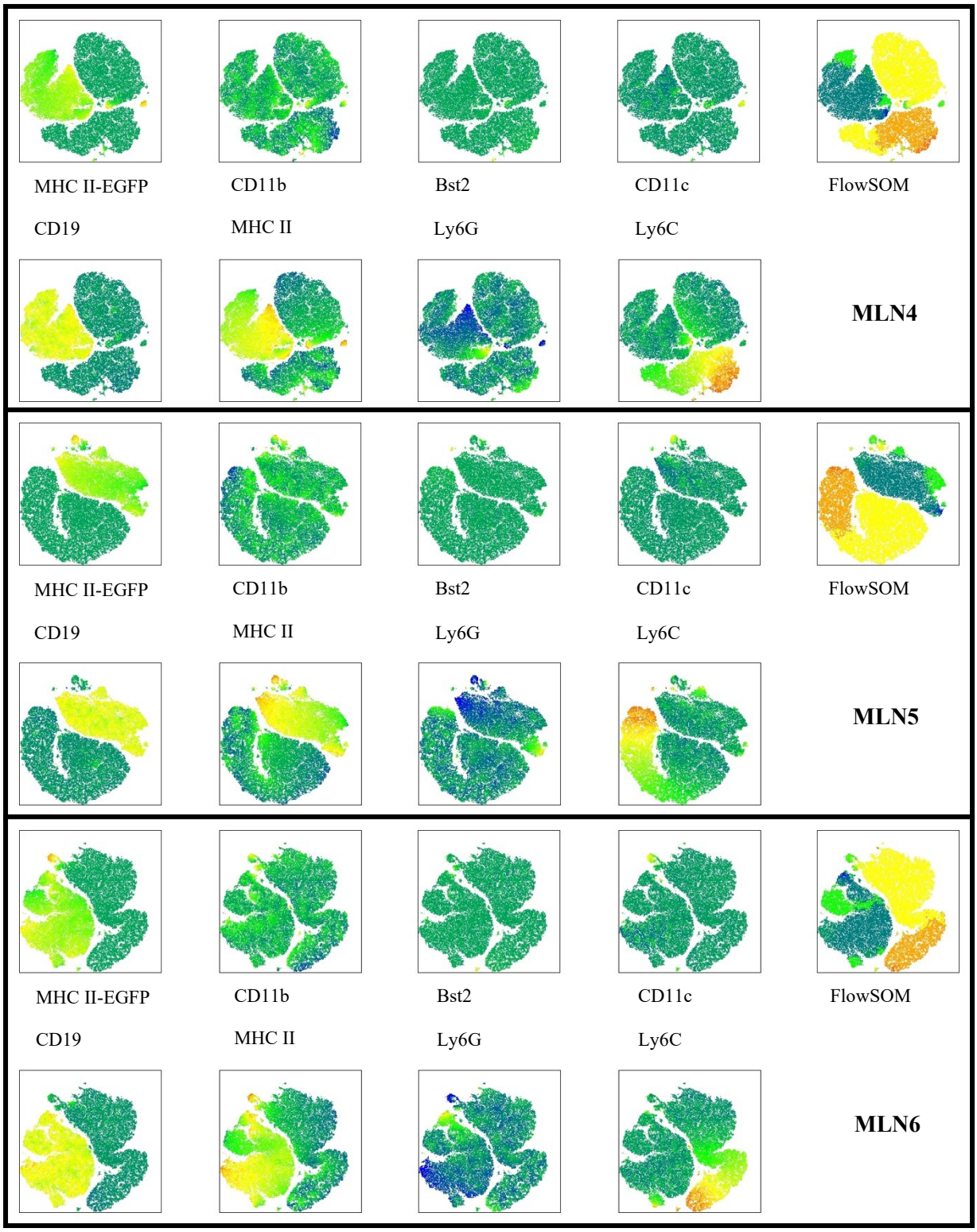

Figure 16: MLNs 4-6 visualized by tSNE – myeloid panel.

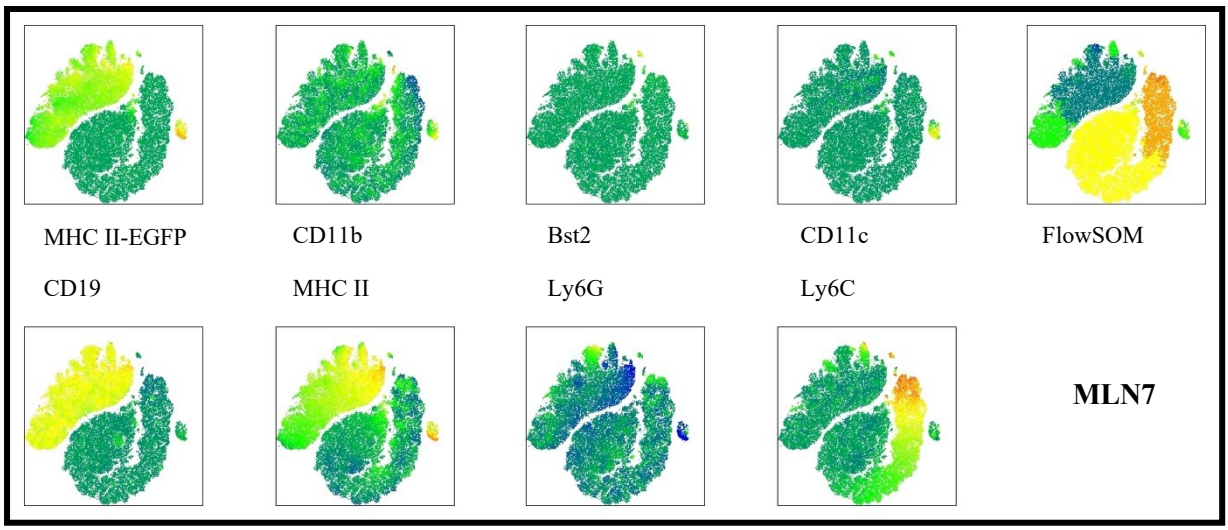

Figure 19: MLN 7 visualized by tSNE – myeloid panel.

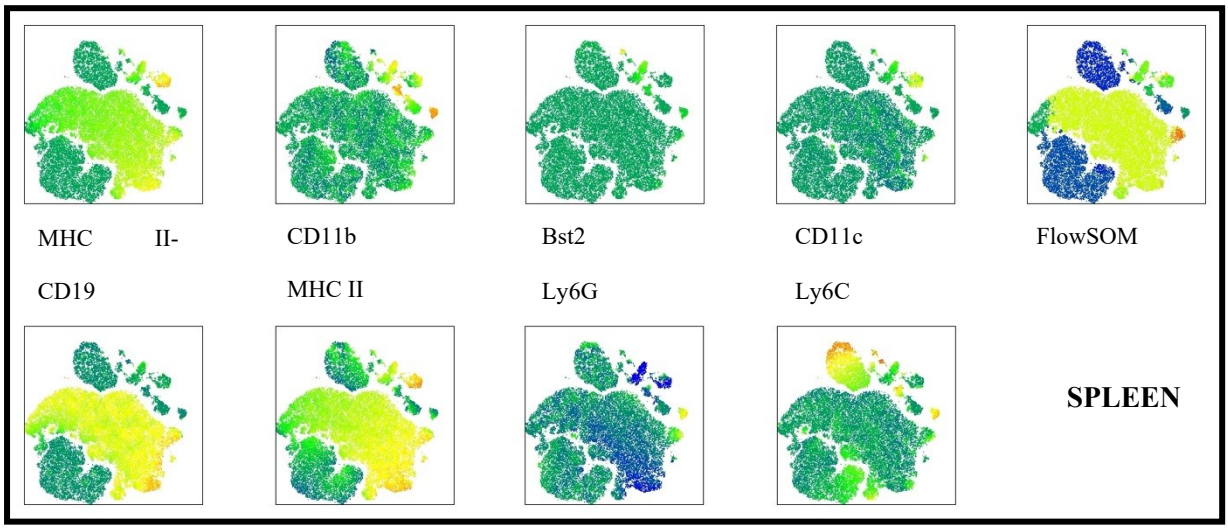

Figure 18: tSNE visualization of spleen - myeloid panel.

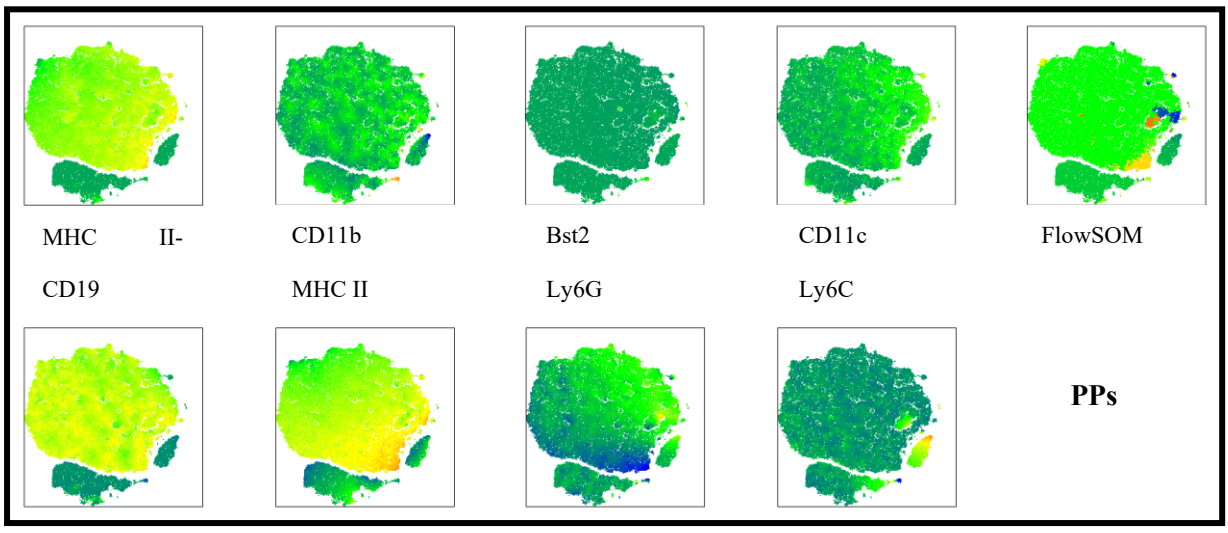

Figure 17: tSNE visualization of concatenated PPs from a single mouse - myeloid panel.

In the case of data containing (sub)complete diagonal of MHC II and CD19 markers, a manual check for each FlowSOM population and sample was performed. Some populations were therefore split

into B-cell and non-B-cell fraction for further analysis not to introduce bias into the data. Only uniform populations with combination of markers characteristic of a distinct well-known population were further analysed.

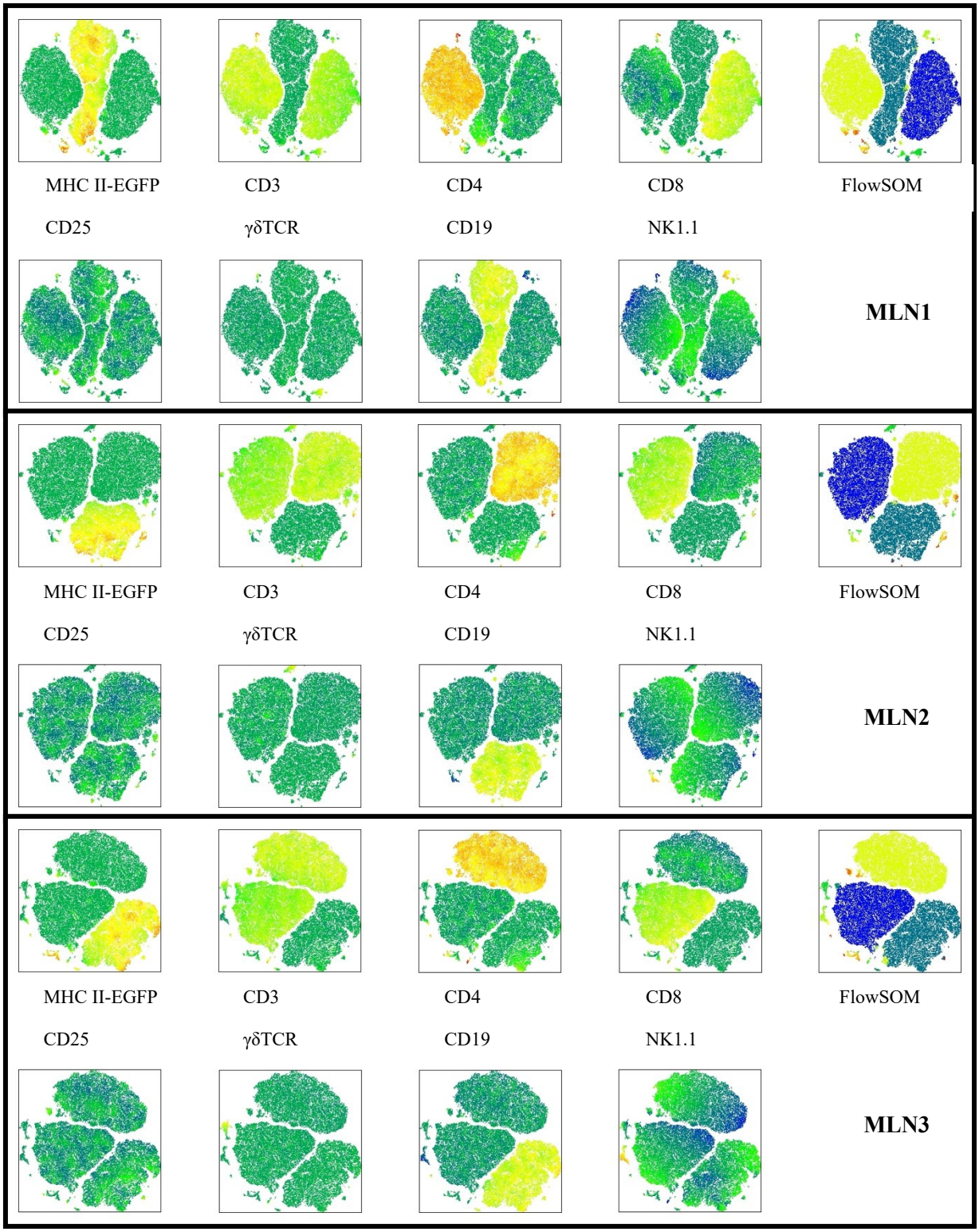

Figure 20: The first 3 out of 7 MLNs visualized by tSNE algorithm – lymphoid panel.

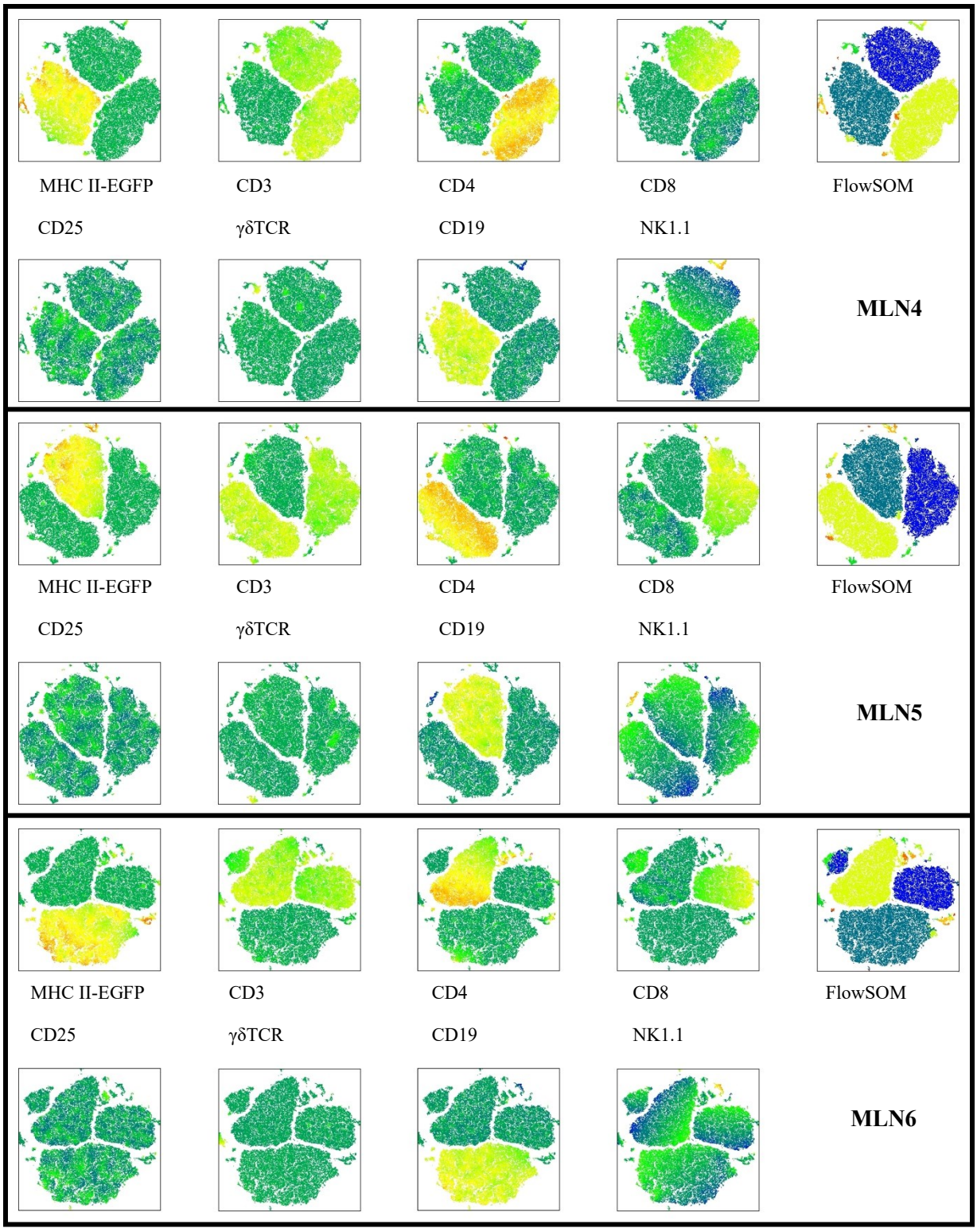

Figure 21: MLNs 4-6 visualized by tSNE –lymphoid panel.

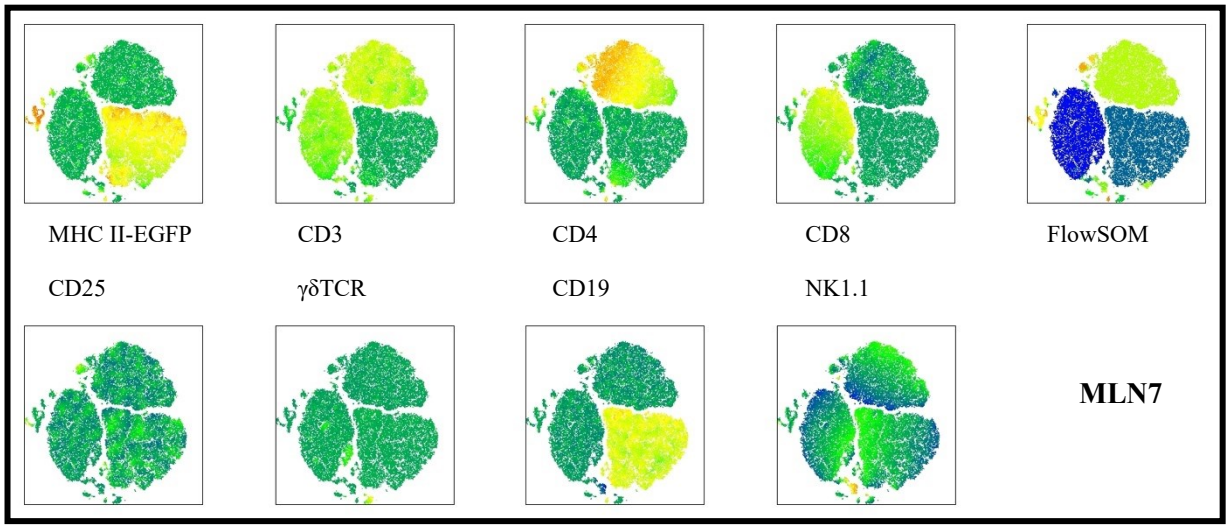

Figure 24: MLN 7 visualized by tSNE – lymphoid panel.

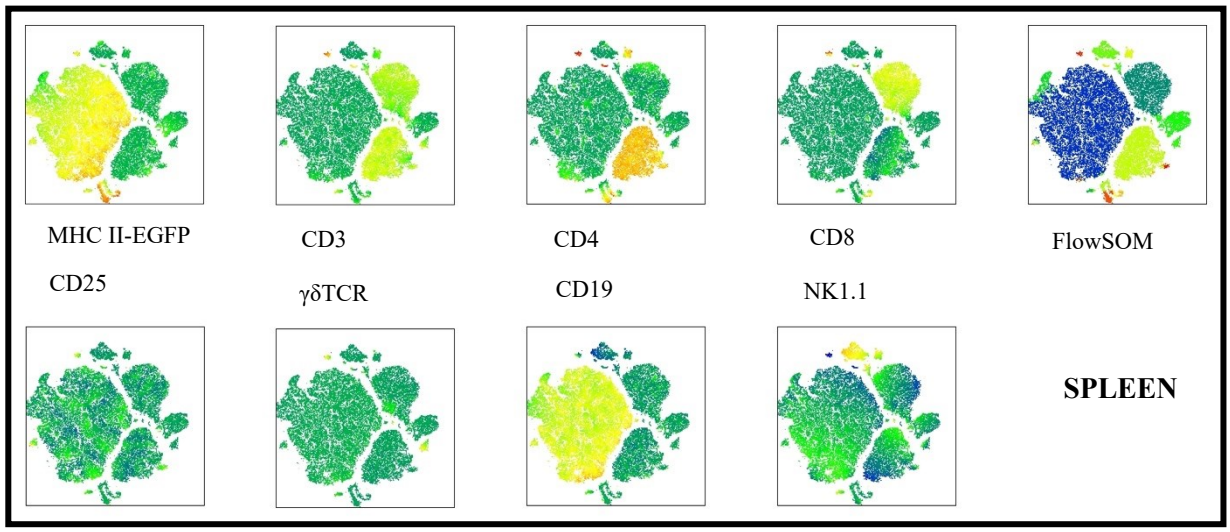

Figure 22: tSNE visualization of spleen - lymphoid panel.

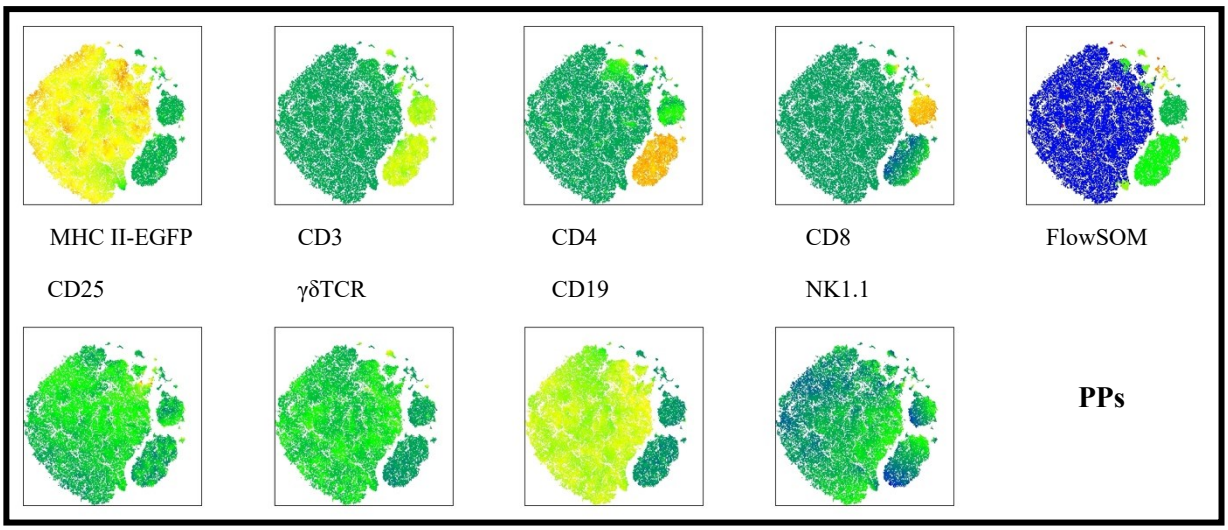

Figure 23: tSNE visualization of concatenated PPs from a single mouse - lymphoid panel.

5.3.4. C57BL/6 mouse vs. MHC II-EGFP *knock-in* mouse

Before the comparison between SPF and GF MHC II-EGFP *knock-in* mouse could be made, C57BL/6 (BL) mouse and MHC II-EGFP *knock-in* mouse (SPF) were compared to verify the previously reported lack of immunological phenotype. The percentages of populations determined by FlowSOM for spleen and pooled MLNs for each panel used are presented in figs.

In spleen, no significant difference between cell percentages was observed between C57BL/6 mice and MHC II-EGFP mice. However, for lymphoid panel, significant differences in "Breg cells" (***, extremely lower in the BL group) and "Treg cells" (**, enhanced in the BL group) were observed. cDC1 (CD3-CD8+) and cDC2 populations (CD3-CD4+) were also quantified in lymphoid panel (data not shown) with significant differences (** and ***, respectively). However, the observation was not supported by the data from myeloid panel, with more reliable cellular markers for cDCs, that served as a control (0,4% and 0,36% of CD45+ cells were cDC1 in BL and SPF mice, respectively, and 0,42% and 0,53% of cells were identified as cDC2s).

In MLNs, higher relative numbers of "memory T cells" were seen in BL mouse (*). This was not correlated by a significant difference in total T cell numbers. Considering lymphoid panel, Th percentages were significantly lower in the BL group (*). No other samples beared any significant difference.

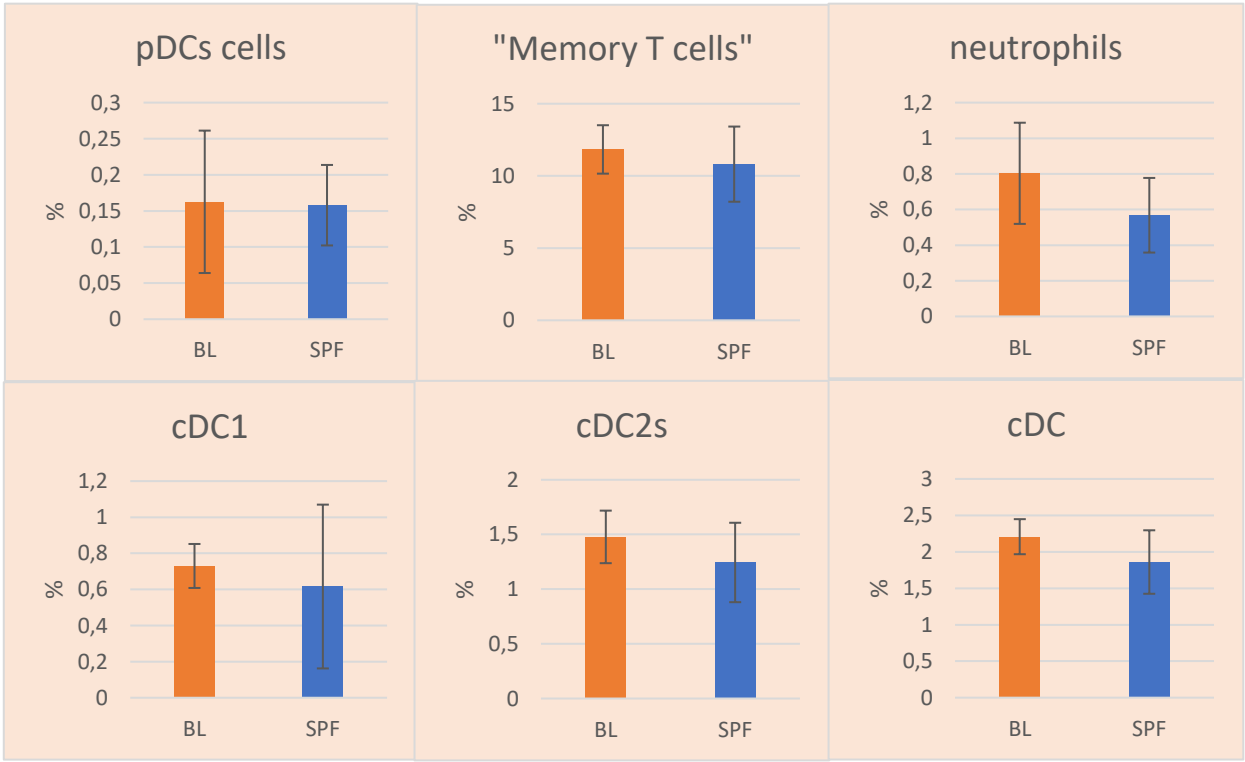

*Figure 25: Representative bar graph charts of comparison between C57BL/6 (BL) and MHC II-EGFP (SPF) - myeloid panel - spleen. Results represent mean ± SD of value. n(BL)=8 mice, n(SPF)=11 mice. *, significant differences with P ≤ 0.05. **, significant differences with P ≤ 0.01. ***, and significant differences with P ≤ 0.001*

The fact that some populations were significantly different between BL and SPF mouse is surprising, as C57BL/6 and MHC II-EGFP mouse model were previously demonstrated to be immunologically equivalent. A possible explanation for these findings is provided in the discussion section.

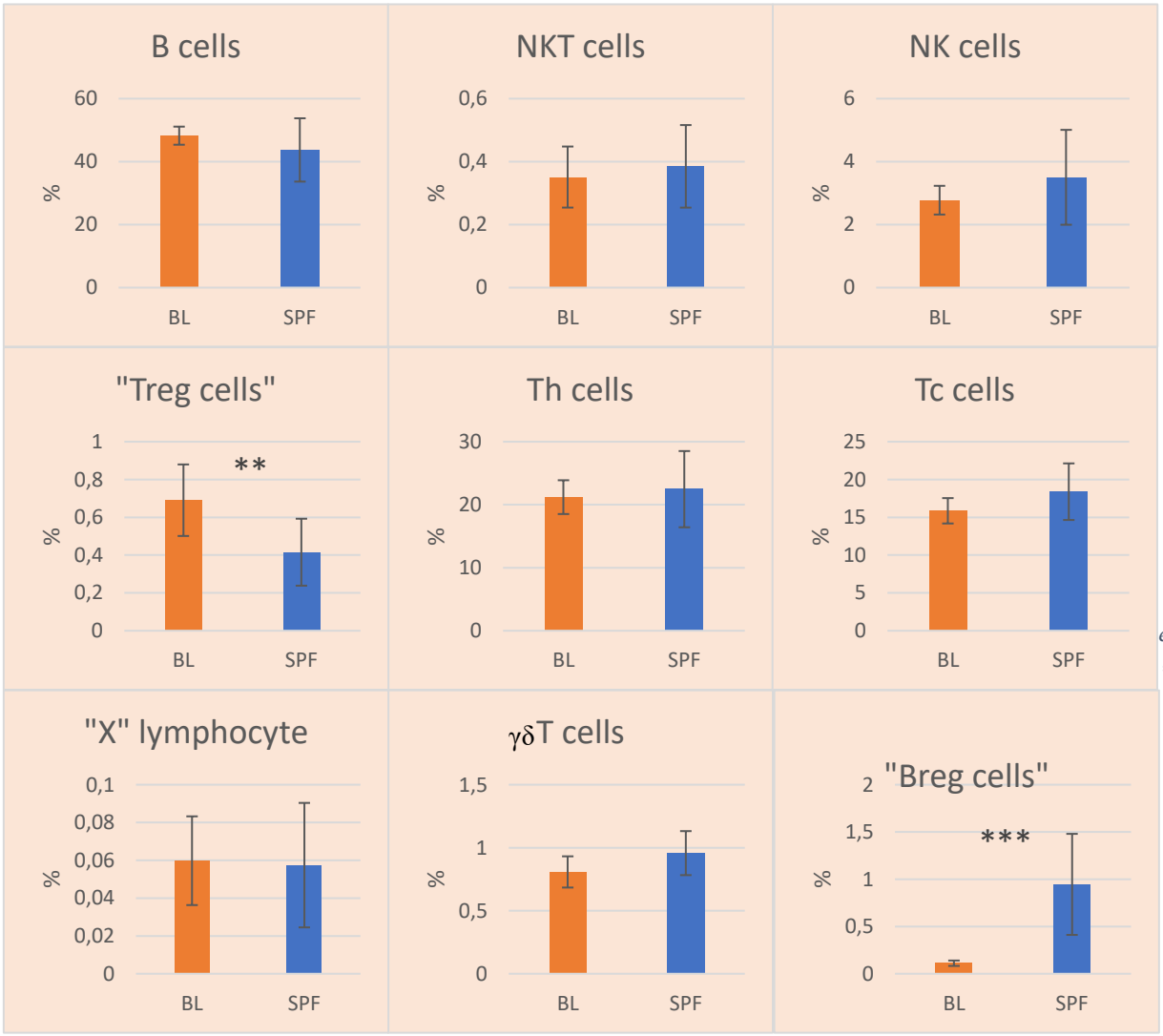

*Figure 27: Representative bar graph charts of comparison between C57BL/6 (BL) and MHC II-EGFP (SPF) - lymphoid panel - spleen. Results represent mean ± SD of value. n(BL)=8 mice, n(SPF)=11 mice. *, significant differences with P ≤ 0.05. **, significant differences with P ≤ 0.01. ***, and significant differences with P ≤ 0.001*

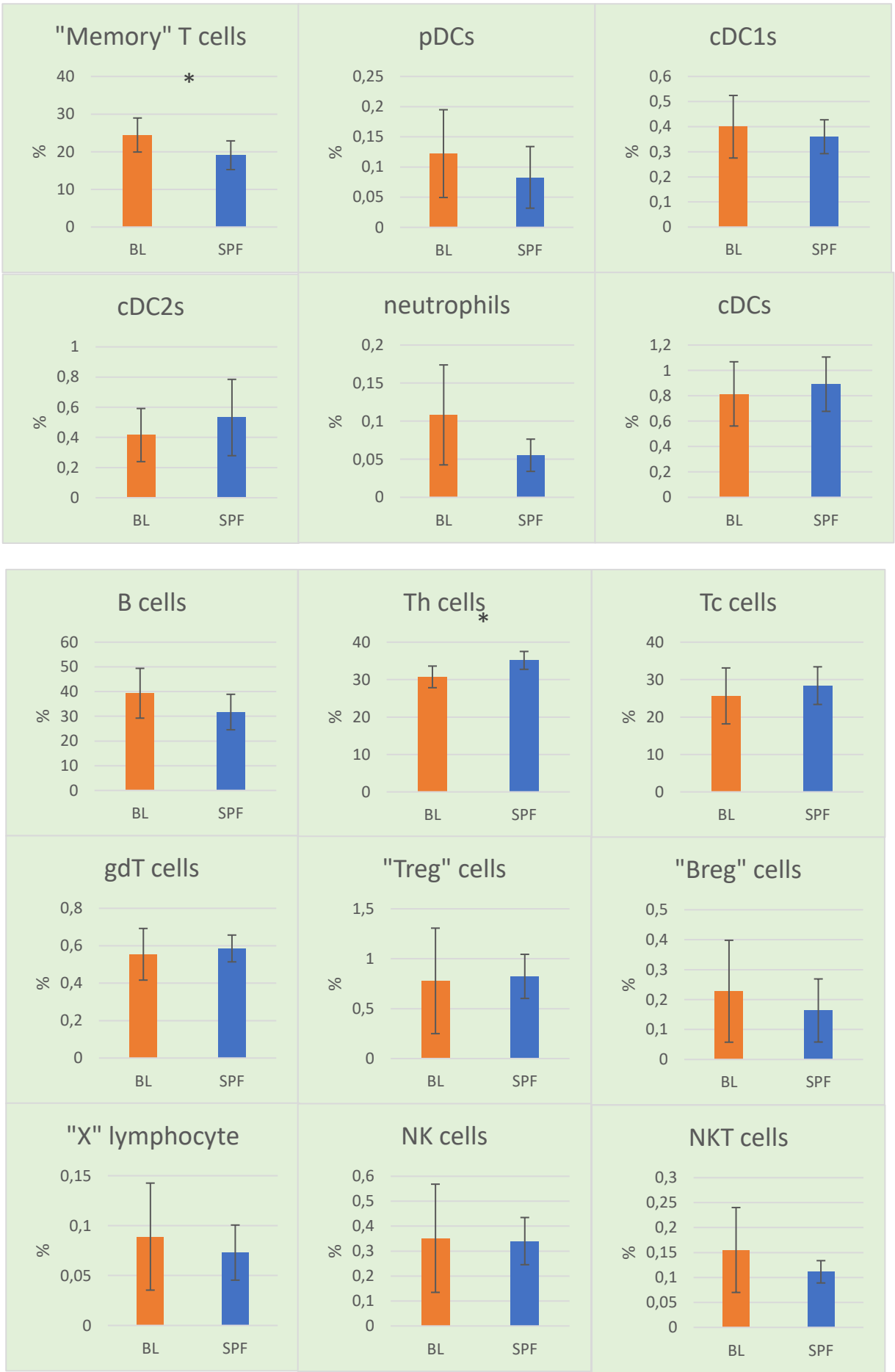
"Memory" T cells
*
40
30
20
10
0
%
BL
SPF
pDCs
0,25
0,2
0,15
0,1
0,05
0
cDC1s
0,6
0,5
0,4
0,3
0,2
0,1
cDC2s
1
0,8
0,6
0,4
0,2
neutrophils
cDCs
1,2
B cells
60
50
Th cells
Tc cells
gdT cells
"Treg" cells
1,5
"Breg" cells
"X" lymphocyte
NK cells
NKT cells

*Figure 28: Representative bar graph charts of comparison between C57BL/6 (BL) and MHC II-EGFP (SPF) - myeloid panel (top), lymphoid panel (bottom) - MLNs. Results represent mean ± SD of value. n(BL)myeloid=8 mice, n(BL)lymphoid=4 mice n(SPF)=11 mice. *, significant differences with P ≤ 0.05. **, significant differences with P ≤ 0.01. ***, and significant differences with P ≤ 0.001*

5.3.5. SPF vs GF MHC II-EGFP *knock-in* mouse

To determine what populations are relatively enriched or reduced in GF mouse compared to SPF model in myeloid panel, the absolute numbers and relative frequencies of cells across populations were determined for each organ type and panel by firstly concatenating the downsampled samples together (samples from a single organ type and panel) to get all the possible populations of cells. The FlowSOM algorithm was run as described in a previous section and the resulting populations were annotated. However, despite all the measures, not all populations of known immune cells were always separated. For spleen, the number of neutrophils could be determined, while for other organs, the neutrophil ratio could not always be determined because neutrophils were present in very low abundance and did not form a discrete population and were therefore omitted from the analysis. For PPs, the cDC populations were not split into cDC1 and cDC2, so only overall percentages could be presented. NKT cell population was also not separated by FlowSOM algorithm in PPs. All populations were determined as stated in the previous chapters.

For MLNs, the first, second to last ("MLN_SI_last" in graphs) and the last (coecal) MLNs were compared statistically for simplification (and the fact that the MLN numbers varied across different samples). For PPs it was the first and last PP in the small intestine (PP1 and PP_SI_last), coecal and colonic patch (figs). In addition, all MLNs and all PPs from the small intestine were plotted in a single graph to visualize differences between patches and a potential MLN/intestinal gradient of cells (figs). Especially for smaller populations, random fluctuations were sometimes observed in a single sample.

In spleen, no significant differences could be observed in myeloid panel for any of the populations (fig). However, the data from the lymphoid panel suggest that B cells are presented in a significantly higher percentage in spleens of GF mice (**, 43,71% in SPF mice vs. 58,98% in GF mice), and, on the contrary, Tc and Th cell percentages are both slightly diminished in GF animals (*, 18,39% of Tc cells in SPF vs. 13,63% in GF animals; and 22,46% in SPF vs. 16,72% in GF mice for Th cells). As B, Th and Tc cells make up the majority of cells in spleen, the difference could be either caused by an increased abundance of B cells, decreased abundance of T cells, or a combination of both, depending on the absolute numbers. Perhaps the most interesting finding is the huge drop in the relative abundance of γδT cells in GF mice (***, 0,96% vs 0,50%).

In MLNs, memory T cells were significantly diminished in GF mice (**), nevertheless, the individual differences among corresponding lymph nodes were not significant. The same holds true for cDC1 and cDC2 cells (*). However, the most significant difference from myeloid cells regards pDCs – while the overal numbers reflect a clear drop in relative abundancies between SPF and GF mice (***),

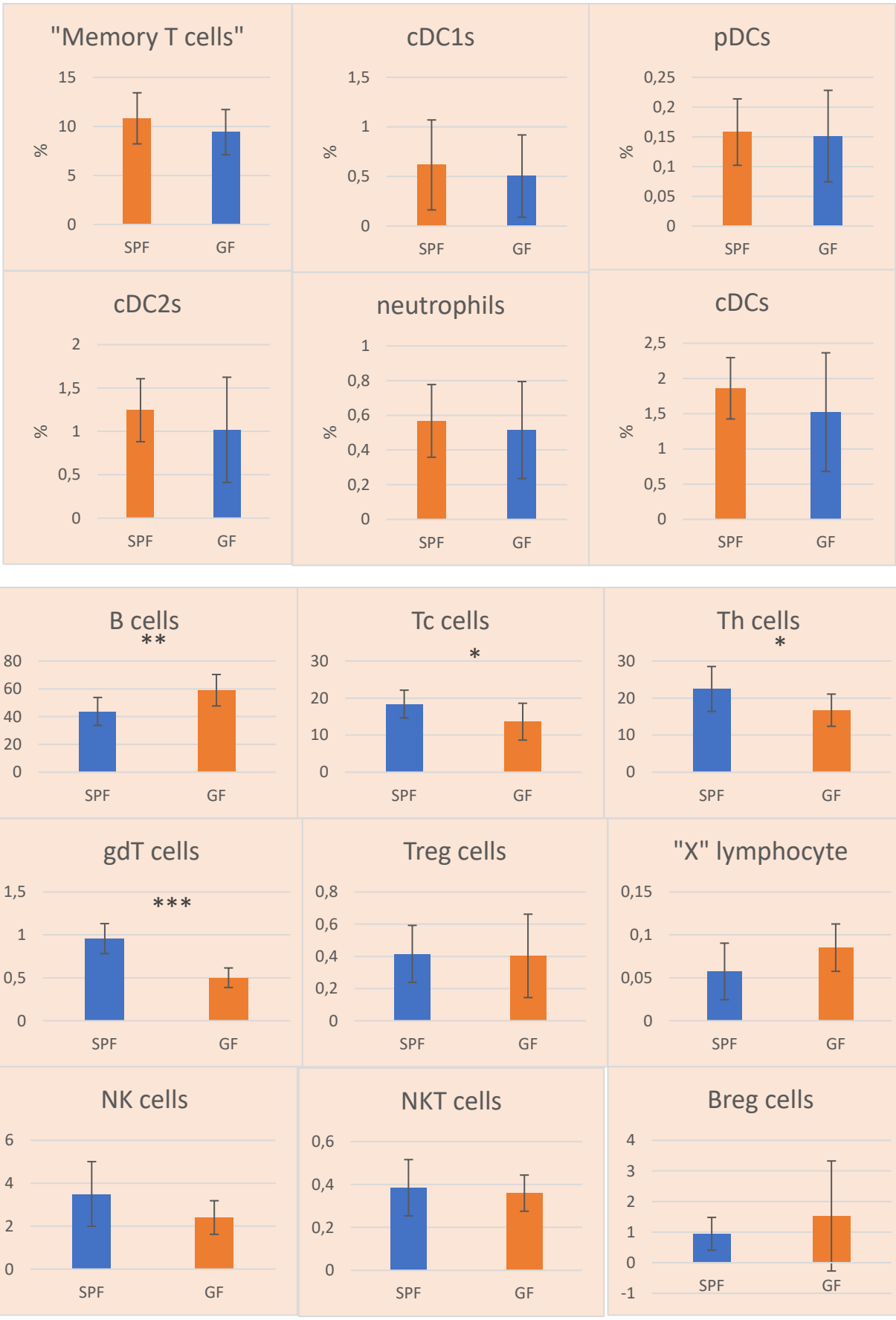

a side-by-side comparison of relative abundancies in colonic lymph node alone is also significant (***, 0,16% vs. 0,04%). Regarding lymphoid cell populations, B cells are again significantly enriched in GF

*Figure 29: Representative bar graph charts of comparison between SPF MHC II-EGFP and GF MHC II-EGFP mouse - myeloid panel (top), lymphoid panel (bottom) - spleen. Results represent mean ± SD of value. n(SPF)myeloid=5 mice, n(SPF)lymphoid=11 mice n(GF)myeloid=5 mice n(GF)lymphoid=8 mice. *, significant differences with P ≤ 0.05. **, significant differences with P ≤ 0.01. ***, and significant differences with P ≤ 0.001*

mouse compared to the SPF mouse (***), and the first (*, 29,10% SPF vs. 43,87% GF) and last small intestinal lymph nodes (**, 30,87 SPF vs. 47,45% GF) both differ on an individual level as well. Tc and Th lymphocytes are relatively diminished in GF mouse in the whole MLN complex (***), and the last MLN draining small intestine is significantly affected as an individual (*, 29,04% SPF vs. 21,19% GF for Tc cells and 34,32% SPF vs. 26,32% GF for Th cells). Analogously to spleen, γδ T cells are also extremely reduced in MLNs (***) and both first and last small intestine-draining lymph nodes reflect this relationship (***, MLN1: 0,79% SPF vs. 0,46% GF, MLN_SI_last: 0,71% SPF vs. 0,44% GF). There is also a clear decreasing gradient between MLN1 and MLN_SI_last in SPF mouse (*), which becomes even clearer when MLN1 and coecal MLN are compared in SPF mouse (***). While neither NK nor NKT cells display a significant difference between SPF and GF animals in any category or as a whole, there is a general difference between individual MLNs (* and ** for NK and NKT cells, respectively) – the relationship is significantly different between MLN1 and MLNlast (colonic) (NK cells) or between the last small intestinal LN and coecal LN (NKT cells, the relationship is significant as a whole and in GF animals). In GF mice, a significant enrichment of coecal lymph node is also observed.

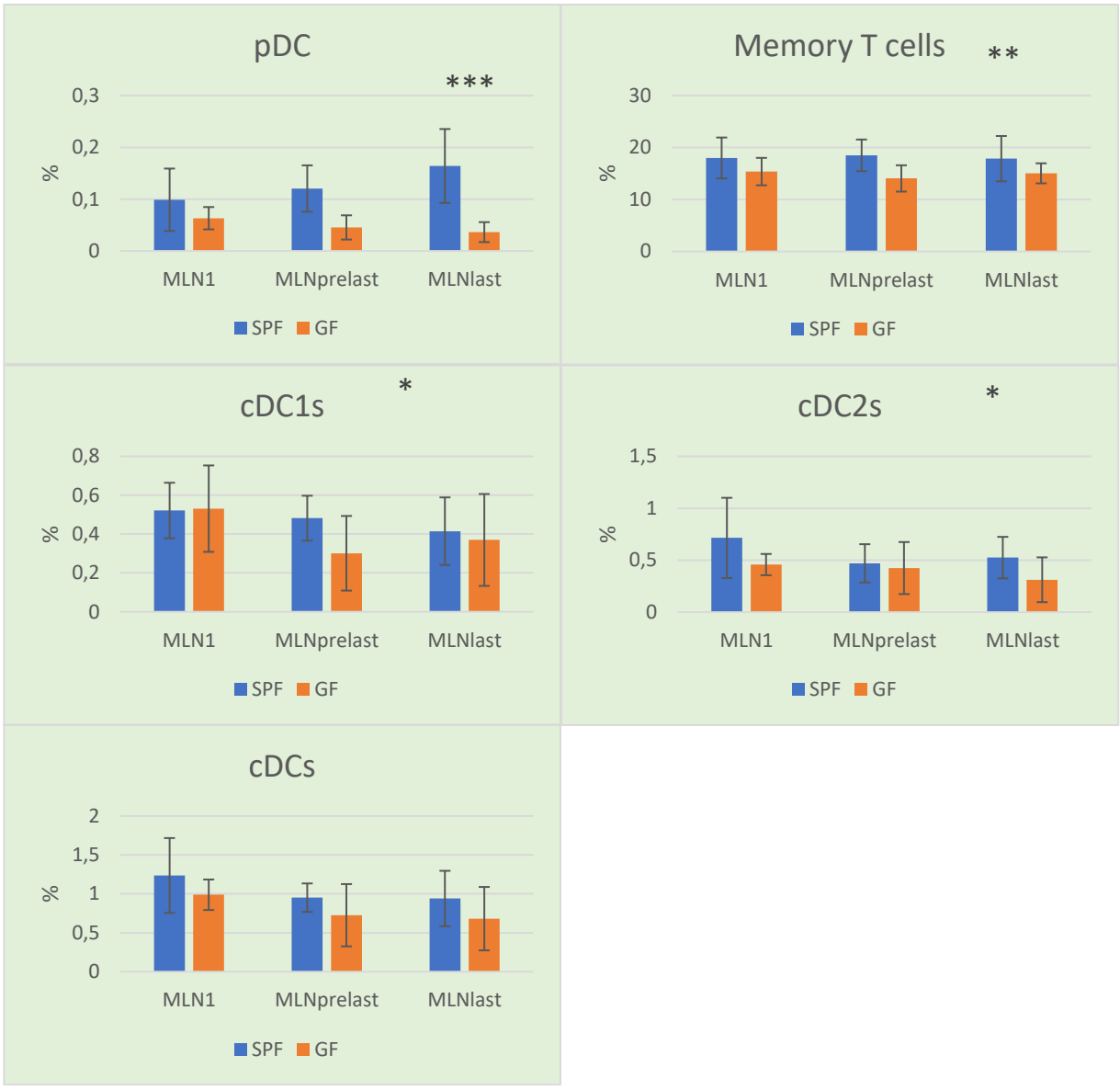

*Figure 30: Representative bar graph charts of comparison between between SPF MHC II-EGFP and GF MHC II-EGFP mouse - myeloid panel - MLNs. Results represent mean ± SD of value. n(SPF)=6 mice, n(GF)=8 mice. *, significant differences with $P \leq 0.05$. **, significant differences with $P \leq 0.01$. ***, and significant differences with $P \leq 0.001$*

In PPs, no significant difference in myeloid cells between SPF and GF mouse could be demonstrated. However, several immune cells reflect the gradient in the intestines. As a whole, the last small intestinal PP has a significantly lower relative abundance of "memory T cells" compared to coecal (***) and colonic (**) patches, while the same applies to the relationship between PP1 and coecal patch

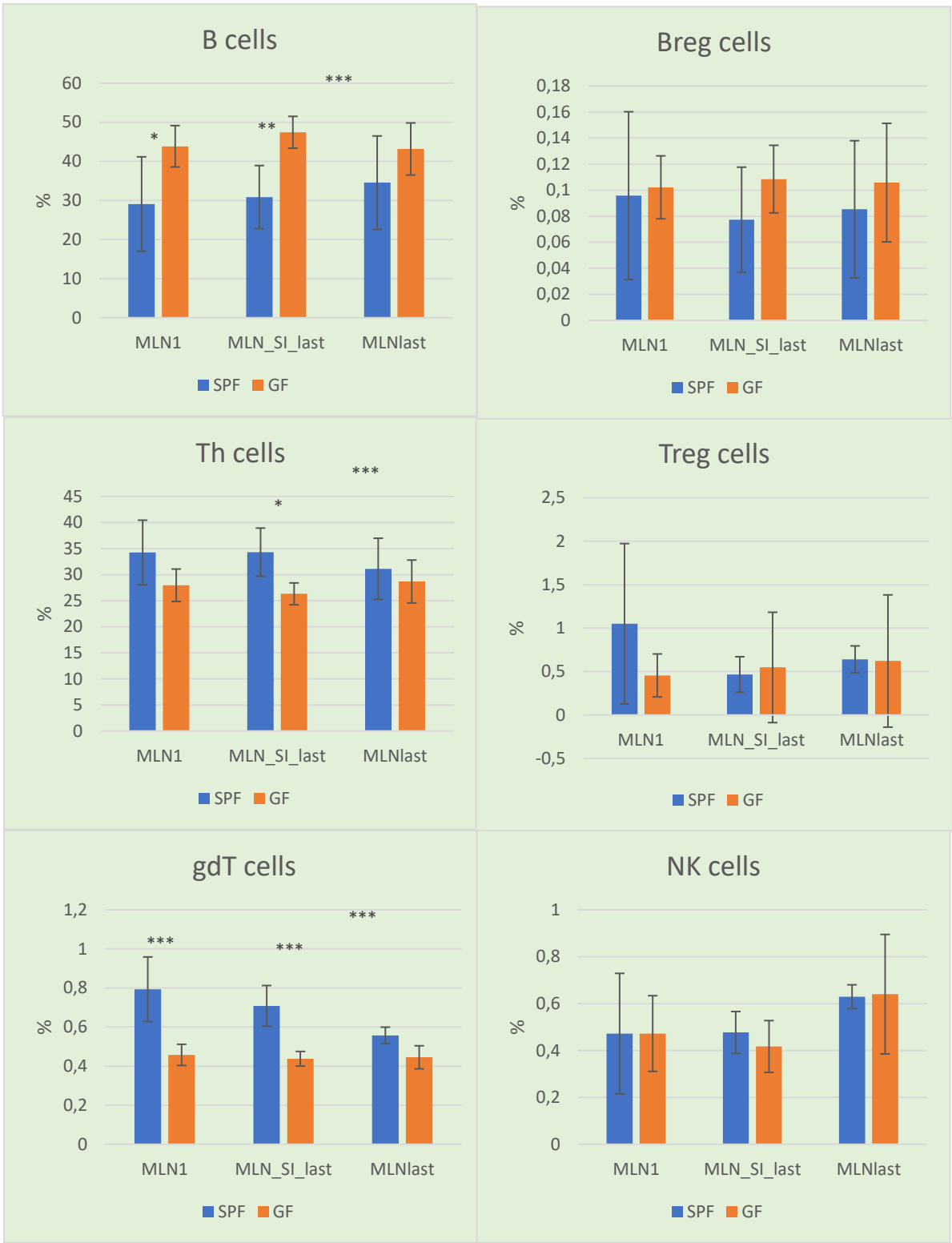

*Figure 31: Representative bar graph charts of comparison between between SPF MHC II-EGFP and GF MHC II-EGFP mouse – lymphoid panel - MLNs. Results represent mean ± SD of value. n(SPF)=6 mice, n(GF)=8 mice. *, significant differences with P ≤ 0.05. **, significant differences with P ≤ 0.01. ***, and significant differences with P ≤ 0.001*

(*). GF mice also demonstrate these relationships significantly (* PP1 (2,61%) : colonic patch (5,00%), * PP_SI_last (1,89%) : coecal patch (4,5%), ** SI_last : colonic patch). B lymphocytes are also differentially (relatively) distributed along the course of GALT (**) in GF mice: the relative

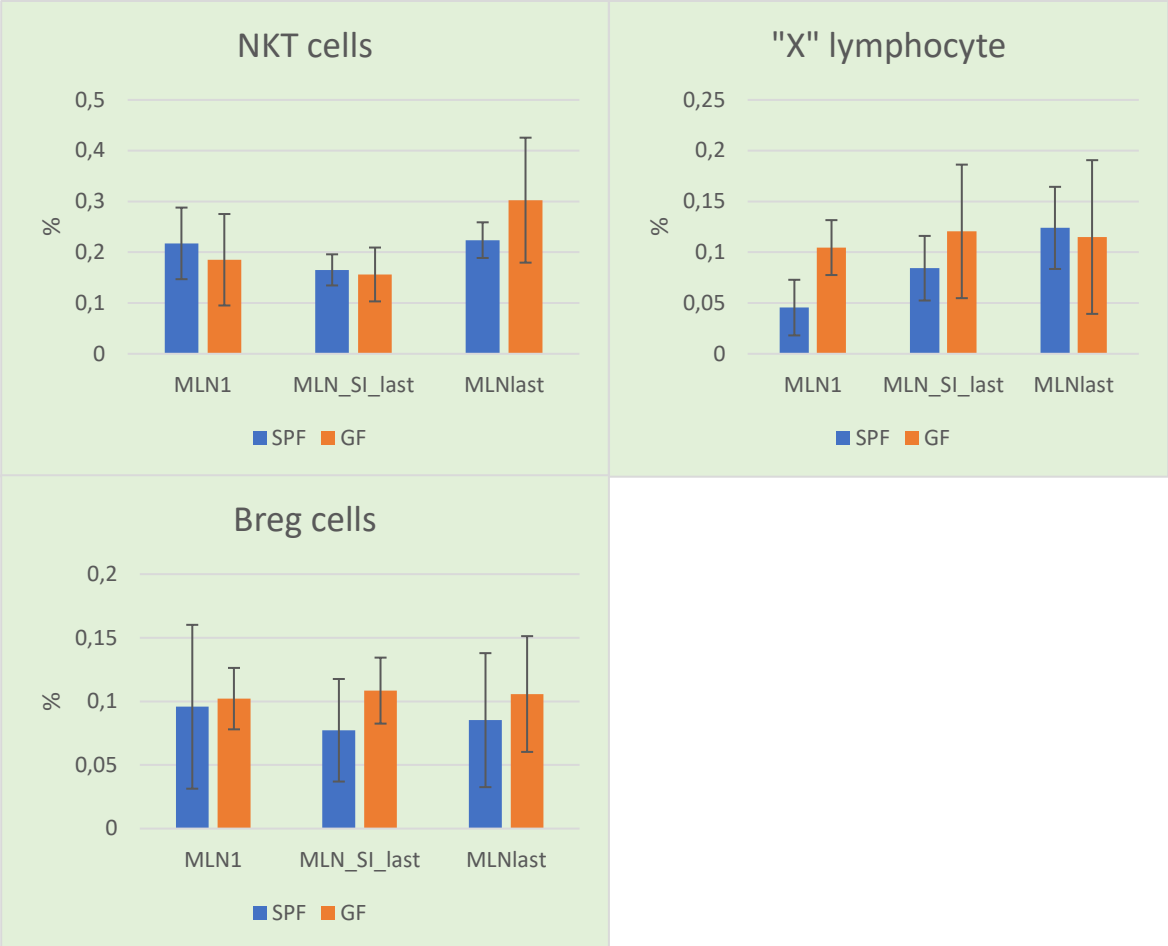

*Figure 33: Representative bar graph charts of comparison between between SPF MHC II-EGFP and GF MHC II-EGFP mouse – lymphoid panel - MLNs. Results represent mean ± SD of value. n(SPF)=6 mice, n(GF)=8 mice. *, significant differences with P ≤ 0.05. **, significant differences with P ≤ 0.01. ***, and significant differences with P ≤ 0.001*

abundance of B lymphocytes in PP_SI_last (86,37%) is significantly higher compared to both coecal (**, 65,64%) and colonic (*, 69,12%). “Bregs” weren’t demonstrated to have a differential distribution along the gut, however, they are significantly higher in abundance in SPF mice in general (*). CD8- γδT cells combine both the significant relationship between SFP and GF mouse in coecum (*, 0,37% SPF vs. 0,82% GF), but there is also a significant increase in abundance between PP_SI_last (0,26%) compared to coecal patch (*). CD8+ γδT lymphocytes, a subset detected exclusively in PPs, is significantly more abundant in the beginning of the small intestine compared to all other studied organs, both for GF (*** within all relationships, PP1: 0,77%, PP_SI_last 0,15%, coecal patch 0,06% and colonic patch 0,02%), and SPF mouse (PP1: 1,23%, PP_SI_last 0,07 *, coecal patch 0,03% **, colonic patch 0,01% **). When both types of γδT cells are summed, the relationship is significant between different organs (* PP1 : Coecum, ** PP1 : Colon, ** PP1 : PP_SI_last). However, concrete mouse housing setting (SPF/GF) is not responsible for this relationship. The abundance of Th also does not seem to be affected by the microbial status of the mouse significantly. Nonetheless, in GF mouse, PP_SI_last (5,70%) seems to have a significantly lower percentage of Th cells compared to colonic PP (*, 12,13%). Last but not least, NK cells offer interesting results. The SPF and GF mice differ

dramatically (***), the difference being mainly the aboral parts of the GALT system – coecal (**, 0,18% SPF vs. 0,85% GF) and colonic (**, 0,1% SPF vs. 0,72% GF) patches show greater relative abundance in GF mice. Both PP1 (0,23% in GF mice) and PP_SI_last (0,21%) differ significantly from both coecal (***) as well as colonic (* and **, respectively) patches.

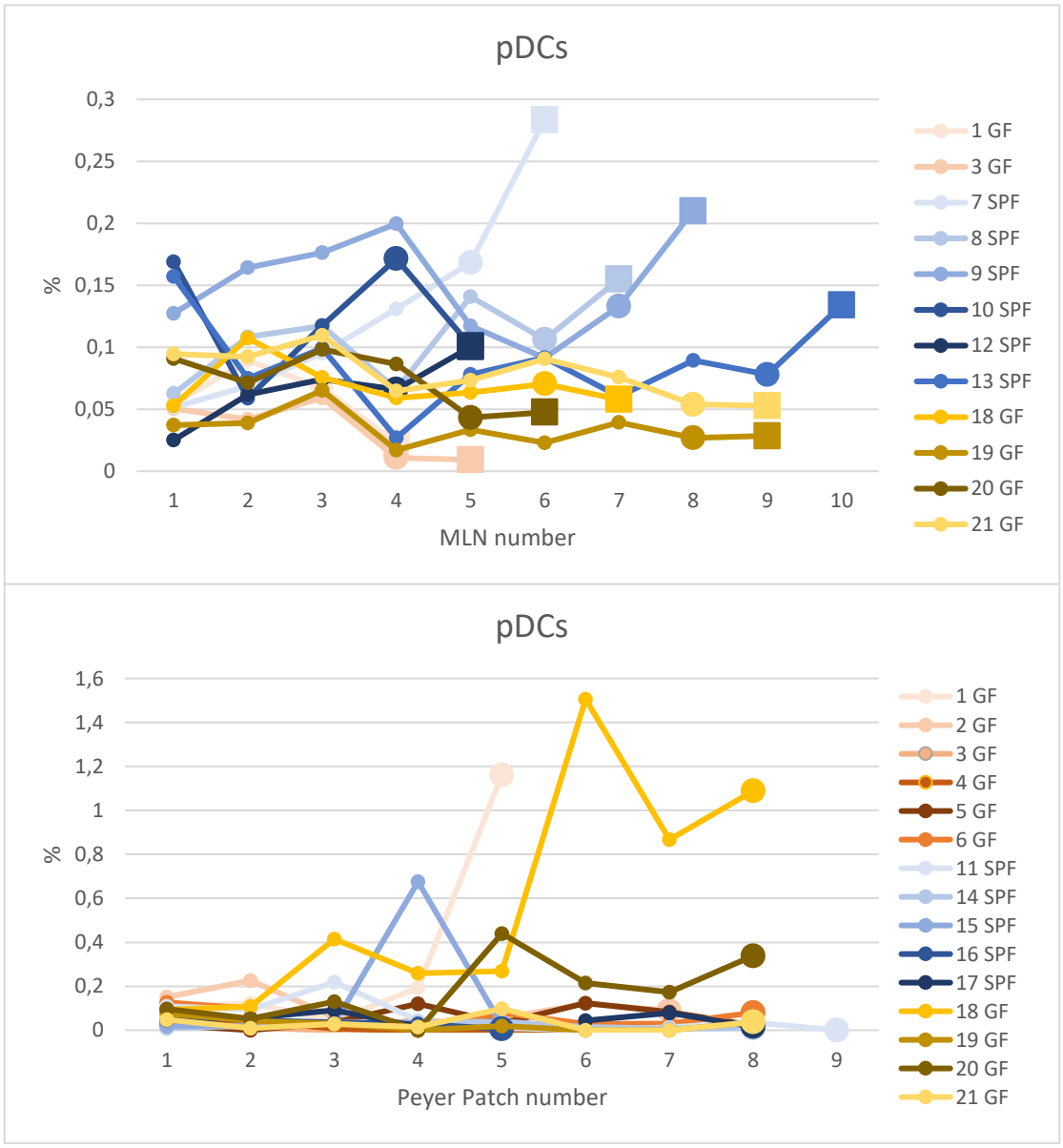

Figure 34: Demonstration line charts of pDC relative abundancies in MLNs and small intestinal PPs of MHC II-EGFP SPF and GF mice.. MLNs: n(SPF)=6 mice, n(GF)=6 mice. PPs: n(SPF)=5 mice, n(GF)=10 mice.

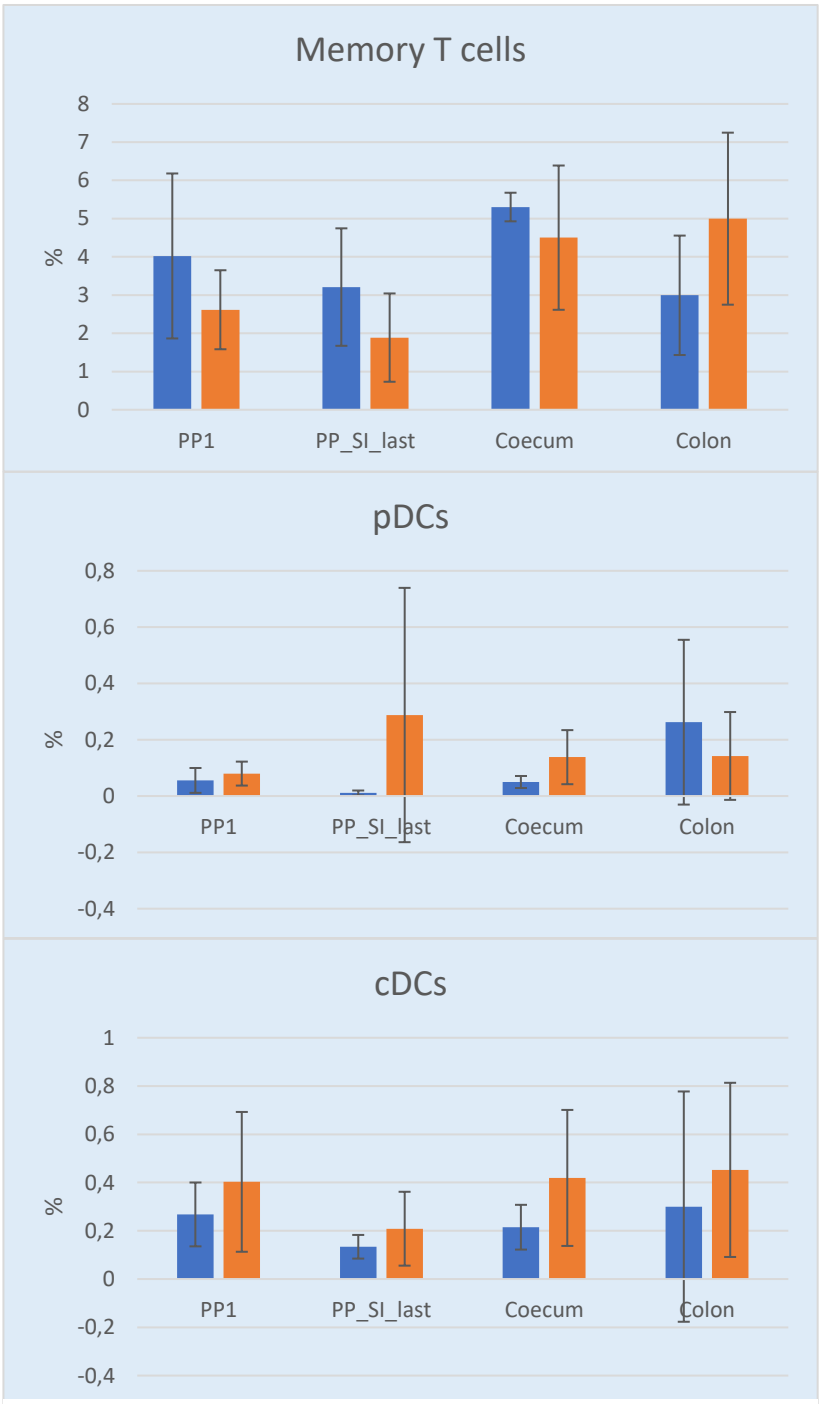

*Figure 35: Representative bar graph charts of comparison between between SPF MHC II-EGFP and GF MHC II-EGFP mouse - myeloid panel - PPs.. Results represent mean ± SD of value. n(SPF)=5 mice, n(GF)=8 mice. *, significant differences with P ≤ 0.05. **, significant differences with P ≤ 0.01. ***, and significant differences with P ≤ 0.001*

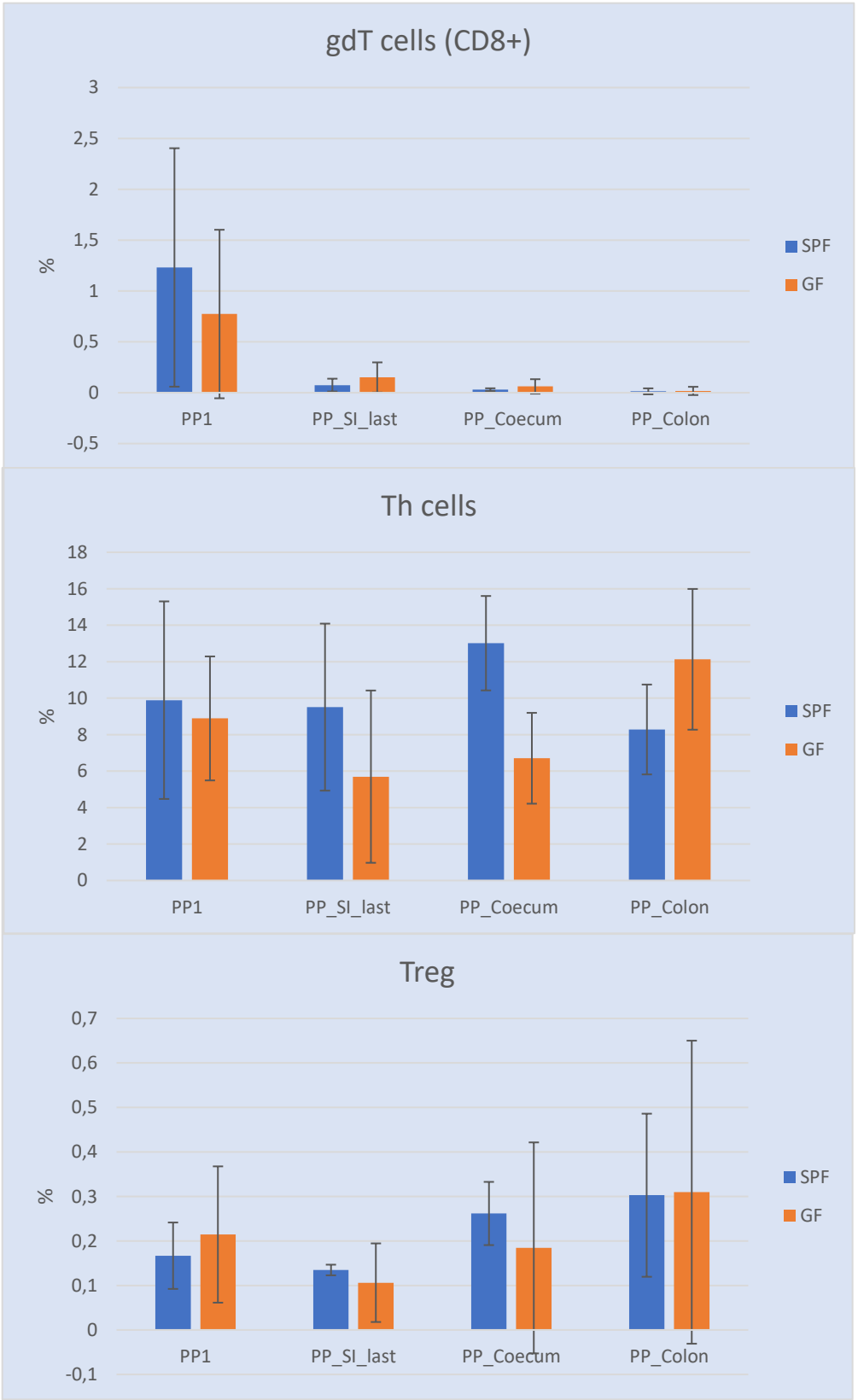

*Figure 36: Representative bar graph charts of comparison between between SPF MHC II-EGFP and GF MHC II-EGFP mouse – lymphoid panel - PPs.. Results represent mean ± SD of value. n(SPF)=5 mice, n(GF)=8 mice. *, significant differences with $P \leq 0.05$. **, significant differences with $P \leq 0.01$. ***, and significant differences with $P \leq 0.001$*

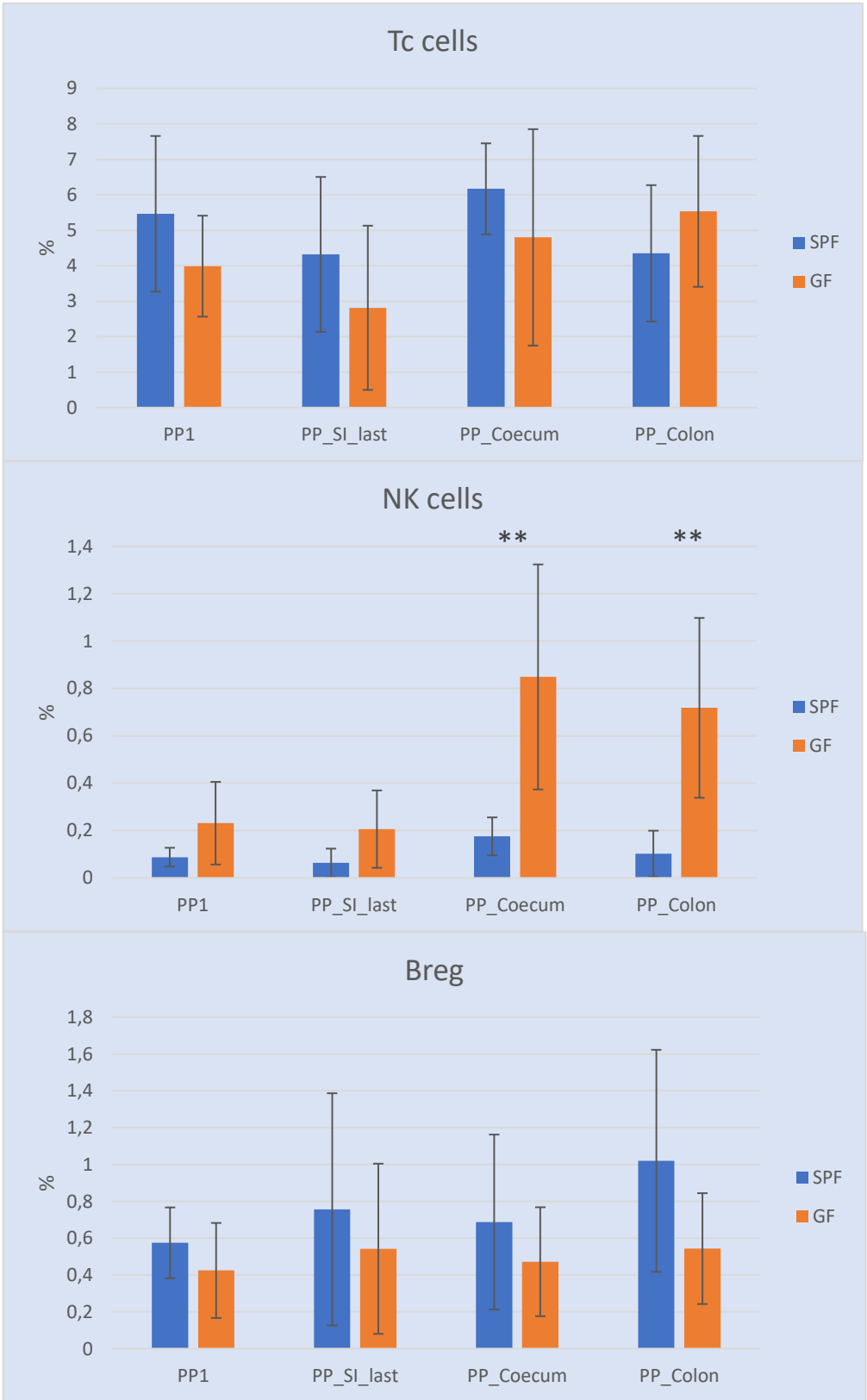

*Figure 37: Representative bar graph charts of comparison between between SPF MHC II-EGFP and GF MHC II-EGFP mouse – lymphoid panel - PPs.. Results represent mean ± SD of value. n(SPF)=5 mice, n(GF)=8 mice. *, significant differences with P ≤ 0.05. **, significant differences with P ≤ 0.01. ***, and significant differences with P ≤ 0.001*

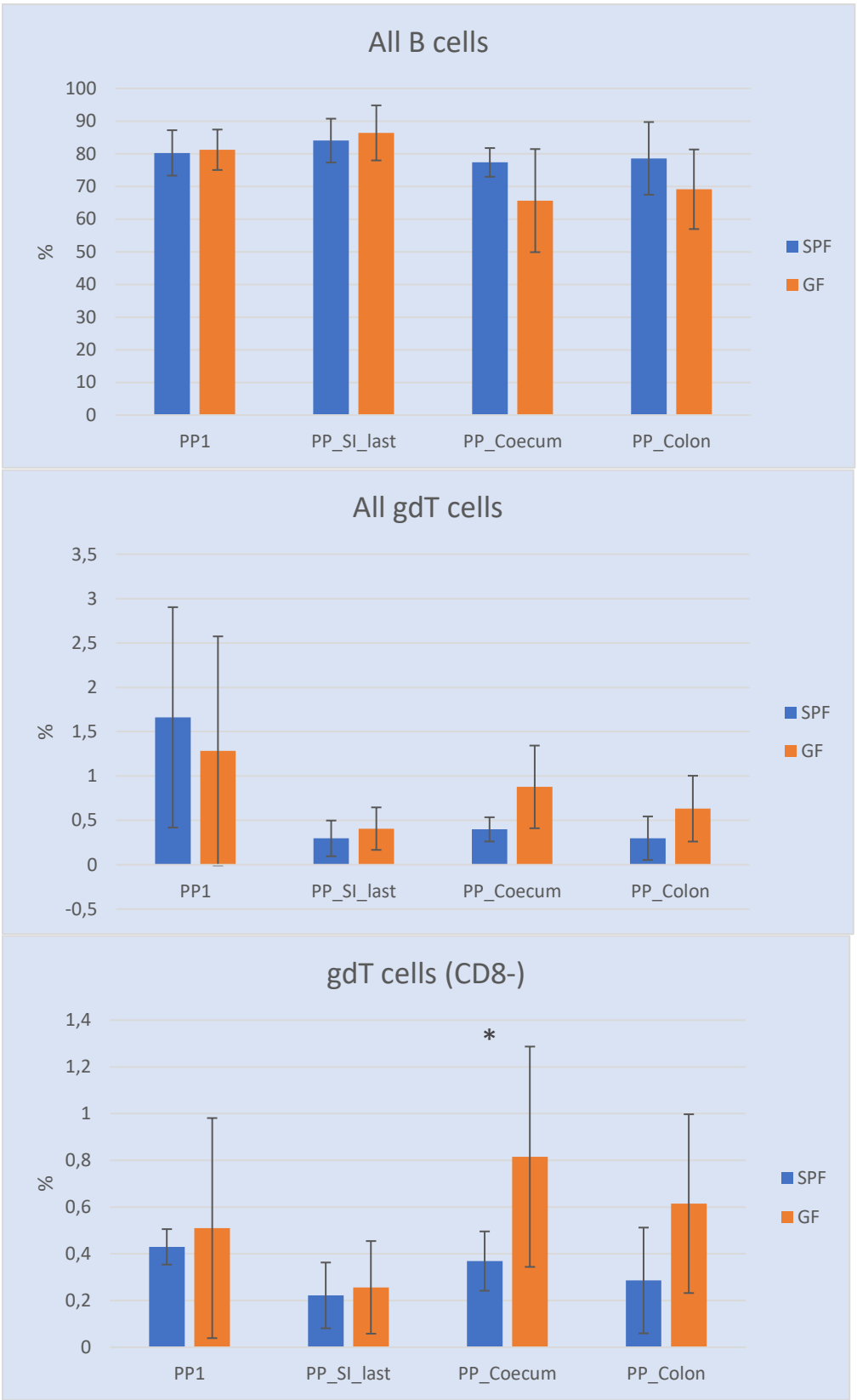

*Figure 38: Representative bar graph charts of comparison between between SPF MHC II-EGFP and GF MHC II-EGFP mouse – lymphoid panel - PPs.. Results represent mean ± SD of value. n(SPF)=5 mice, n(GF)=8 mice. *, significant differences with P ≤ 0.05. **, significant differences with P ≤ 0.01. ***, and significant differences with P ≤ 0.001*

5.3.6. SPF vs. GF – absolute numbers

Last but not least, absolute numbers of cells in different organs in SPF vs. GF mice were determined. These were calculated from the total number of CD45-positive (or TER-119-negative in lymphoid panel) cells. In the case of separated MLNs and PPs, where all the cells were used this number was determined as number of events * 200 / 160 * 2 (half of cells were stained by each panel and 160 out of 200 µl were used for measurements in FACS). For spleen, the total number was determined as number of events * 200 / 160 * 200 (as 100 µl were used per sample from the 20 ml the whole spleen was diluted in after digestion). The data for lymph nodes and small intestinal PPs were pooled and averaged as each mouse could have a different number of MLNs and PPs, but the overal number of cells, especially for MLNs, does not have to change. No significant differences in the total number of cells was found for MLNs and spleen (data not shown), however, in the case of PPs, the average number of cells per small intestinal PP as well as for the coecal patch was significantly lower in GF animals (* and **, respectively, concordantly with the observations from stereomicroscope). Subsequently, absolute numbers of cells were tested for significance, as denoted in graphs (fig).

From absolute numbers, the “memory T cell” counts were found to be significantly lower in GF animals(***), especially in PPs from the small intestine (***, 2285 in SPF mouse cells vs. 769 cells in GF mouse per 1 PP) and coecal patch (***, 9629 cells in SPF mouse vs. 1557 cells in GF). Absolute B cell counts reflected the drastic difference between the number of cells in SFP and GF mice in coecal patch (**, 109925 vs. 22758 cells in SPF and GF mice, respectively. “Breg” and “Treg” cells were also significantly lower in GF mice (** and ***, respectively; “Breg”: 818 SPF vs. 134 cells in GF mouse and “Treg”: 398 vs. 47 cells per coecal patch in SPF and GF mice, respectively). Last but not least, Tc cells and Th cells had both significantly lower cell counts in coecal patch (***, 8478 SPF vs. 1426 GF cells for Tc cells and 17502 SPF and 2467 GF Th cells) as well as in small intestinal PPs (** and * for Tc and Th cells, respectively, 2294 SPF vs. 991 GF Tc cells and 4876 SPF vs. 2185 Th cells). Other differences proved insignificant. However, exactly these “insignificancies” could mean shifts in the composition of immune microenvironment, as the total numer of cells is significantly different. That is the reason, while absolute numbers offer the proportional representation of cellular numbers, the relative abundance could affect the actuall immunological processes more in a given spot.

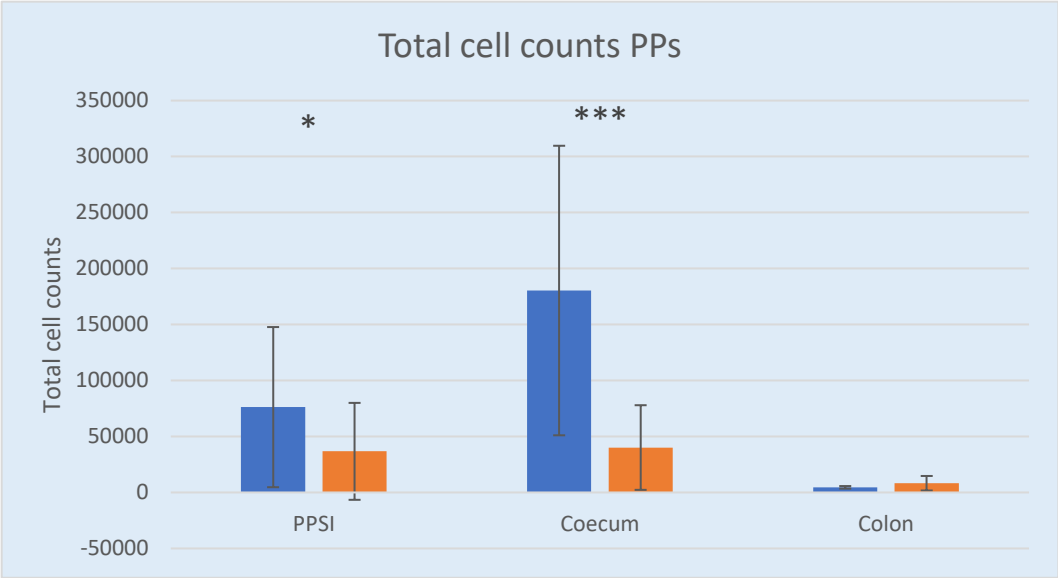

*Figure 39: Representative bar graph charts of comparison between between absolute numbers in SPF MHC II-EGFP and GF MHC II-EGFP mouse - PPs.. Results represent mean ± SD of value. n(SPF)=5 mice, n(GF)=8 mice. *, significant differences with P ≤ 0.05. **, significant differences with P ≤ 0.01. ***, and significant differences with P ≤ 0.001*

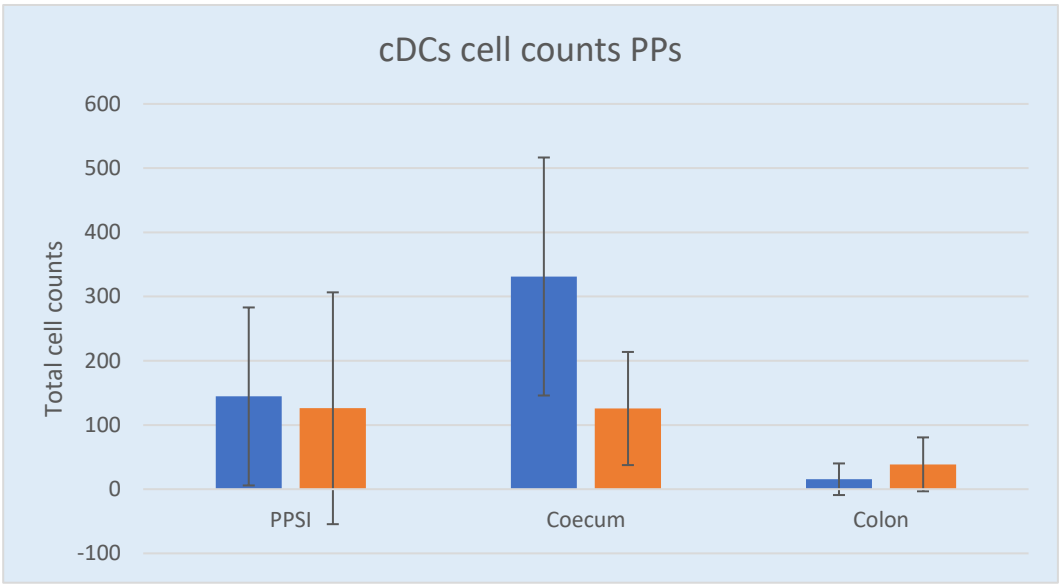
cDCs cell counts PPs
Total cell counts
600
500
400
300
200
100
0
-100
PPSI
Coecum
Colon

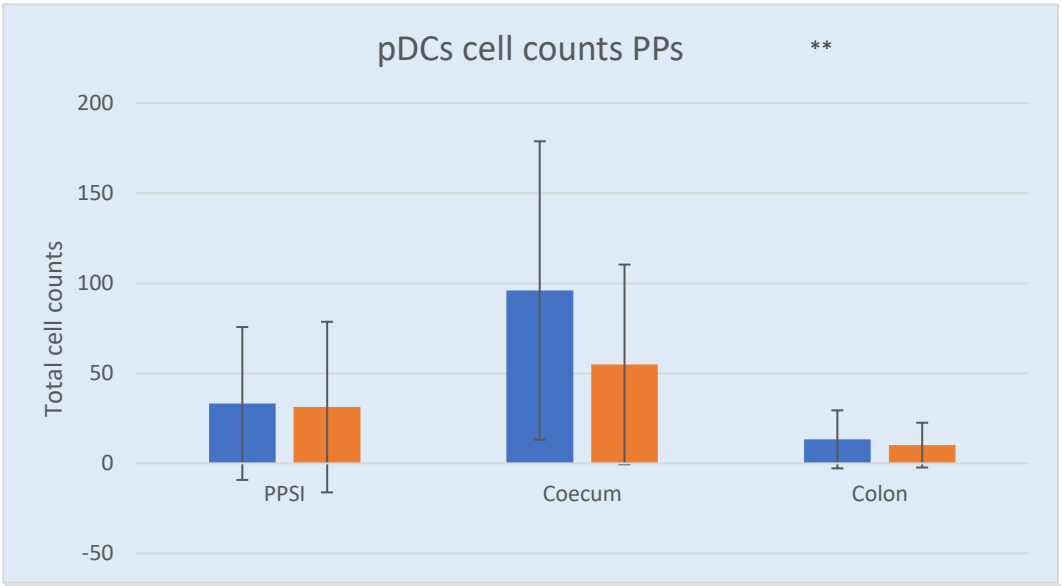
pDCs cell counts PPs
**
Total cell counts
200
150
100
50
0
-50
PPSI
Coecum
Colon

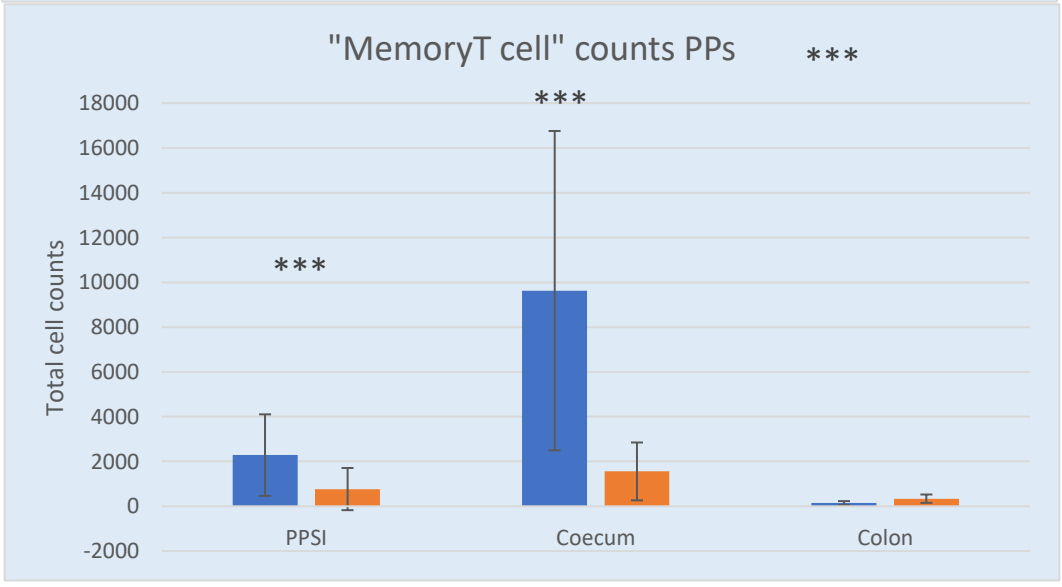
"MemoryT cell" counts PPs
***
***
***
Total cell counts
18000
16000
14000
12000
10000
8000
6000
4000
2000
0
-2000
PPSI
Coecum
Colon

*Figure 41: Representative bar graph charts of comparison between between absolute numbers in SPF MHC II-EGFP and GF MHC II-EGFP mouse – myeloid panel - PPs.. Results represent mean ± SD of value. n(SPF)=5 mice, n(GF)=8 mice. *, significant differences with P ≤ 0.05. **, significant differences with P ≤ 0.01. ***, and significant differences with P ≤ 0.001*

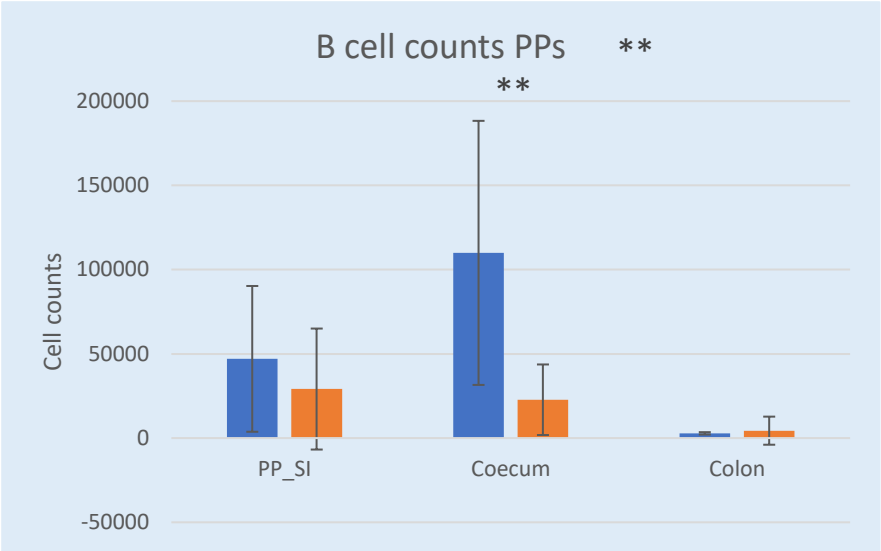

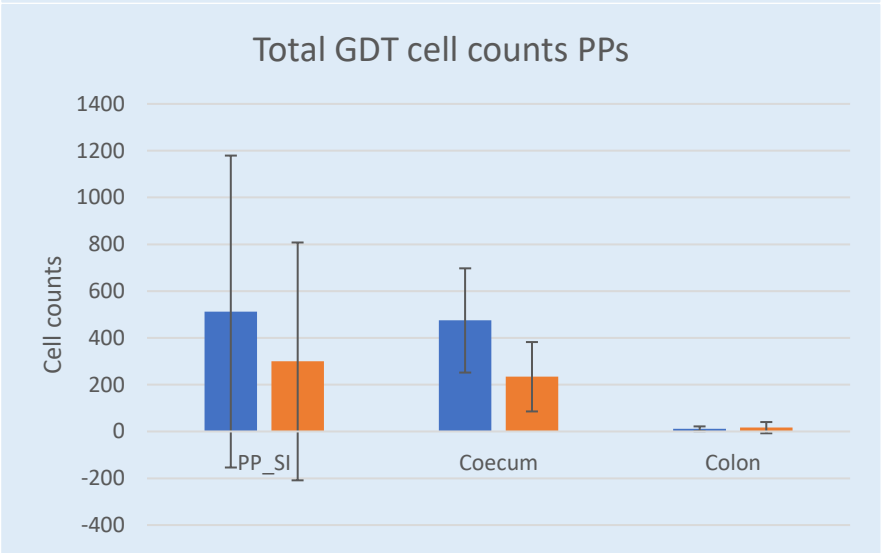

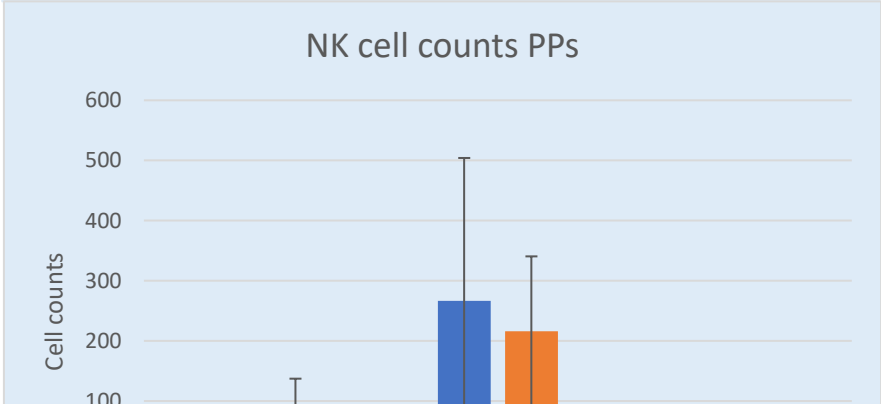

*Figure 40: Representative bar graph charts of comparison between between absolute numbers in SPF MHC II-EGFP and GF MHC II-EGFP mouse – lymphoid panel - PPs.. Results represent mean ± SD of value. n(SPF)=5 mice, n(GF)=8 mice. *, significant differences with P ≤ 0.05. **, significant differences with P ≤ 0.01. ***, and significant differences with P ≤ 0.001*

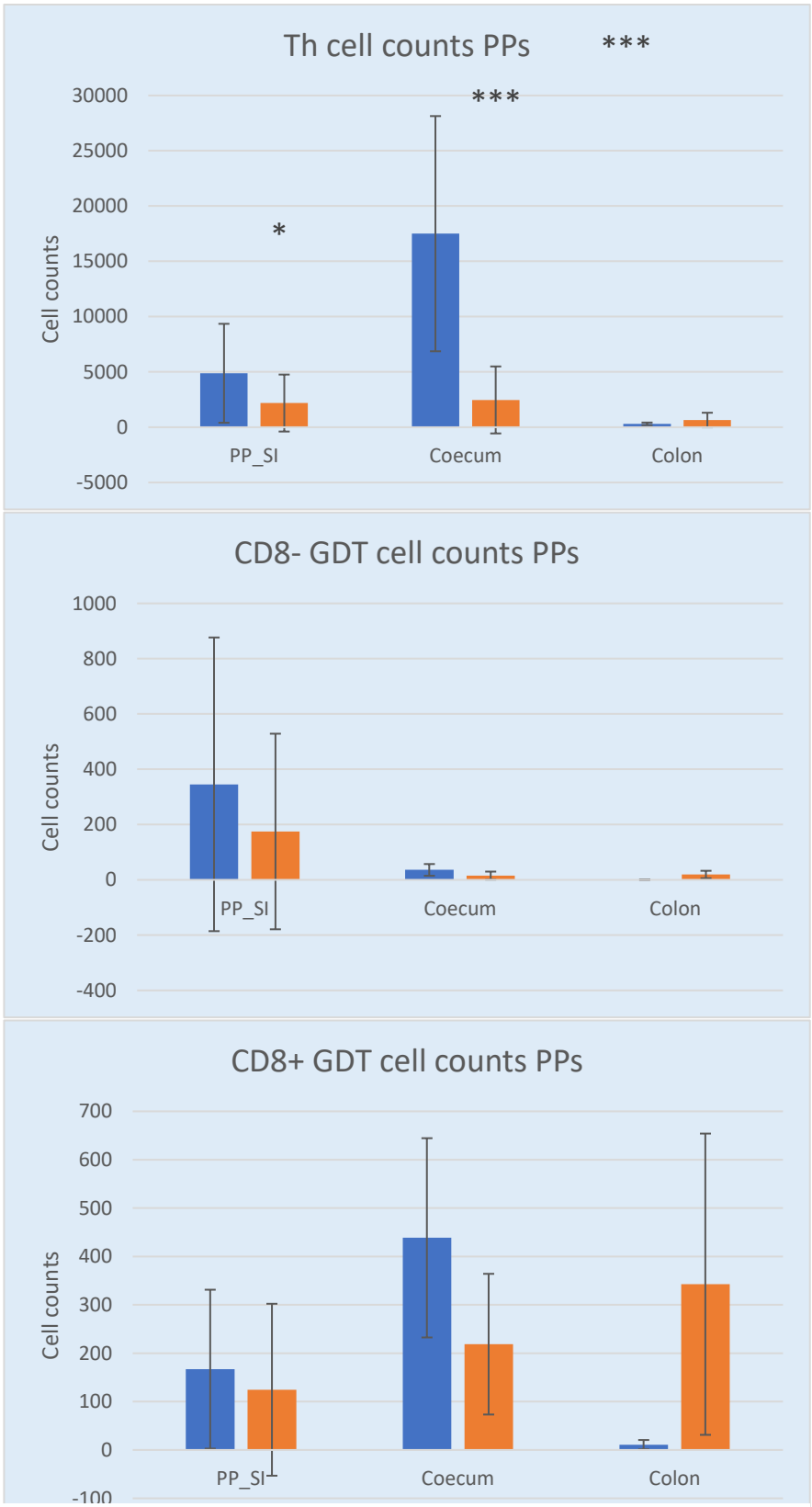

*Figure 42: Representative bar graph charts of comparison between between absolute numbers in SPF MHC II-EGFP and GF MHC II-EGFP mouse – lymphoid panel - PPs.. Results represent mean ± SD of value. n(SPF)=5 mice, n(GF)=8 mice. *, significant differences with $P \leq 0.05$. **, significant differences with $P \leq 0.01$. ***, and significant differences with $P \leq 0.001$*

5.3.7. Ly6C vs. CD3

To further verify the observations of a relatively huge percentage of Ly6C-positive cells (especially in MLNs) negative for any other myeloid marker, a separate experiment was performed only with the use of CD3 and Ly6C antibodies. Single stains were measured to compute the compensation matrix, which was then applied to a mixed sample. The results are shown in Figure 43. The numbers of Ly6C-positive T cells (10,2% in BL spleen, 7,21% in MHC II_EGFP spleen and 21,4% for MLNs for all live cells) roughly correlate with the numbers observed by myeloid panel (however, no accurate determination could be used because of the absence of other parameters, such as CD45 or TER-119).

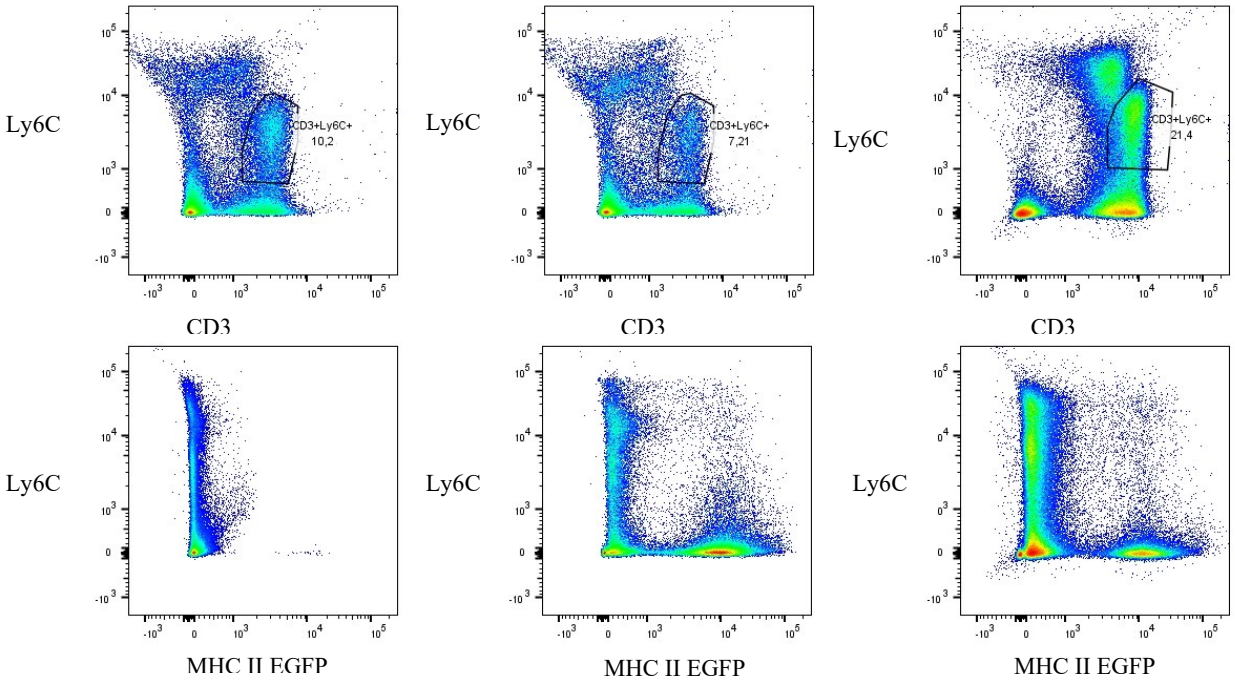

Figure 43: CD3 vs. Ly6C representative dotplots of spleen of wtC57BL/6 mouse (left), MHC II-EGFP knock-in *mouse (middle), and MLNs of MHC II-EGFP* knock-in *mouse (right).*

6. Discussion

The focus of this work is in the development and optimalization of detailed dissection, microscopic (LSM) and flow cytometric methods with the usage of the unique MHC II-EGFP mouse model for several secondary lymphoid organs. This included a unique approach of dissecting the MLN complex into single units, complemented by a sequential dissection of PPs throughout the whole intestine, including coecal and colonic patches. Flow cytometry provided the quantitative data abouth cellular numbers, while LSM was used to gain the 3D structural information about MLNs and PPs with the least number of artifacts possible introduced by sample preparation. This work forms a basis of a bigger project in the laboratory I am enrolled in, that will try to envision the entero-mammary pathway, whose details are still a highly discussed topic[51–53]. Future work will focus on the visualization of bacterial transfer from the gut (PPs) to the mammary gland, possibly via DCs or other MHC II-positive cells, using the monocolonisation of GF MHC II-EGFP mice by the fluorescently-tagged bacterium Lactobacillus plantarum. However, to enable further analysis, studied organs in both SPF and GF mice of MHC II-EGFP mouse model needed to be characterized in detail to become familiarized with the effects microbiota can bear on the structural and functional basis of secondary lymphoid organs studied. This work is a set of pilot experiments in the laboratory and many aspects may be optimized further in the future to yield the desired results of fully correlating cytometric and microscopic data.

I successfully managed to dissect MLN complex of MHC II-EGFP mouse model into separate structural units in a sequential order, as well as to analyze the whole set of PPs, coecal and colonic patches, in a sequential manner. Provided stereomicroscopical pictures clearly demonstrated the degree of variability in the number and 3D composition of MLNs and variable morphology and set-up of PPs, coecal and colonic patches along the gut, supported by the previously published results, where the number of PPs in the small intestine varied from 5 to 9 in a C57BL/6 mouse[71].

During the dissection of the samples for LSFM, a very careful approach had to be taken not to squeeze tiny PPs or MLNs with the dissection tools, which could cause artifact formation. On the other hand, all the fat from the fatty capsule of MLNs had to be eliminated to be able to see the sample properly, as the fat-bound DRAQ5 would make the samples practically unacquirable due to its high fluorescence. As the samples were quite small and relatively easy to diffuse into, a relatively high dilution of DRAQ5 could be used. Demonstrative 2D “sheets” as well as a visualization of samples in 3D (data not shown) provided interesting insights into the structure of both MLNs and PPs without the artifacts that would be brought in by the preparation of physical slides. However, the small lymphocytic cells were packed so densely together that it has been unattainable to count the cellular numbers to date, even after deconvolution algorithms were used. By means of further optimalization, an algorithm using the artificial intelligence will have to be developed or adapted (from the previous work of my colleague Karolína Knížková) on the computed dataset to get an output approaching real numbers of cells in the organs.

Flow cytometry data aquisition and analysis was by far the biggest component of my research. I helped with the optimalization of two fluorescence panels as well as by the troubleshooting of tissue digestion enzyme used. Dispase vs. collagenase tissue dissociation protocols were tested, and, as collagenase provided higher cellular yields, it was therefore used for further analysis. The downside of collagenase digestion is a longer sample preparation, which could lead to selective dying of susceptible cells during longer experiments.

My next task was to compare CD57BL/6 mouse model with MHC II-EGFP, and subsequently MHC II-EGFP mice under SPF and GF housing conditions. As the cytometric panels were multiparametric and manual gating of all possible populations would be timely and biased by the hierarchy used (needless to say also highly subjective), the unsupervised analysis approach by FlowJo plugin FlowSOM was chosen, complemented by tSNE algorithm, which allows for easier visualization of clusters. The reason tSNE was not performed of all samples was because of its slow computational rate compared to FlowSOM (also limiting the maximum effective sample size), the stochasticity and subsequent inability to compare populations across multiple samples as well as the need for subsequent (manual) gating, causing possible bias. The number of chosen metaclusters in FlowSOM were also a subject of optimalisation, as lower numbers did not separate the (almost) full potential of populations distinguishable by the panels, but higher numbers were more timely in subsequent analysis and an unnecessary clustering of a single cellular population was observed. Grid size, a parameter enabling finer differentiation of populations, also needed to be tweaked in order to capture the desired rare populations. Regarding population naming, while CD3+CD4+CD25+ were denoted as “Treg cells”, and CD19+CD25+(MHC II-EGFP+) population as “Breg cells”, this was purely for the simplification purposes and I am aware that CD3+CD4+CD25+ also contains activated Th cells (and that the characteristic marker of Treg cells is FoxP3, which the both panels lack) and That “Bregs” are still a highly discussed population with different subsets and is rather characteristic by IL-10 production. Regarding the “memory T cell” subset, as it was defined in myeloid panel by the sole expression of Ly6C, may not be entirely correct as myeloid panel does not contain CD3 antibody (and was therefore verified separately). Regarding the “lymphocyte X” (CD3+CD19+), it is still a very controversial population, so while it was quanified, any findings regarding its existence and abundance are still highly preliminary and will need verification in the future.

While CD57BL/6 and MHC II-EGFP mouse models are documented as immunologically equivalent, several populations showed significant differences when the mice were compared. However, this should not be automatically interpreted as a real result. As CD57BL/6 mice lack the fluorescently tagged MHC II, they had to be analysed separately by FlowSOM. Having one less reliable parameter for population clustering, the generated clusters could be different (especially in lymphoid panel where most significant relationships were demonstrated, as no “control” MHC II antibody was used) from the situation in GFP mouse. Another point is that as sometimes the mesenteric lymph nodes are localised outside of the main “stream”, by the classical dissection of the whole MLN complex, not all of the lymph

nodes may be included. This information further proves how it is necessary to search for possible bias when interpreting (cytometrical) data.

Afterwards, MLNs, spleen and PPs were compared accross SFP and GF mice. Differences among the organ group were also observed. As the number of MLNs and PPs is very variable, as well as their configuration and distribution, I could not compare the sequential number of MLNs or PPs, as the numbers would not always correspond to the same drainage site in the gut. Therefore, I only compared the first, last (coecal) and second to last MLN (draining the last part of small intestine) and the first and last (small intestinal) PP, coecal and colonic patches. The rest of the samples were not evaluated statistically at the moment, however, there is and ongoing search for an approach that would allow comparison of all the acquired data. A collaboration with Karel Fišer, Department of Bioinformatics, Second Faculty of Medicine, Charles University, is under way to use the data to their full capacity.

Considering the comparison of relative numbers, a few interesting significancies will be mentioned. A recurring theme in all organs are relatively lower numbers of γδT cells in germ-free mice, that also present a gradient across MLN and PP sequences. I have not encountered this information in any papers. Therefore, while it definitely needs further verification, this information could be a novel finding regarding GF mice physiology as well as the demonstration that by pooling MLNs/PPs, a significant positional information could be persistently lost. Other recurring significant differences among spleen and MLNs are a relative increase in B cells and decrease in both Th and Tc cells. This is a clear demonstration as to why it is essential to look at both the absolute and relative numbers. As T and B cells make up for the majority of cells in spleen and especially in MLNs, an absolute decrease in one variable inevitably leads to the relative increase of other. Therefore, without the quantification of cellular numbers, one cannot state whether the observed phenotype is due to an absolute increase in B cells, a decrease in T cells, or a combination of both. As the total number of cells was not significantly different for MLNs or spleen in my settings, the latter seems probable. Indeed, lower absolute numbers of both Th and Tc were observed in MLNs (and sometimes spleen)[56,271]. However, the data regarding B cells in MLNs are lacking (but in spleen, similar numbers were described)[56]. Another interesting and unique trend described in GF mouse is the steep increase of relative abundance of NK cells in coecal and colonic patches. This phenomenon, to my knowledge, is also previously unknown. Last but not least, a decrease in all DCs (especially pDCs), was observed in MLNs. This finding is supported by an article, however, pDCs are not regarded separately and a decrease was also observed in spleen, where no significant difference could be noted by me[272].

Paralelly to relative abundances, I also analysed quantitative data. This type of data is often completely omitted in scientific work, and many works regarding cellular numbers are dated and not challenged further by novel quantitative approaches. I acquired my data in a highly standardized and quatitative manner, so I could determine the absolute numbers for spleen, per average MLN, per average PP, coecal and colonic patches. Again, the quantification could not be done for each sequential number

for MLNs and PPs, because every mouse has different number and configuration of their GALT system. I only observed significant differences between the absolute numbers in average small intestinal PP and coecal patch, which were analysed further. B and T cells all copied the pattern of total cell counts significantly (especially for coecal patch). However, as the total cell numbers were significantly different, the "significant" finding could actually be in other populations, where the difference between cells is not significant across SPF and GF mice, which could mean a difference in the relative abundance. Therefore, a combination of both relative and absolute numbers provides the best representation of the actual conditions inside the body.

Despite the quantification and calculations, the presented "total" cell numbers are not entirely complete, as no correction was done accounting for cells dying or being washed off in the process. As me and my colleague Jan Pačes determined (external data), only about 48% of cells from small intestinal PPs make it to the FACS measurements live when staining with panels compared to measuring the number of cells directly after the collagenase treatment. This may be partially accounted to more washing steps, as well as longer time before measurements, as PPs are a quite delicate tissue (compared to spleen and MLNs). Similar correction was not yet determined for spleen or MLNs, however, the percentages may be slightly higher due to their higher durability.

Last but not least, I combined CD3 and Ly6C staining to verify my observations and calculations of a relatively big Ly6C-positive population. Ly6C is a marker for central (as well as virtual memory T cells), but not effector memory cells[132,272]. Memory T cells increase during aging, so it was critical for me to use mice of the same age (in my case, 8 weeks) across all my experiments, to avoid any bias regarding their abundance[133]. My observations indicate that there may be a significant difference in their abundance between SPF and GF mice in MLNs) and that their abundances vary significantly in PPs across their intestinal gradient (esp. in GF mice). However, to verify these resunt, staining with bost CD3 and Ly6C will need to be performed.

7. Conclusion

In this work, I fulfilled my aim to optimize the spectroscopical, LSM and flow cytometrical methods to MHC II-EGFP *knock-in* mouse model, with the future perspective of using it to research entero-mammary pathway in detail. The use of LSM to count all/MHC II+ will be attempted in the future with the help of artificial intelligence. For cytometrical measurements, two variants of unsupervised data analysis were used complementarily.

I also described both MLNs as well as PPs both qualitatively and quantitatively, using the optimalized toolbox.

I identified several populations in MLNs and PPs in both myeloid and lymphoid panels and tested both the frequencies as well as absolute numbers of cells in each sample to determine differences between SPF and GF mouse model, with significant results.

The results indicate several shifts in the relative abundances of cellular populations between SPF and GF mouse models. These include lower abundances of γδ T cells across all samples, higher B cell percentage and lower Th and Tc cell abundances in spleen and MLNs, lower pDC and cDC cell numbers in MLNs, and more. Several markers exhibited differential expression only in some of the tissues, e.g. NK cells were enriched in coecal and colonic patches in GF mouse. Total cell numbers were significantly lower in small intestinal PPs and coecal patch of GF mouse, which was also reglected by B, Th or Tc populations. Taken together, both SPF vs. GF housing settings, as well as the gradient along MLNs and PPs, were found to have a significant impact on the cellular composition of secondary myeloid organs.

8. References

1. Pickard JM, Zeng MY, Caruso R, Núñez G. Gut microbiota: Role in pathogen colonization, immune responses, and inflammatory disease. *Immunol Rev*. 2017;279(1):70-89. doi:10.1111/imr.12567
2. Ahlawat S, Asha, Sharma KK. Gut–organ axis: a microbial outreach and networking. *Lett Appl Microbiol*. 2021;72(6):636-668. doi:10.1111/lam.13333
3. Wang G, Huang S, Wang Y, et al. Bridging intestinal immunity and gut microbiota by metabolites. *Cell Mol Life Sci*. 2019;76(20):3917-3937. doi:10.1007/s00018-019-03190-6
4. Postler TS, Ghosh S. Understanding the Holobiont: How Microbial Metabolites Affect Human Health and Shape the Immune System. *Cell Metab*. 2017;26(1):110-130. doi:10.1016/j.cmet.2017.05.008
5. Yoo JY, Groer M, Dutra SVO, Sarkar A, McSkimming DI. Gut Microbiota and Immune System Interactions. *Microorganisms*. 2020;8(10). doi:10.3390/microorganisms8101587
6. Rooks MG, Garrett WS. Gut microbiota, metabolites and host immunity. *Nat Rev Immunol*. 2016;16(6):341-352. doi:10.1038/nri.2016.42
7. Macpherson AJ, Uhr T. Induction of protective IgA by intestinal dendritic cells carrying commensal bacteria. *Science*. 2004;303(5664):1662-1665. doi:10.1126/science.1091334
8. Sawa S, Lochner M, Satoh-Takayama N, et al. RORγt+ innate lymphoid cells regulate intestinal homeostasis by integrating negative signals from the symbiotic microbiota. *Nat Immunol*. 2011;12(4):320-326. doi:10.1038/ni.2002
9. Cording S, Fleissner D, Heimesaat MM, et al. Commensal microbiota drive proliferation of conventional and Foxp3+ regulatory CD4+ T cells in mesenteric lymph nodes and Peyer's patches. *Eur J Microbiol Immunol (Bp)*. 2013;3(1):1. doi:10.1556/EUJMI.3.2013.1.1
10. Kau AL, Ahern PP, Griffin NW, Goodman AL, Gordon JI. Human nutrition, the gut microbiome and the immune system. *Nature*. 2011;474(7351):327-336. doi:10.1038/nature10213
11. Everard A, Cani PD. Diabetes, obesity and gut microbiota. *Best Pract Res Clin Gastroenterol*. 2013;27(1):73-83. doi:10.1016/j.bpg.2013.03.007
12. Miele L, Giorgio V, Alberelli MA, De Candia E, Gasbarrini A, Grieco A. Impact of Gut Microbiota on Obesity, Diabetes, and Cardiovascular Disease Risk. *Curr Cardiol Rep*. 2015;17(12):120. doi:10.1007/s11886-015-0671-z
13. Jiao Y, Wu L, Huntington ND, Zhang X. Crosstalk Between Gut Microbiota and Innate Immunity and Its Implication in Autoimmune Diseases. *Front Immunol*. 2020;11:282. doi:10.3389/fimmu.2020.00282
14. Thaiss CA, Zmora N, Levy M, Elinav E. The microbiome and innate immunity. *Nature*.

2016;535(7610):65-74. doi:10.1038/nature18847

15. Amoroso C, Perillo F, Strati F, Fantini MC, Caprioli F, Facciotti F. The Role of Gut Microbiota Biomodulators on Mucosal Immunity and Intestinal Inflammation. *Cells*. 2020;9(5). doi:10.3390/cells9051234
16. Garrett WS, Gallini CA, Yatsunenko T, et al. Enterobacteriaceae act in concert with the gut microbiota to induce spontaneous and maternally transmitted colitis. *Cell Host Microbe*. 2010;8(3):292-300. doi:10.1016/j.chom.2010.08.004
17. Paramsothy S, Kamm MA, Kaakoush NO, et al. Multidonor intensive faecal microbiota transplantation for active ulcerative colitis: a randomised placebo-controlled trial. *Lancet (London, England)*. 2017;389(10075):1218-1228. doi:10.1016/S0140-6736(17)30182-4
18. Yang Q, Wang Y, Jia A, Wang Y, Bi Y, Liu G. The crosstalk between gut bacteria and host immunity in intestinal inflammation. *J Cell Physiol*. 2021;236(4):2239-2254. doi:10.1002/jcp.30024
19. Reyes-Castillo Z, Valdés-Miramontes E, Llamas-Covarrubias M, Muñoz-Valle JF. Troublesome friends within us: the role of gut microbiota on rheumatoid arthritis etiopathogenesis and its clinical and therapeutic relevance. *Clin Exp Med*. 2021;21(1):1-13. doi:10.1007/s10238-020-00647-y
20. Kesika P, Suganthy N, Sivamaruthi BS, Chaiyasut C. Role of gut-brain axis, gut microbial composition, and probiotic intervention in Alzheimer's disease. *Life Sci*. 2021;264:118627. doi:10.1016/J.LFS.2020.118627
21. Maiuolo J, Gliozzi M, Musolino V, et al. The Contribution of Gut Microbiota–Brain Axis in the Development of Brain Disorders. *Front Neurosci*. 2021;15. doi:10.3389/FNINS.2021.616883
22. Erny D, Hrabě de Angelis AL, Jaitin D, et al. Host microbiota constantly control maturation and function of microglia in the CNS. *Nat Neurosci*. 2015;18(7):965-977. doi:10.1038/nn.4030
23. Xu J-Y, Liu M-T, Tao T, Zhu X, Fei F-Q. The role of gut microbiota in tumorigenesis and treatment. *Biomed Pharmacother*. 2021;138:111444. doi:10.1016/J.BIOPHA.2021.111444
24. Qiu Q, Lin Y, Ma Y, et al. Exploring the Emerging Role of the Gut Microbiota and Tumor Microenvironment in Cancer Immunotherapy. *Front Immunol*. 2020;11:612202. doi:10.3389/fimmu.2020.612202
25. Ma J, Zhu W, Liu B. Role of gut microbiome in the outcome of cancer immunotherapy. *Int J Cancer*. 2021;149(4):760-768. doi:10.1002/ijc.33524
26. Rezasoltani S, Yadegar A, Asadzadeh Aghdaei H, Reza Zali M. Modulatory effects of gut microbiome in cancer immunotherapy: A novel paradigm for blockade of immune checkpoint inhibitors. *Cancer Med*. 2021;10(3):1141-1154. doi:10.1002/cam4.3694
27. Sivan A, Corrales L, Hubert N, et al. Commensal Bifidobacterium promotes antitumor immunity and facilitates anti-PD-L1 efficacy. *Science*. 2015;350(6264):1084-1089.

doi:10.1126/science.aac4255

28. Vétizou M, Pitt JM, Daillère R, et al. Anticancer immunotherapy by CTLA-4 blockade relies on the gut microbiota. *Science*. 2015;350(6264):1079-1084. doi:10.1126/science.aad1329
29. Fransen F, Zagato E, Mazzini E, et al. BALB/c and C57BL/6 Mice Differ in Polyreactive IgA Abundance, which Impacts the Generation of Antigen-Specific IgA and Microbiota Diversity. *Immunity*. 2015;43(3):527-540. doi:10.1016/J.IMMUNI.2015.08.011
30. Ivanov II, Atarashi K, Manel N, et al. Induction of intestinal Th17 cells by segmented filamentous bacteria. *Cell*. 2009;139(3):485. doi:10.1016/J.CELL.2009.09.033
31. Sanos SL, Bui VL, Mortha A, et al. RORγt and commensal microflora are required for the differentiation of mucosal interleukin 22–producing NKp46+ cells. *Nat Immunol*. 2009;10(1):83. doi:10.1038/NI.1684
32. Martínez-López M, Iborra S, Conde-Garrosa R, et al. Microbiota Sensing by Mincle-Syk Axis in Dendritic Cells Regulates Interleukin-17 and -22 Production and Promotes Intestinal Barrier Integrity. *Immunity*. 2019;50(2):446. doi:10.1016/J.IMMUNI.2018.12.020
33. Atarashi K, Tanoue T, Shima T, et al. Induction of Colonic Regulatory T Cells by Indigenous Clostridium Species. *Science*. 2011;331(6015):337. doi:10.1126/SCIENCE.1198469
34. Atarashi K, Tanoue T, Oshima K, et al. Treg induction by a rationally selected mixture of Clostridia strains from the human microbiota. *Nature*. 2013;500(7461):232-236. doi:10.1038/nature12331
35. Round JL, Mazmanian SK. Inducible Foxp3+ regulatory T-cell development by a commensal bacterium of the intestinal microbiota. *Proc Natl Acad Sci U S A*. 2010;107(27):12204. doi:10.1073/PNAS.0909122107
36. Mazmanian SK, Liu CH, Tzianabos AO, Kasper DL. An Immunomodulatory Molecule of Symbiotic Bacteria Directs Maturation of the Host Immune System. *Cell*. 2005;122(1):107-118. doi:10.1016/J.CELL.2005.05.007
37. Geva-Zatorsky N, Sefik E, Kua L, et al. Mining the Human Gut Microbiota for Immunomodulatory Organisms. *Cell*. 2017;168(5):928-943.e11. doi:10.1016/j.cell.2017.01.022
38. Schwarzer M, Makki K, Storelli G, et al. Lactobacillus plantarum strain maintains growth of infant mice during chronic undernutrition. *Science*. 2016;351(6275):854-857. doi:10.1126/science.aad8588
39. Al Nabhani Z, Eberl G. Imprinting of the immune system by the microbiota early in life. *Mucosal Immunol*. 2020;13(2):183-189. doi:10.1038/s41385-020-0257-y
40. Schulfer AF, Battaglia T, Alvarez Y, et al. Intergenerational transfer of antibiotic-perturbed microbiota enhances colitis in susceptible mice. *Nat Microbiol*. 2018;3(2):234-242. doi:10.1038/s41564-017-0075-5

41. de Goffau MC, Lager S, Sovio U, et al. Human placenta has no microbiome but can contain potential pathogens. *Nature*. 2019;572(7769):329-334. doi:10.1038/s41586-019-1451-5
42. Aagaard K, Ma J, Antony KM, Ganu R, Petrosino J, Versalovic J. The placenta harbors a unique microbiome. *Sci Transl Med*. 2014;6(237):237ra65. doi:10.1126/scitranslmed.3008599
43. Bashir MEH, Louie S, Shi HN, Nagler-Anderson C. Toll-like receptor 4 signaling by intestinal microbes influences susceptibility to food allergy. *J Immunol*. 2004;172(11):6978-6987. doi:10.4049/jimmunol.172.11.6978
44. Reyman M, van Houten MA, van Baarle D, et al. Impact of delivery mode-associated gut microbiota dynamics on health in the first year of life. *Nat Commun*. 2019;10(1):4997. doi:10.1038/s41467-019-13014-7
45. Urbaniak C, Cummins J, Brackstone M, et al. Microbiota of human breast tissue. *Appl Environ Microbiol*. 2014;80(10):3007-3014. doi:10.1128/AEM.00242-14
46. Hieken TJ, Chen J, Hoskin TL, et al. The Microbiome of Aseptically Collected Human Breast Tissue in Benign and Malignant Disease. *Sci Rep*. 2016;6. doi:10.1038/SREP30751
47. Ward TL, Hosid S, Ioshikhes I, Altosaar I. Human milk metagenome: a functional capacity analysis. *BMC Microbiol*. 2013;13:116. doi:10.1186/1471-2180-13-116
48. Urbaniak C, Angelini M, Gloor GB, Reid G. Human milk microbiota profiles in relation to birthing method, gestation and infant gender. *Microbiome*. 2016;4:1. doi:10.1186/s40168-015-0145-y
49. Harmsen HJ, Wildeboer-Veloo AC, Raangs GC, et al. Analysis of intestinal flora development in breast-fed and formula-fed infants by using molecular identification and detection methods. *J Pediatr Gastroenterol Nutr*. 2000;30(1):61-67. doi:10.1097/00005176-200001000-00019
50. Sakata S, Tonooka T, Ishizeki S, et al. Culture-independent analysis of fecal microbiota in infants, with special reference to Bifidobacterium species. *FEMS Microbiol Lett*. 2005;243(2):417-423. doi:10.1016/j.femsle.2005.01.002
51. Perez PF, Doré J, Leclerc M, et al. Bacterial imprinting of the neonatal immune system: lessons from maternal cells? *Pediatrics*. 2007;119(3):e724-32. doi:10.1542/peds.2006-1649
52. Donnet-Hughes A, Perez PF, Doré J, et al. Potential role of the intestinal microbiota of the mother in neonatal immune education. *Proc Nutr Soc*. 2010;69(3):407-415. doi:10.1017/S0029665110001898
53. Urbaniak C, Burton JP, Reid G. Breast, milk and microbes: a complex relationship that does not end with lactation. *Womens Health (Lond Engl)*. 2012;8(4):385-398. doi:10.2217/whe.12.23
54. Rodríguez JM. The origin of human milk bacteria: is there a bacterial entero-mammary pathway during late pregnancy and lactation? *Adv Nutr*. 2014;5(6):779-784. doi:10.3945/an.114.007229
55. Ojo-Okunola A, Nicol M, du Toit E. Human Breast Milk Bacteriome in Health and Disease. *Nutrients*. 2018;10(11). doi:10.3390/nu10111643

56. Kennedy EA, King KY, Baldridge MT. Mouse Microbiota Models: Comparing Germ-Free Mice and Antibiotics Treatment as Tools for Modifying Gut Bacteria. *Front Physiol*. 2018;9:1534. doi:10.3389/fphys.2018.01534

57. Brandl K, Plitas G, Mihu CN, et al. Vancomycin-resistant enterococci exploit antibiotic-induced innate immune deficits. *Nature*. 2008;455(7214):804-807. doi:10.1038/nature07250

58. Ekmekciu I, von Klitzing E, Fiebiger U, et al. Immune Responses to Broad-Spectrum Antibiotic Treatment and Fecal Microbiota Transplantation in Mice. *Front Immunol*. 2017;8:397. doi:10.3389/fimmu.2017.00397

59. Khosravi A, Yáñez A, Price JG, et al. Gut microbiota promote hematopoiesis to control bacterial infection. *Cell Host Microbe*. 2014;15(3):374-381. doi:10.1016/j.chom.2014.02.006

60. Bouskra D, Brézillon C, Bérard M, et al. Lymphoid tissue genesis induced by commensals through NOD1 regulates intestinal homeostasis. *Nature*. 2008;456(7221):507-510. doi:10.1038/nature07450

61. Lorenz RG, Chaplin DD, McDonald KG, McDonough JS, Newberry RD. Isolated lymphoid follicle formation is inducible and dependent upon lymphotoxin-sufficient B lymphocytes, lymphotoxin beta receptor, and TNF receptor I function. *J Immunol*. 2003;170(11):5475-5482. doi:10.4049/jimmunol.170.11.5475

62. BAUER H, HOROWITZ RE, LEVENSON SM, POPPER H. The response of the lymphatic tissue to the microbial flora. Studies on germfree mice. *Am J Pathol*. 1963;42(4):471-483. http://www.ncbi.nlm.nih.gov/pubmed/13966929. Accessed July 6, 2021.

63. Ruddle NH, Akirav EM. Secondary lymphoid organs: responding to genetic and environmental cues in ontogeny and the immune response. *J Immunol*. 2009;183(4):2205-2212. doi:10.4049/jimmunol.0804324

64. Buettner M, Lochner M. Development and Function of Secondary and Tertiary Lymphoid Organs in the Small Intestine and the Colon. *Front Immunol*. 2016;7:342. doi:10.3389/fimmu.2016.00342

65. Mowat AM, Agace WW. Regional specialization within the intestinal immune system. *Nat Rev Immunol*. 2014;14(10):667-685. doi:10.1038/nri3738

66. Rhee K-J, Sethupathi P, Driks A, Lanning DK, Knight KL, Koga Y. Role of commensal bacteria in development of gut-associated lymphoid tissues and preimmune antibody repertoire. *J Immunol*. 2004;172(2):1118-1124. doi:10.4049/jimmunol.172.2.1118

67. Pastori C, Lopalco L. Isolation and in vitro Activation of Mouse Peyer's Patch Cells from Small Intestine Tissue. *BIO-PROTOCOL*. 2014;4(21). doi:10.21769/BioProtoc.1282

68. Reboldi A, Cyster JG. Peyer's patches: organizing B-cell responses at the intestinal frontier. *Immunol Rev*. 2016;271(1):230-245. doi:10.1111/imr.12400

69. Cebra JJ, Periwal SB, Lee G, Lee F, Shroff KE. Development and maintenance of the gut-associated lymphoid tissue (GALT): the roles of enteric bacteria and viruses. *Dev Immunol*. 1998;6(1-2):13-18. doi:10.1155/1998/68382

70. Pollard M, Sharon N. Responses of the Peyer's Patches in Germ-Free Mice to Antigenic Stimulation. *Infect Immun*. 1970;2(1):96-100. doi:10.1128/iai.2.1.96-100.1970

71. Duriancik DM, Hoag KA. The identification and enumeration of dendritic cell populations from individual mouse spleen and Peyer's patches using flow cytometric analysis. *Cytom Part A*. 2009;75A(11):951-959. doi:10.1002/cyto.a.20794

72. Schulz O, Ugur M, Friedrichsen M, et al. Hypertrophy of infected Peyer's patches arises from global, interferon-receptor, and CD69-independent shutdown of lymphocyte egress. *Mucosal Immunol*. 2014;7(4):892-904. doi:10.1038/mi.2013.105

73. Carlson JR, Heyworth MF, Owen RL. Response of Peyer's patch lymphocyte subsets to Giardia muris infection in BALB/c mice: I. T-cell subsets. *Cell Immunol*. 1986;97(1):44-50. doi:10.1016/0008-8749(86)90373-4

74. Nochi T, Denton PW, Wahl A, Garcia JV. Cryptopatches are essential for the development of human GALT. *Cell Rep*. 2013;3(6):1874-1884. doi:10.1016/j.celrep.2013.05.037

75. Hamada H, Hiroi T, Nishiyama Y, et al. Identification of multiple isolated lymphoid follicles on the antimesenteric wall of the mouse small intestine. *J Immunol*. 2002;168(1):57-64. doi:10.4049/jimmunol.168.1.57

76. Manzano M, Abadía-Molina AC, García-Olivares E, Gil A, Rueda R. Absolute Counts and Distribution of Lymphocyte Subsets in Small Intestine of BALB/c Mice Change during Weaning. *J Nutr*. 2002;132(9):2757-2762. doi:10.1093/jn/132.9.2757

77. Houston SA, Cerovic V, Thomson C, Brewer J, Mowat AM, Milling S. The lymph nodes draining the small intestine and colon are anatomically separate and immunologically distinct. *Mucosal Immunol*. 2016;9(2):468-478. doi:10.1038/mi.2015.77

78. Buettner M, Bode U. Lymph node dissection--understanding the immunological function of lymph nodes. *Clin Exp Immunol*. 2012;169(3):205-212. doi:10.1111/j.1365-2249.2012.04602.x

79. Willard-Mack CL. Normal structure, function, and histology of lymph nodes. *Toxicol Pathol*. 2006;34(5):409-424. doi:10.1080/01926230600867727

80. Qu J, Yu X, Jin C, et al. TLR7 Modulated T Cell Response in the Mesenteric Lymph Node of *Schistosoma japonicum* -Infected C57BL/6 Mice. *J Immunol Res*. 2019;2019:1-14. doi:10.1155/2019/2691808

81. Parker SJ, Inchley CJ. Heligmosomoides polygyrus: influence of infection on lymphocyte subpopulations in mouse mesenteric lymph nodes. *Exp Parasitol*. 1990;71(3):249-258. doi:10.1016/0014-4894(90)90029-c

82. Macpherson AJ, Smith K. Mesenteric lymph nodes at the center of immune anatomy. *J Exp Med*. 2006;203(3):497-500. doi:10.1084/jem.20060227

83. Worbs T, Bode U, Yan S, et al. Oral tolerance originates in the intestinal immune system and relies on antigen carriage by dendritic cells. *J Exp Med*. 2006;203(3):519-527. doi:10.1084/jem.20052016

84. Kunkel D, Kirchhoff D, Nishikawa S-I, Radbruch A, Scheffold A. Visualization of peptide presentation following oral application of antigen in normal and Peyer's patches-deficient mice. *Eur J Immunol*. 2003;33(5):1292-1301. doi:10.1002/eji.200323383

85. Voedisch S, Koenecke C, David S, et al. Mesenteric lymph nodes confine dendritic cell-mediated dissemination of Salmonella enterica serovar Typhimurium and limit systemic disease in mice. *Infect Immun*. 2009;77(8):3170-3180. doi:10.1128/IAI.00272-09

86. Jang MH, Sougawa N, Tanaka T, et al. CCR7 is critically important for migration of dendritic cells in intestinal lamina propria to mesenteric lymph nodes. *J Immunol*. 2006;176(2):803-810. doi:10.4049/jimmunol.176.2.803

87. Kashimura M. The human spleen as the center of the blood defense system. *Int J Hematol*. 2020;112(2):147-158. doi:10.1007/s12185-020-02912-y

88. Bronte V, Pittet MJ. The spleen in local and systemic regulation of immunity. *Immunity*. 2013;39(5):806-818. doi:10.1016/j.immuni.2013.10.010

89. Mebius RE, Kraal G. Structure and function of the spleen. *Nat Rev Immunol*. 2005;5(8):606-616. doi:10.1038/nri1669

90. Lewis SM, Williams A, Eisenbarth SC. Structure and function of the immune system in the spleen. *Sci Immunol*. 2019;4(33). doi:10.1126/sciimmunol.aau6085

91. Pellegrini A, Guinazu N, Aoki MP, et al. Spleen B cells from BALB/c are more prone to activation than spleen B cells from C57BL/6 mice during a secondary immune response to cruzipain. *Int Immunol*. 2007;19(12):1395-1402. doi:10.1093/intimm/dxm107

92. Hrncir T, Stepankova R, Kozakova H, Hudcovic T, Tlaskalova-Hogenova H. Gut microbiota and lipopolysaccharide content of the diet influence development of regulatory T cells: studies in germ-free mice. *BMC Immunol*. 2008;9(1):65. doi:10.1186/1471-2172-9-65

93. Collin M, McGovern N, Haniffa M. Human dendritic cell subsets. *Immunology*. 2013;140(1):22-30. doi:10.1111/imm.12117

94. Hermiston ML, Xu Z, Weiss A. CD45: a critical regulator of signaling thresholds in immune cells. *Annu Rev Immunol*. 2003;21:107-137. doi:10.1146/annurev.immunol.21.120601.140946

95. Holmes N. CD45: all is not yet crystal clear. *Immunology*. 2006;117(2):145-155. doi:10.1111/j.1365-2567.2005.02265.x

96. Loken MR, Brosnan JM, Bach BA, Ault KA. Establishing optimal lymphocyte gates for

immunophenotyping by flow cytometry. *Cytometry*. 1990;11(4):453-459. doi:10.1002/cyto.990110402

97. Irie-Sasaki J, Sasaki T, Matsumoto W, et al. CD45 is a JAK phosphatase and negatively regulates cytokine receptor signalling. *Nature*. 2001;409(6818):349-354. doi:10.1038/35053086
98. Victora GD, Nussenzweig MC. Germinal centers. *Annu Rev Immunol*. 2012;30:429-457. doi:10.1146/annurev-immunol-020711-075032
99. Clark EA. A Short History of the B-Cell-Associated Surface Molecule CD40. *Front Immunol*. 2014;5:472. doi:10.3389/fimmu.2014.00472
100. Fujimoto M, Fujimoto Y, Poe JC, et al. CD19 regulates Src family protein tyrosine kinase activation in B lymphocytes through processive amplification. *Immunity*. 2000;13(1):47-57. doi:10.1016/s1074-7613(00)00007-8
101. Uchida J, Lee Y, Hasegawa M, et al. Mouse CD20 expression and function. *Int Immunol*. 2004;16(1):119-129. doi:10.1093/intimm/dxh009
102. Renno T, Attinger A, Rimoldi D, Hahne M, Tschopp J, MacDonald HR. Expression of B220 on activated T cell blasts precedes apoptosis. *Eur J Immunol*. 1998;28(2):540-547. doi:10.1002/(SICI)1521-4141(199802)28:02<540::AID-IMMU540>3.0.CO;2-Y
103. Ferrero I, Held W, Wilson A, Tacchini-Cottier F, Radtke F, MacDonald HR. Mouse CD11c(+) B220(+) Gr1(+) plasmacytoid dendritic cells develop independently of the T-cell lineage. *Blood*. 2002;100(8):2852-2857. doi:10.1182/blood-2002-01-0214
104. Martín P, Del Hoyo GM, Anjuère F, et al. Characterization of a new subpopulation of mouse CD8alpha+ B220+ dendritic cells endowed with type 1 interferon production capacity and tolerogenic potential. *Blood*. 2002;100(2):383-390. doi:10.1182/blood.v100.2.383
105. Segura E, Wong J, Villadangos JA. Cutting edge: B220+CCR9- dendritic cells are not plasmacytoid dendritic cells but are precursors of conventional dendritic cells. *J Immunol*. 2009;183(3):1514-1517. doi:10.4049/jimmunol.0901524
106. Wilmore JR, Jones DD, Allman D. Protocol for improved resolution of plasma cell subpopulations by flow cytometry. *Eur J Immunol*. 2017;47(8):1386-1388. doi:10.1002/eji.201746944
107. McCarron MJ, Park PW, Fooksman DR. CD138 mediates selection of mature plasma cells by regulating their survival. *Blood*. 2017;129(20):2749-2759. doi:10.1182/blood-2017-01-761643
108. Won W-J, Kearney JF, Dick MD, et al. CD9 is a unique marker for marginal zone B cells, B1 cells, and plasma cells in mice. *J Immunol*. 2002;168(11):5605-5611. doi:10.4049/jimmunol.168.11.5605
109. Yoshimoto M. The ontogeny of murine B-1a cells. *Int J Hematol*. 2020;111(5):622-627. doi:10.1007/s12185-019-02787-8

110. Rosser EC, Mauri C. Regulatory B Cells: Origin, Phenotype, and Function. *Immunity*. 2015;42(4):607-612. doi:10.1016/J.IMMUNI.2015.04.005

111. Bankoti R, Gupta K, Levchenko A, Stäger S. Marginal zone B cells regulate antigen-specific T cell responses during infection. *J Immunol*. 2012;188(8):3961-3971. doi:10.4049/jimmunol.1102880

112. Yanaba K, Bouaziz J-D, Haas KM, Poe JC, Fujimoto M, Tedder TF. A regulatory B cell subset with a unique CD1dhiCD5+ phenotype controls T cell-dependent inflammatory responses. *Immunity*. 2008;28(5):639-650. doi:10.1016/j.immuni.2008.03.017

113. Ahmed R, Omidian Z, Giwa A, et al. A Public BCR Present in a Unique Dual-Receptor-Expressing Lymphocyte from Type 1 Diabetes Patients Encodes a Potent T Cell Autoantigen. *Cell*. 2019;177(6):1583-1599.e16. doi:10.1016/j.cell.2019.05.007

114. Japp AS, Meng W, Rosenfeld AM, et al. TCR+/BCR+ dual-expressing cells and their associated public BCR clonotype are not enriched in type 1 diabetes. *Cell*. 2021;184(3):827-839.e14. doi:10.1016/j.cell.2020.11.035

115. Burel JG, Pomaznoy M, Lindestam Arlehamn CS, et al. The Challenge of Distinguishing Cell-Cell Complexes from Singlet Cells in Non-Imaging Flow Cytometry and Single-Cell Sorting. *Cytometry A*. 2020;97(11):1127-1135. doi:10.1002/cyto.a.24027

116. STORIE I, WILSON GA, GRANGER V, BARNETT D, REILLY JT. Circulating CD20dim T-lymphocytes increase with age: evidence for a memory cytotoxic phenotype. *Clin Lab Haematol*. 1995;17(4):323-328. doi:10.1111/J.1365-2257.1995.TB01272.X

117. Hultin LE, Hausner MA, Hultin PM, Giorgi J V. CD20 (pan-B cell) antigen is expressed at a low level on a subpopulation of human T lymphocytes. *Cytometry*. 1993;14(2):196-204. doi:10.1002/cyto.990140212

118. Quintanilla-Martinez L, Preffer F, Rubin D, Ferry JA, Harris NL. CD20+ T-cell lymphoma. Neoplastic transformation of a normal T-cell subset. *Am J Clin Pathol*. 1994;102(4):483-489. doi:10.1093/ajcp/102.4.483

119. Henry C, Ramadan A, Montcuquet N, et al. CD3+CD20+ cells may be an artifact of flow cytometry: Comment on the article by Wilk et al. *Arthritis Rheum*. 2010;62(8):2561-2563. doi:10.1002/art.27527

120. Nagel A, Möbs C, Raifer H, Wiendl H, Hertl M, Eming R. CD3-positive B cells: a storage-dependent phenomenon. *PLoS One*. 2014;9(10):e110138. doi:10.1371/journal.pone.0110138

121. Martina MN, Noel S, Saxena A, Rabb H, Hamad ARA. Double negative (DN) αβ T cells: misperception and overdue recognition. *Immunol Cell Biol*. 2015;93(3):305-310. doi:10.1038/icb.2014.99

122. Nascimbeni M, Shin E-C, Chiriboga L, Kleiner DE, Rehermann B. Peripheral CD4(+)CD8(+) T cells

are differentiated effector memory cells with antiviral functions. *Blood*. 2004;104(2):478-486. doi:10.1182/blood-2003-12-4395

123. Das G, Augustine MM, Das J, Bottomly K, Ray P, Ray A. An important regulatory role for CD4+CD8 alpha alpha T cells in the intestinal epithelial layer in the prevention of inflammatory bowel disease. *Proc Natl Acad Sci U S A*. 2003;100(9):5324-5329. doi:10.1073/pnas.0831037100
124. Mousset CM, Hobo W, Woestenenk R, Preijers F, Dolstra H, van der Waart AB. Comprehensive Phenotyping of T Cells Using Flow Cytometry. *Cytom Part A*. 2019;95(6):647-654. doi:10.1002/cyto.a.23724
125. Kessel A, Haj T, Peri R, et al. Human CD19(+)CD25(high) B regulatory cells suppress proliferation of CD4(+) T cells and enhance Foxp3 and CTLA-4 expression in T-regulatory cells. *Autoimmun Rev*. 2012;11(9):670-677. doi:10.1016/j.autrev.2011.11.018
126. Kalyan S, Kabelitz D. Defining the nature of human γδ T cells: a biographical sketch of the highly empathetic. *Cell Mol Immunol*. 2013;10(1):21-29. doi:10.1038/cmi.2012.44
127. Kadivar M, Petersson J, Svensson L, Marsal J. CD8αβ+ γδ T Cells: A Novel T Cell Subset with a Potential Role in Inflammatory Bowel Disease. *J Immunol*. 2016;197(12):4584-4592. doi:10.4049/jimmunol.1601146
128. Brandes M, Willimann K, Moser B. Professional antigen-presentation function by human gammadelta T Cells. *Science*. 2005;309(5732):264-268. doi:10.1126/science.1110267
129. Durek P, Nordström K, Gasparoni G, et al. Epigenomic Profiling of Human CD4+ T Cells Supports a Linear Differentiation Model and Highlights Molecular Regulators of Memory Development. *Immunity*. 2016;45(5):1148-1161. doi:10.1016/j.immuni.2016.10.022
130. van Aalderen MC, van den Biggelaar M, Remmerswaal EBM, et al. Label-free Analysis of CD8+ T Cell Subset Proteomes Supports a Progressive Differentiation Model of Human-Virus-Specific T Cells. *Cell Rep*. 2017;19(5):1068-1079. doi:10.1016/j.celrep.2017.04.014
131. Sallusto F, Lenig D, Förster R, Lipp M, Lanzavecchia A. Two subsets of memory T lymphocytes with distinct homing potentials and effector functions. *Nature*. 1999;401(6754):708-712. doi:10.1038/44385
132. Hänninen A, Maksimow M, Alam C, Morgan DJ, Jalkanen S. Ly6C supports preferential homing of central memory CD8+ T cells into lymph nodes. *Eur J Immunol*. 2011;41(3):634-644. doi:10.1002/eji.201040760
133. Sathaliyawala T, Kubota M, Yudanin N, et al. Distribution and compartmentalization of human circulating and tissue-resident memory T cell subsets. *Immunity*. 2013;38(1):187-197. doi:10.1016/j.immuni.2012.09.020
134. Mueller SN, Mackay LK. Tissue-resident memory T cells: local specialists in immune defence. *Nat Rev Immunol*. 2016;16(2):79-89. doi:10.1038/nri.2015.3

135. Gattinoni L, Lugli E, Ji Y, et al. A human memory T cell subset with stem cell-like properties. *Nat Med*. 2011;17(10):1290-1297. doi:10.1038/nm.2446

136. Tian Y, Babor M, Lane J, et al. Unique phenotypes and clonal expansions of human CD4 effector memory T cells re-expressing CD45RA. *Nat Commun*. 2017;8(1):1473. doi:10.1038/s41467-017-01728-5

137. Haluszczak C, Akue AD, Hamilton SE, et al. The antigen-specific CD8+ T cell repertoire in unimmunized mice includes memory phenotype cells bearing markers of homeostatic expansion. *J Exp Med*. 2009;206(2):435-448. doi:10.1084/jem.20081829

138. Cortez VS, Colonna M. Diversity and function of group 1 innate lymphoid cells. *Immunol Lett*. 2016;179:19-24. doi:10.1016/j.imlet.2016.07.005

139. Walzer T, Bléry M, Chaix J, et al. Identification, activation, and selective in vivo ablation of mouse NK cells via NKp46. *Proc Natl Acad Sci U S A*. 2007;104(9):3384-3389. doi:10.1073/pnas.0609692104

140. Ziegler S, Weiss E, Schmitt A-L, et al. CD56 Is a Pathogen Recognition Receptor on Human Natural Killer Cells. *Sci Rep*. 2017;7(1):6138. doi:10.1038/s41598-017-06238-4

141. Reichlin A, Yokoyama WM. Natural killer cell proliferation induced by anti-NK1.1 and IL-2. *Immunol Cell Biol*. 1998;76(2):143-152. doi:10.1046/j.1440-1711.1998.00726.x

142. Wensveen FM, Jelenčić V, Polić B. NKG2D: A Master Regulator of Immune Cell Responsiveness. *Front Immunol*. 2018;9:441. doi:10.3389/fimmu.2018.00441

143. Abel AM, Yang C, Thakar MS, Malarkannan S. Natural Killer Cells: Development, Maturation, and Clinical Utilization. *Front Immunol*. 2018;9:1869. doi:10.3389/fimmu.2018.01869

144. Chiossone L, Chaix J, Fuseri N, Roth C, Vivier E, Walzer T. Maturation of mouse NK cells is a 4-stage developmental program. *Blood*. 2009;113(22):5488-5496. doi:10.1182/blood-2008-10-187179

145. Krovi SH, Gapin L. Invariant Natural Killer T Cell Subsets—More Than Just Developmental Intermediates. *Front Immunol*. 2018;9:1393. doi:10.3389/fimmu.2018.01393

146. Giorda R, Weisberg EP, Ip TK, Trucco M. Genomic structure and strain-specific expression of the natural killer cell receptor NKR-P1. *J Immunol*. 1992;149(6):1957-1963. http://www.ncbi.nlm.nih.gov/pubmed/1517565. Accessed July 24, 2021.

147. Walzer T, Bléry M, Chaix J, et al. Identification, activation, and selective in vivo ablation of mouse NK cells via NKp46. *Proc Natl Acad Sci U S A*. 2007;104(9):3384-3389. doi:10.1073/pnas.0609692104

148. Hameg A, Apostolou I, Leite-De-Moraes M, et al. A subset of NKT cells that lacks the NK1.1 marker, expresses CD1d molecules, and autopresents the alpha-galactosylceramide antigen. *J Immunol*. 2000;165(9):4917-4926. doi:10.4049/jimmunol.165.9.4917

149. Kawano T, Cui J, Koezuka Y, et al. CD1d-restricted and TCR-mediated activation of valpha14 NKT cells by glycosylceramides. *Science*. 1997;278(5343):1626-1629. doi:10.1126/science.278.5343.1626

150. Uldrich AP, Patel O, Cameron G, et al. A semi-invariant Vα10+ T cell antigen receptor defines a population of natural killer T cells with distinct glycolipid antigen-recognition properties. *Nat Immunol*. 2011;12(7):616-623. doi:10.1038/ni.2051

151. M S, M S, A E, et al. Surface receptors identify mouse NK1.1+ T cell subsets distinguished by function and T cell receptor type. *Eur J Immunol*. 2004;34(1). doi:10.1002/EJI.200323963

152. Watarai H, Sekine-Kondo E, Shigeura T, et al. Development and function of invariant natural killer T cells producing T(h)2- and T(h)17-cytokines. *PLoS Biol*. 2012;10(2):e1001255. doi:10.1371/journal.pbio.1001255

153. Sag D, Krause P, Hedrick CC, Kronenberg M, Wingender G. IL-10-producing NKT10 cells are a distinct regulatory invariant NKT cell subset. *J Clin Invest*. 2014;124(9):3725-3740. doi:10.1172/JCI72308

154. Monteiro M, Almeida CF, Caridade M, et al. Identification of regulatory Foxp3+ invariant NKT cells induced by TGF-beta. *J Immunol*. 2010;185(4):2157-2163. doi:10.4049/jimmunol.1000359

155. Takahashi T, Chiba S, Nieda M, et al. Cutting edge: analysis of human V alpha 24+CD8+ NK T cells activated by alpha-galactosylceramide-pulsed monocyte-derived dendritic cells. *J Immunol*. 2002;168(7):3140-3144. doi:10.4049/jimmunol.168.7.3140

156. Krijgsman D, Hokland M, Kuppen PJK. The Role of Natural Killer T Cells in Cancer—A Phenotypical and Functional Approach. *Front Immunol*. 2018;9:367. doi:10.3389/fimmu.2018.00367

157. Terashima A, Watarai H, Inoue S, et al. A novel subset of mouse NKT cells bearing the IL-17 receptor B responds to IL-25 and contributes to airway hyperreactivity. *J Exp Med*. 2008;205(12):2727-2733. doi:10.1084/jem.20080698

158. Mars LT, Gautron A-S, Novak J, et al. Invariant NKT cells regulate experimental autoimmune encephalomyelitis and infiltrate the central nervous system in a CD1d-independent manner. *J Immunol*. 2008;181(4):2321-2329. doi:10.4049/jimmunol.181.4.2321

159. van de Pavert SA. Lymphoid Tissue inducer (LTi) cell ontogeny and functioning in embryo and adult. *Biomed J*. 2021;44(2):123-132. doi:10.1016/J.BJ.2020.12.003

160. Yoshida H, Honda K, Shinkura R, et al. IL-7 receptor α+ CD3– cells in the embryonic intestine induces the organizing center of Peyer's patches. *Int Immunol*. 1999;11(5):643-655. doi:10.1093/intimm/11.5.643

161. Wang S, Xia P, Chen Y, et al. Regulatory Innate Lymphoid Cells Control Innate Intestinal Inflammation. *Cell*. 2017;171(1):201-216.e18. doi:10.1016/j.cell.2017.07.027

162. Colonna M. Innate Lymphoid Cells: Diversity, Plasticity, and Unique Functions in Immunity. *Immunity*. 2018;48(6):1104-1117. doi:10.1016/j.immuni.2018.05.013

163. Vivier E, Artis D, Colonna M, et al. Innate Lymphoid Cells: 10 Years On. *Cell*. 2018;174(5):1054-1066. doi:10.1016/j.cell.2018.07.017

164. Panda SK, Colonna M. Innate Lymphoid Cells in Mucosal Immunity. *Front Immunol*. 2019;10:861. doi:10.3389/fimmu.2019.00861

165. Sanos SL, Bui VL, Mortha A, et al. RORgammat and commensal microflora are required for the differentiation of mucosal interleukin 22-producing NKp46+ cells. *Nat Immunol*. 2009;10(1):83-91. doi:10.1038/ni.1684

166. Vonarbourg C, Mortha A, Bui VL, et al. Regulated expression of nuclear receptor RORγt confers distinct functional fates to NK cell receptor-expressing RORγt(+) innate lymphocytes. *Immunity*. 2010;33(5):736-751. doi:10.1016/j.immuni.2010.10.017

167. Sonnenberg GF, Monticelli LA, Elloso MM, Fouser LA, Artis D. CD4+ Lymphoid Tissue-Inducer Cells Promote Innate Immunity in the Gut. *Immunity*. 2011;34(1):122-134. doi:10.1016/J.IMMUNI.2010.12.009

168. Oliphant CJ, Hwang YY, Walker JA, et al. MHCII-mediated dialog between group 2 innate lymphoid cells and CD4(+) T cells potentiates type 2 immunity and promotes parasitic helminth expulsion. *Immunity*. 2014;41(2):283-295. doi:10.1016/j.immuni.2014.06.016

169. Hepworth MR, Monticelli LA, Fung TC, et al. Innate lymphoid cells regulate CD4+ T-cell responses to intestinal commensal bacteria. *Nature*. 2013;498(7452):113-117. doi:10.1038/nature12240

170. Meininger I, Carrasco A, Rao A, Soini T, Kokkinou E, Mjösberg J. Tissue-Specific Features of Innate Lymphoid Cells. *Trends Immunol*. 2020;41(10):902-917. doi:10.1016/J.IT.2020.08.009

171. Gurka S, Hartung E, Becker M, Kroczek RA. Mouse Conventional Dendritic Cells Can be Universally Classified Based on the Mutually Exclusive Expression of XCR1 and SIRPα. *Front Immunol*. 2015;6:35. doi:10.3389/fimmu.2015.00035

172. Guilliams M, Dutertre C-A, Scott CL, et al. Unsupervised High-Dimensional Analysis Aligns Dendritic Cells across Tissues and Species. *Immunity*. 2016;45(3):669-684. doi:10.1016/j.immuni.2016.08.015

173. Merad M, Sathe P, Helft J, Miller J, Mortha A. The dendritic cell lineage: ontogeny and function of dendritic cells and their subsets in the steady state and the inflamed setting. *Annu Rev Immunol*. 2013;31:563-604. doi:10.1146/annurev-immunol-020711-074950

174. Ardavin C, Shortman K. Cell surface marker analysis of mouse thymic dendritic cells. *Eur J Immunol*. 1992;22(3):859-862. doi:10.1002/eji.1830220334

175. Vremec D, Pooley J, Hochrein H, et al. CD4 and CD8 expression by dendritic cell subtypes in

mouse thymus and spleen. *J Immunol*. 2000;164(6):2978-2986. doi:10.4049/jimmunol.164.6.2978

176. Flores-Langarica A, Cook C, Müller Luda K, et al. Intestinal CD103+CD11b+ cDC2 Conventional Dendritic Cells Are Required for Primary CD4+ T and B Cell Responses to Soluble Flagellin. *Front Immunol*. 2018;9:2409. doi:10.3389/fimmu.2018.02409
177. Flores-Langarica A, Müller Luda K, Persson EK, et al. CD103+CD11b+ mucosal classical dendritic cells initiate long-term switched antibody responses to flagellin. *Mucosal Immunol*. 2018;11(3):681-692. doi:10.1038/mi.2017.105
178. Förster R, Schubel A, Breitfeld D, et al. CCR7 coordinates the primary immune response by establishing functional microenvironments in secondary lymphoid organs. *Cell*. 1999;99(1):23-33. doi:10.1016/s0092-8674(00)80059-8
179. Singh-Jasuja H, Thiolat A, Ribon M, et al. The mouse dendritic cell marker CD11c is down-regulated upon cell activation through Toll-like receptor triggering. *Immunobiology*. 2013;218(1):28-39. doi:10.1016/J.IMBIO.2012.01.021
180. Musumeci A, Lutz K, Winheim E, Krug AB. What Makes a pDC: Recent Advances in Understanding Plasmacytoid DC Development and Heterogeneity. *Front Immunol*. 2019;10:1222. doi:10.3389/fimmu.2019.01222
181. Epelman S, Lavine KJ, Randolph GJ. Origin and functions of tissue macrophages. *Immunity*. 2014;41(1):21-35. doi:10.1016/j.immuni.2014.06.013
182. Mildner A, Marinkovic G, Jung S. Murine Monocytes: Origins, Subsets, Fates, and Functions. *Microbiol Spectr*. 2016;4(5). doi:10.1128/microbiolspec.MCHD-0033-2016
183. Zhang X, Goncalves R, Mosser DM. The isolation and characterization of murine macrophages. *Curr Protoc Immunol*. 2008;Chapter 14:Unit 14.1. doi:10.1002/0471142735.im1401s83
184. Gautier EL, Shay T, Miller J, et al. Gene-expression profiles and transcriptional regulatory pathways that underlie the identity and diversity of mouse tissue macrophages. *Nat Immunol*. 2012;13(11):1118-1128. doi:10.1038/ni.2419
185. Misharin A V, Morales-Nebreda L, Mutlu GM, Budinger GRS, Perlman H. Flow cytometric analysis of macrophages and dendritic cell subsets in the mouse lung. *Am J Respir Cell Mol Biol*. 2013;49(4):503-510. doi:10.1165/rcmb.2013-0086MA
186. Jablonski KA, Amici SA, Webb LM, et al. Novel Markers to Delineate Murine M1 and M2 Macrophages. *PLoS One*. 2015;10(12):e0145342. doi:10.1371/journal.pone.0145342
187. Ghosn EEB, Cassado AA, Govoni GR, et al. Two physically, functionally, and developmentally distinct peritoneal macrophage subsets. *Proc Natl Acad Sci U S A*. 2010;107(6):2568-2573. doi:10.1073/pnas.0915000107
188. Cassado A dos A, Dâ€™ImpÃ©rio Lima MR, Bortoluci KR. Revisiting Mouse Peritoneal

Macrophages: Heterogeneity, Development, and Function. *Front Immunol*. 2015;6:225. doi:10.3389/fimmu.2015.00225

189. Gray EE, Cyster JG. Lymph Node Macrophages. *J Innate Immun*. 2012;4(5-6):424-436. doi:10.1159/000337007
190. Fujiyama S, Nakahashi-Oda C, Abe F, Wang Y, Sato K, Shibuya A. Identification and isolation of splenic tissue-resident macrophage sub-populations by flow cytometry. *Int Immunol*. 2019;31(1):51-56. doi:10.1093/intimm/dxy064
191. Bonnardel J, Da Silva C, Henri S, et al. Innate and adaptive immune functions of peyer's patch monocyte-derived cells. *Cell Rep*. 2015;11(5):770-784. doi:10.1016/j.celrep.2015.03.067
192. Vorobjeva N V, Chernyak B V. NETosis: Molecular Mechanisms, Role in Physiology and Pathology. *Biochemistry (Mosc)*. 2020;85(10):1178-1190. doi:10.1134/S0006297920100065
193. Teschner D, Cholaszczyńska A, Ries F, et al. CD11b Regulates Fungal Outgrowth but Not Neutrophil Recruitment in a Mouse Model of Invasive Pulmonary Aspergillosis. *Front Immunol*. 2019;10:123. doi:10.3389/fimmu.2019.00123
194. Fleming TJ, Fleming ML, Malek TR. Selective expression of Ly-6G on myeloid lineage cells in mouse bone marrow. RB6-8C5 mAb to granulocyte-differentiation antigen (Gr-1) detects members of the Ly-6 family. *J Immunol*. 1993;151(5):2399-2408. http://www.ncbi.nlm.nih.gov/pubmed/8360469. Accessed July 26, 2021.
195. Lee PY, Wang J-X, Parisini E, Dascher CC, Nigrovic PA. Ly6 family proteins in neutrophil biology. *J Leukoc Biol*. 2013;94(4):585-594. doi:10.1189/jlb.0113014
196. Rosales C. Neutrophil: A Cell with Many Roles in Inflammation or Several Cell Types? *Front Physiol*. 2018;9:113. doi:10.3389/fphys.2018.00113
197. Zhang D, Chen G, Manwani D, et al. Neutrophil ageing is regulated by the microbiome. *Nature*. 2015;525(7570):528-532. doi:10.1038/nature15367
198. Casanova-Acebes M, Pitaval C, Weiss LA, et al. Rhythmic Modulation of the Hematopoietic Niche through Neutrophil Clearance. *Cell*. 2013;153(5):1025-1035. doi:10.1016/j.cell.2013.04.040
199. Cerutti A, Puga I, Magri G. The B cell helper side of neutrophils. *J Leukoc Biol*. 2013;94(4):677-682. doi:10.1189/jlb.1112596
200. Beauvillain C, Cunin P, Doni A, et al. CCR7 is involved in the migration of neutrophils to lymph nodes. *Blood*. 2011;117(4):1196-1204. doi:10.1182/blood-2009-11-254490
201. Ssemaganda A, Kindinger L, Bergin P, et al. Characterization of Neutrophil Subsets in Healthy Human Pregnancies. Zenclussen AC, ed. *PLoS One*. 2014;9(2):e85696. doi:10.1371/journal.pone.0085696
202. Clarke TB, Davis KM, Lysenko ES, Zhou AY, Yu Y, Weiser JN. Recognition of peptidoglycan from

the microbiota by Nod1 enhances systemic innate immunity. *Nat Med*. 2010;16(2):228-231. doi:10.1038/nm.2087

203. Hergott CB, Roche AM, Tamashiro E, et al. Peptidoglycan from the gut microbiota governs the lifespan of circulating phagocytes at homeostasis. *Blood*. 2016;127(20):2460-2471. doi:10.1182/blood-2015-10-675173
204. Piertney SB, Oliver MK. The evolutionary ecology of the major histocompatibility complex. *Heredity (Edinb)*. 2006;96(1):7-21. doi:10.1038/sj.hdy.6800724
205. Cresswell P. Invariant chain structure and MHC class II function. *Cell*. 1996;84(4):505-507. doi:10.1016/s0092-8674(00)81025-9
206. Ting JP-Y, Trowsdale J. Genetic control of MHC class II expression. *Cell*. 2002;109 Suppl:S21-33. doi:10.1016/s0092-8674(02)00696-7
207. Muhlethaler-Mottet A, Otten LA, Steimle V, Mach B. Expression of MHC class II molecules in different cellular and functional compartments is controlled by differential usage of multiple promoters of the transactivator CIITA. *EMBO J*. 1997;16(10):2851-2860. doi:10.1093/emboj/16.10.2851
208. Chang CH, Fontes JD, Peterlin M, Flavell RA. Class II transactivator (CIITA) is sufficient for the inducible expression of major histocompatibility complex class II genes. *J Exp Med*. 1994;180(4):1367-1374. doi:10.1084/jem.180.4.1367
209. Dienes HP, Hütteroth T, Hess G, Meuer SC. Immunoelectron microscopic observations on the inflammatory infiltrates and HLA antigens in hepatitis B and non-A, non-B. *Hepatology*. 1987;7(6):1317-1325. doi:10.1002/hep.1840070623
210. Herkel J, Jagemann B, Wiegard C, et al. MHC class II-expressing hepatocytes function as antigen-presenting cells and activate specific CD4 T lymphocyutes. *Hepatology*. 2003;37(5):1079-1085. doi:10.1053/jhep.2003.50191
211. Cannella B, Aquino DA, Raine CS. MHC II expression in the CNS after long-term demyelination. *J Neuropathol Exp Neurol*. 1995;54(4):521-530. doi:10.1097/00005072-199507000-00006
212. Hanafusa T, Pujol-Borrell R, Chiovato L, Russell RC, Doniach D, Bottazzo GF. Aberrant expression of HLA-DR antigen on thyrocytes in Graves' disease: relevance for autoimmunity. *Lancet (London, England)*. 1983;2(8359):1111-1115. doi:10.1016/s0140-6736(83)90628-1
213. Scott NA, Zhao Y, Krishnamurthy B, Mannering SI, Kay TWH, Thomas HE. IFNγ-Induced MHC Class II Expression on Islet Endothelial Cells Is an Early Marker of Insulitis but Is Not Required for Diabetogenic CD4+ T Cell Migration. *Front Immunol*. 2018;9:2800. doi:10.3389/fimmu.2018.02800
214. Abi Abdallah DS, Egan CE, Butcher BA, Denkers EY. Mouse neutrophils are professional antigen-presenting cells programmed to instruct Th1 and Th17 T-cell differentiation. *Int Immunol*.

2011;23(5):317-326. doi:10.1093/intimm/dxr007

215. SCOTT H, SOLHEIM BG, BRANDTZAEG P, THORSBY E. HLA-DR-like Antigens in the Epithelium of the Human Small Intestine. *Scand J Immunol*. 1980;12(1):77-82. doi:10.1111/j.1365-3083.1980.tb00043.x

216. Byrne B, Madrigal-Estebas L, McEvoy A, et al. Human duodenal epithelial cells constitutively express molecular components of antigen presentation but not costimulatory molecules. *Hum Immunol*. 2002;63(11):977-986. doi:10.1016/S0198-8859(02)00436-6

217. Hepworth MR, Monticelli LA, Fung TC, et al. Innate lymphoid cells regulate CD4+ T-cell responses to intestinal commensal bacteria. *Nature*. 2013;498(7452):113-117. doi:10.1038/nature12240

218. Borcherding F, Nitschke M, Hundorfean G, et al. The CD40-CD40L pathway contributes to the proinflammatory function of intestinal epithelial cells in inflammatory bowel disease. *Am J Pathol*. 2010;176(4):1816-1827. doi:10.2353/ajpath.2010.090461

219. Zimmer KP, Poremba C, Weber P, Ciclitira PJ, Harms E. Translocation of gliadin into HLA-DR antigen containing lysosomes in coeliac disease enterocytes. *Gut*. 1995;36(5):703-709. doi:10.1136/gut.36.5.703

220. Biton M, Haber AL, Rogel N, et al. T Helper Cell Cytokines Modulate Intestinal Stem Cell Renewal and Differentiation. *Cell*. 2018;175(5):1307-1320.e22. doi:10.1016/j.cell.2018.10.008

221. Dubrot J, Duraes F V, Potin L, et al. Lymph node stromal cells acquire peptide-MHCII complexes from dendritic cells and induce antigen-specific $CD4^+$ T cell tolerance. *J Exp Med*. 2014;211(6):1153-1166. doi:10.1084/jem.20132000

222. Mori T, Wu GM, Mori E, et al. Expression of class II major histocompatibility complex antigen on mouse sperm and its roles in fertilization. *Am J Reprod Immunol*. 1990;24(1):9-14. doi:10.1111/j.1600-0897.1990.tb00688.x

223. Zhang Y, Liu Y, Liu H, Tang WH. Exosomes: biogenesis, biologic function and clinical potential. *Cell Biosci*. 2019;9(1):19. doi:10.1186/s13578-019-0282-2

224. Bettadapur A, Miller HW, Ralston KS. Biting Off What Can Be Chewed: Trogocytosis in Health, Infection, and Disease. Ottemann KM, ed. *Infect Immun*. 2020;88(7). doi:10.1128/IAI.00930-19

225. Dupont M, Souriant S, Lugo-Villarino G, Maridonneau-Parini I, Vérollet C. Tunneling Nanotubes: Intimate Communication between Myeloid Cells. *Front Immunol*. 2018;9:43. doi:10.3389/fimmu.2018.00043

226. Sokol CL, Chu N-Q, Yu S, Nish SA, Laufer TM, Medzhitov R. Basophils function as antigen-presenting cells for an allergen-induced T helper type 2 response. *Nat Immunol*. 2009;10(7):713-720. doi:10.1038/ni.1738

227. Perrigoue JG, Saenz SA, Siracusa MC, et al. MHC class II-dependent basophil-CD4+ T cell

interactions promote T(H)2 cytokine-dependent immunity. *Nat Immunol*. 2009;10(7):697-705. doi:10.1038/ni.1740

228. Sharma M, Hegde P, Aimanianda V, et al. Circulating human basophils lack the features of professional antigen presenting cells. *Sci Rep*. 2013;3(1):1188. doi:10.1038/srep01188
229. Miyake K, Shiozawa N, Nagao T, Yoshikawa S, Yamanishi Y, Karasuyama H. Trogocytosis of peptide-MHC class II complexes from dendritic cells confers antigen-presenting ability on basophils. *Proc Natl Acad Sci U S A*. 2017;114(5):1111-1116. doi:10.1073/pnas.1615973114
230. van Niel G, Raposo G, Candalh C, et al. Intestinal epithelial cells secrete exosome-like vesicles. *Gastroenterology*. 2001;121(2):337-349. doi:10.1053/gast.2001.26263
231. Mallegol J, Van Niel G, Lebreton C, et al. T84-intestinal epithelial exosomes bear MHC class II/peptide complexes potentiating antigen presentation by dendritic cells. *Gastroenterology*. 2007;132(5):1866-1876. doi:10.1053/j.gastro.2007.02.043
232. Karlsson M, Lundin S, Dahlgren U, Kahu H, Pettersson I, Telemo E. "Tolerosomes"; are produced by intestinal epithelial cells. *Eur J Immunol*. 2001;31(10):2892-2900. doi:10.1002/1521-4141(2001010)31:10<2892::aid-immu2892>3.0.co;2-i
233. Tsang JYS, Chai JG, Lechler R. Antigen presentation by mouse CD4+ T cells involving acquired MHC class II:peptide complexes: another mechanism to limit clonal expansion? *Blood*. 2003;101(7):2704-2710. doi:10.1182/blood-2002-04-1230
234. SHIMOMURA O, JOHNSON FH, SAIGA Y. Extraction, purification and properties of aequorin, a bioluminescent protein from the luminous hydromedusan, Aequorea. *J Cell Comp Physiol*. 1962;59:223-239. doi:10.1002/jcp.1030590302
235. Kremers G-J, Gilbert SG, Cranfill PJ, Davidson MW, Piston DW. Fluorescent proteins at a glance. *J Cell Sci*. 2011;124(Pt 2):157-160. doi:10.1242/jcs.072744
236. Zhang G, Gurtu V, Kain SR. An enhanced green fluorescent protein allows sensitive detection of gene transfer in mammalian cells. *Biochem Biophys Res Commun*. 1996;227(3):707-711. doi:10.1006/bbrc.1996.1573
237. Ikawa M, Kominami K, Yoshimura Y, Tanaka K, Nishimune Y, Okabe M. Green fluorescent protein as a marker in transgenic mice. *Dev Growth Differ*. 1995;37(4):455-459. doi:10.1046/j.1440-169X.1995.t01-2-00012.x
238. Boes M, Cerny J, Massol R, et al. T-cell engagement of dendritic cells rapidly rearranges MHC class II transport. *Nature*. 2002;418(6901):983-988. doi:10.1038/nature01004
239. Huisken J, Swoger J, Del Bene F, Wittbrodt J, Stelzer EHK. Optical sectioning deep inside live embryos by selective plane illumination microscopy. *Science*. 2004;305(5686):1007-1009. doi:10.1126/science.1100035
240. Huisken J, Stainier DYR. Even fluorescence excitation by multidirectional selective plane

illumination microscopy (mSPIM). *Opt Lett*. 2007;32(17):2608-2610. doi:10.1364/ol.32.002608

241. Chen B-C, Legant WR, Wang K, et al. Lattice light-sheet microscopy: imaging molecules to embryos at high spatiotemporal resolution. *Science*. 2014;346(6208):1257998. doi:10.1126/science.1257998
242. Fadero TC, Gerbich TM, Rana K, et al. LITE microscopy: Tilted light-sheet excitation of model organisms offers high resolution and low photobleaching. *J Cell Biol*. 2018;217(5):1869-1882. doi:10.1083/jcb.201710087
243. Wu Y, Chandris P, Winter PW, et al. Simultaneous multiview capture and fusion improves spatial resolution in wide-field and light-sheet microscopy. *Optica*. 2016;3(8):897-910. doi:10.1364/OPTICA.3.000897
244. Mertz J, Kim J. Scanning light-sheet microscopy in the whole mouse brain with HiLo background rejection. *J Biomed Opt*. 2010;15(1):016027. doi:10.1117/1.3324890
245. Chhetri RK, Amat F, Wan Y, Höckendorf B, Lemon WC, Keller PJ. Whole-animal functional and developmental imaging with isotropic spatial resolution. *Nat Methods*. 2015;12(12):1171-1178. doi:10.1038/nmeth.3632
246. Udan RS, Piazza VG, Hsu C-W, Hadjantonakis A-K, Dickinson ME. Quantitative imaging of cell dynamics in mouse embryos using light-sheet microscopy. *Development*. 2014;141(22):4406-4414. doi:10.1242/dev.111021
247. Icha J, Schmied C, Sidhaye J, Tomancak P, Preibisch S, Norden C. Using Light Sheet Fluorescence Microscopy to Image Zebrafish Eye Development. *J Vis Exp*. 2016;(110):e53966. doi:10.3791/53966
248. Kaufmann A, Mickoleit M, Weber M, Huisken J. Multilayer mounting enables long-term imaging of zebrafish development in a light sheet microscope. *Development*. 2012;139(17):3242-3247. doi:10.1242/dev.082586
249. Mzinza DT, Fleige H, Laarmann K, et al. Application of light sheet microscopy for qualitative and quantitative analysis of bronchus-associated lymphoid tissue in mice. *Cell Mol Immunol*. 2018;15(10):875-887. doi:10.1038/cmi.2017.150
250. Männ L, Klingberg A, Gunzer M, Hasenberg M. Quantitative Visualization of Leukocyte Infiltrate in a Murine Model of Fulminant Myocarditis by Light Sheet Microscopy. *J Vis Exp*. 2017;(123). doi:10.3791/55450
251. Amich J, Mokhtari Z, Strobel M, et al. Three-Dimensional Light Sheet Fluorescence Microscopy of Lungs To Dissect Local Host Immune-Aspergillus fumigatus Interactions. *MBio*. 2020;11(1). doi:10.1128/mBio.02752-19
252. Glaser AK, Reder NP, Chen Y, et al. Light-sheet microscopy for slide-free non-destructive pathology of large clinical specimens. *Nat Biomed Eng*. 2017;1(7). doi:10.1038/s41551-017-

0084

253. Susaki EA, Tainaka K, Perrin D, et al. Whole-brain imaging with single-cell resolution using chemical cocktails and computational analysis. *Cell*. 2014;157(3):726-739. doi:10.1016/j.cell.2014.03.042

254. Maiuri L, Candeo A, Sana I, et al. Virtual unfolding of light sheet fluorescence microscopy dataset for quantitative analysis of the mouse intestine. *J Biomed Opt*. 2016;21(05):1. doi:10.1117/1.JBO.21.5.056001

255. Saeys Y, Van Gassen S, Lambrecht BN. Computational flow cytometry: helping to make sense of high-dimensional immunology data. *Nat Rev Immunol*. 2016;16(7):449-462. doi:10.1038/nri.2016.56

256. Nolan JP, Condello D. Spectral flow cytometry. *Curr Protoc Cytom*. 2013;Chapter 1:Unit1.27. doi:10.1002/0471142956.cy0127s63

257. Ornatsky O, Bandura D, Baranov V, Nitz M, Winnik MA, Tanner S. Highly multiparametric analysis by mass cytometry. *J Immunol Methods*. 2010;361(1-2):1-20. doi:10.1016/j.jim.2010.07.002

258. van der Maaten L, Hinton G. Visualizing Data using t-SNE. *J Mach Learn Res*. 2008;9(86):2579-2605. http://jmlr.org/papers/v9/vandermaaten08a.html.

259. McInnes L, Healy J, Melville J. UMAP: Uniform Manifold Approximation and Projection for Dimension Reduction. February 2018. https://arxiv.org/abs/1802.03426. Accessed August 4, 2021.

260. Becht E, Dutertre C-A, Kwok IWH, Ng LG, Ginhoux F, Newell EW. Evaluation of UMAP as an alternative to t-SNE for single-cell data. *bioRxiv*. April 2018:298430. doi:10.1101/298430

261. Becht E, McInnes L, Healy J, et al. Dimensionality reduction for visualizing single-cell data using UMAP. *Nat Biotechnol*. December 2018. doi:10.1038/nbt.4314

262. Kobak D, Linderman GC. UMAP does not preserve global structure any better than t-SNE when using the same initialization. *bioRxiv*. December 2019:2019.12.19.877522. doi:10.1101/2019.12.19.877522

263. Ferrer-Font L, Mayer JU, Old S, Hermans IF, Irish J, Price KM. High-Dimensional Data Analysis Algorithms Yield Comparable Results for Mass Cytometry and Spectral Flow Cytometry Data. *Cytometry A*. 2020;97(8):824-831. doi:10.1002/cyto.a.24016

264. Van Gassen S, Callebaut B, Van Helden MJ, et al. FlowSOM: Using self-organizing maps for visualization and interpretation of cytometry data. *Cytometry A*. 2015;87(7):636-645. doi:10.1002/cyto.a.22625

265. Kratochvíl M, Koladiya A, Vondrášek J. Generalized EmbedSOM on quadtree-structured self-organizing maps. *F1000Research*. 2019;8:2120. doi:10.12688/f1000research.21642.2

266. Kratochvíl M, Bednárek D, Sieger T, Fišer K, Vondrášek J. ShinySOM: graphical SOM-based analysis of single-cell cytometry data. *Bioinformatics*. 2020;36(10):3288-3289. doi:10.1093/bioinformatics/btaa091

267. Lucchesi S, Nolfi E, Pettini E, et al. Computational Analysis of Multiparametric Flow Cytometric Data to Dissect B Cell Subsets in Vaccine Studies. *Cytom Part A*. 2020;97(3):259-267. doi:10.1002/cyto.a.23922

268. Mazza EMC, Brummelman J, Alvisi G, et al. Background fluorescence and spreading error are major contributors of variability in high-dimensional flow cytometry data visualization by t-distributed stochastic neighboring embedding. *Cytometry A*. 2018;93(8):785-792. doi:10.1002/cyto.a.23566

269. Toghi Eshghi S, Au-Yeung A, Takahashi C, et al. Quantitative Comparison of Conventional and t-SNE-guided Gating Analyses. *Front Immunol*. 2019;10:1194. doi:10.3389/fimmu.2019.01194

270. Lee J-Y, Hamilton SE, Akue AD, Hogquist KA, Jameson SC. Virtual memory CD8 T cells display unique functional properties. *Proc Natl Acad Sci U S A*. 2013;110(33):13498-13503. doi:10.1073/pnas.1307572110

271. Huang T, Wei B, Velazquez P, Borneman J, Braun J. Commensal microbiota alter the abundance and TCR responsiveness of splenic naïve CD4+ T lymphocytes. *Clin Immunol*. 2005;117(3):221-230. doi:10.1016/J.CLIM.2005.09.012

272. Walton KLW, He J, Kelsall BL, Sartor RB, Fisher NC. Dendritic cells in germ-free and specific pathogen-free mice have similar phenotypes and in vitro antigen presenting function. *Immunol Lett*. 2006;102(1):16-24. doi:10.1016/J.IMLET.2005.07.001

273. Olarte OE, Andilla J, Gualda EJ, Loza-Alvarez P. Light-sheet microscopy: a tutorial. *Adv Opt Photonics*. 2018;10(1):111-179. doi:10.1364/AOP.10.000111

9. Supplementary figure

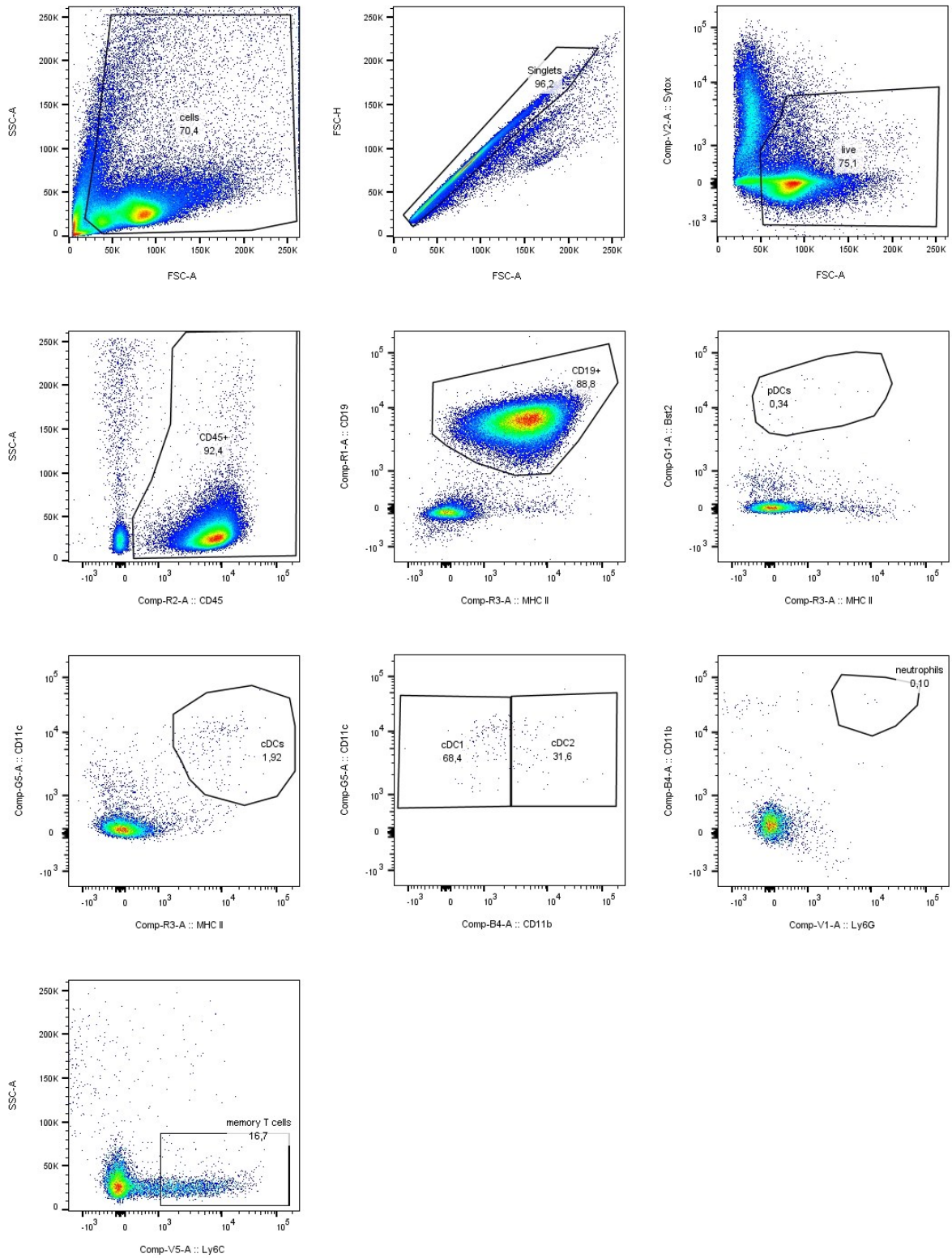

S_Figure 1: Gating strategy: myeloid panel PPs.

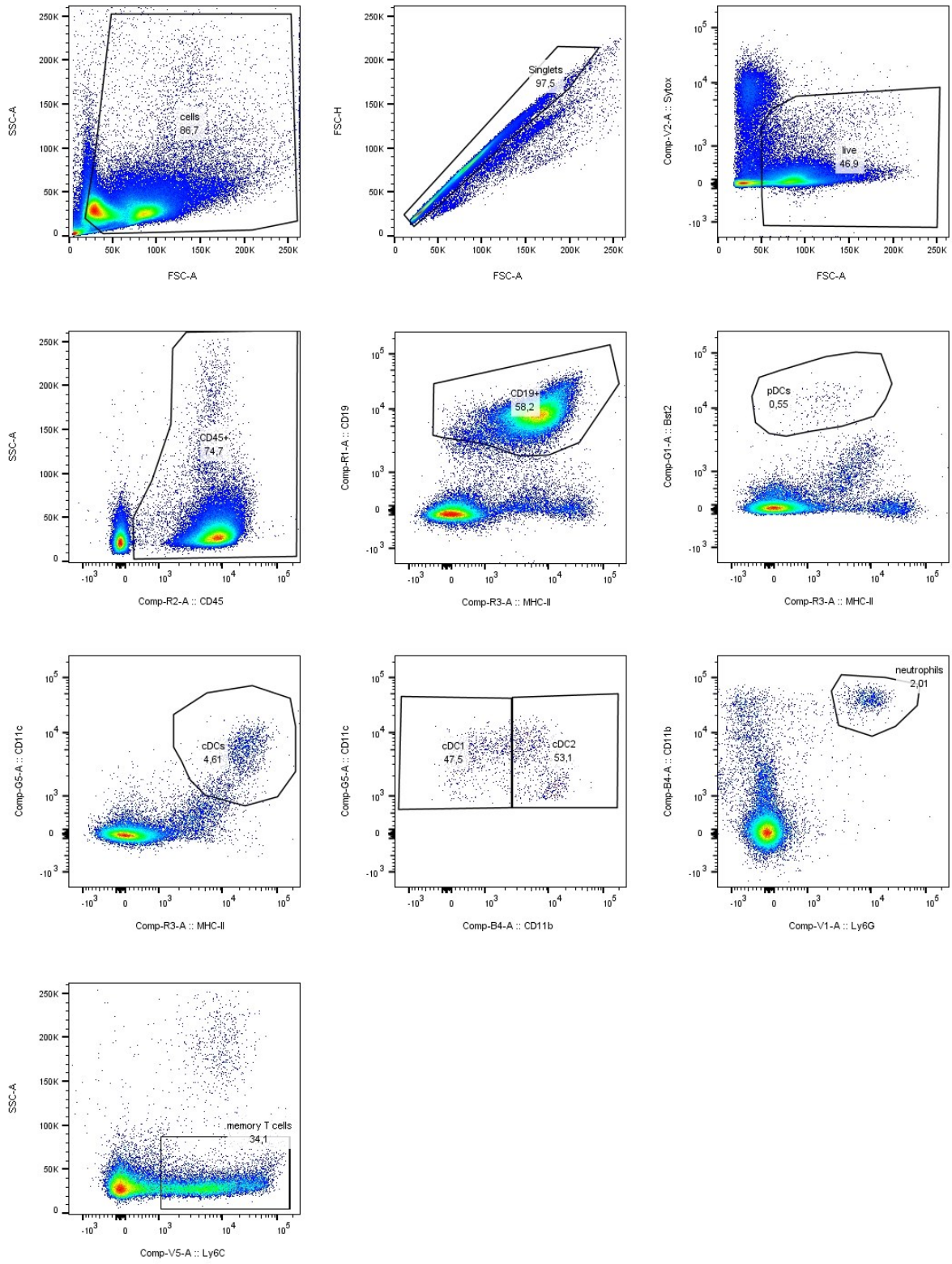

S_Figure 2: Gating strategy: myeloid panel Spleen.

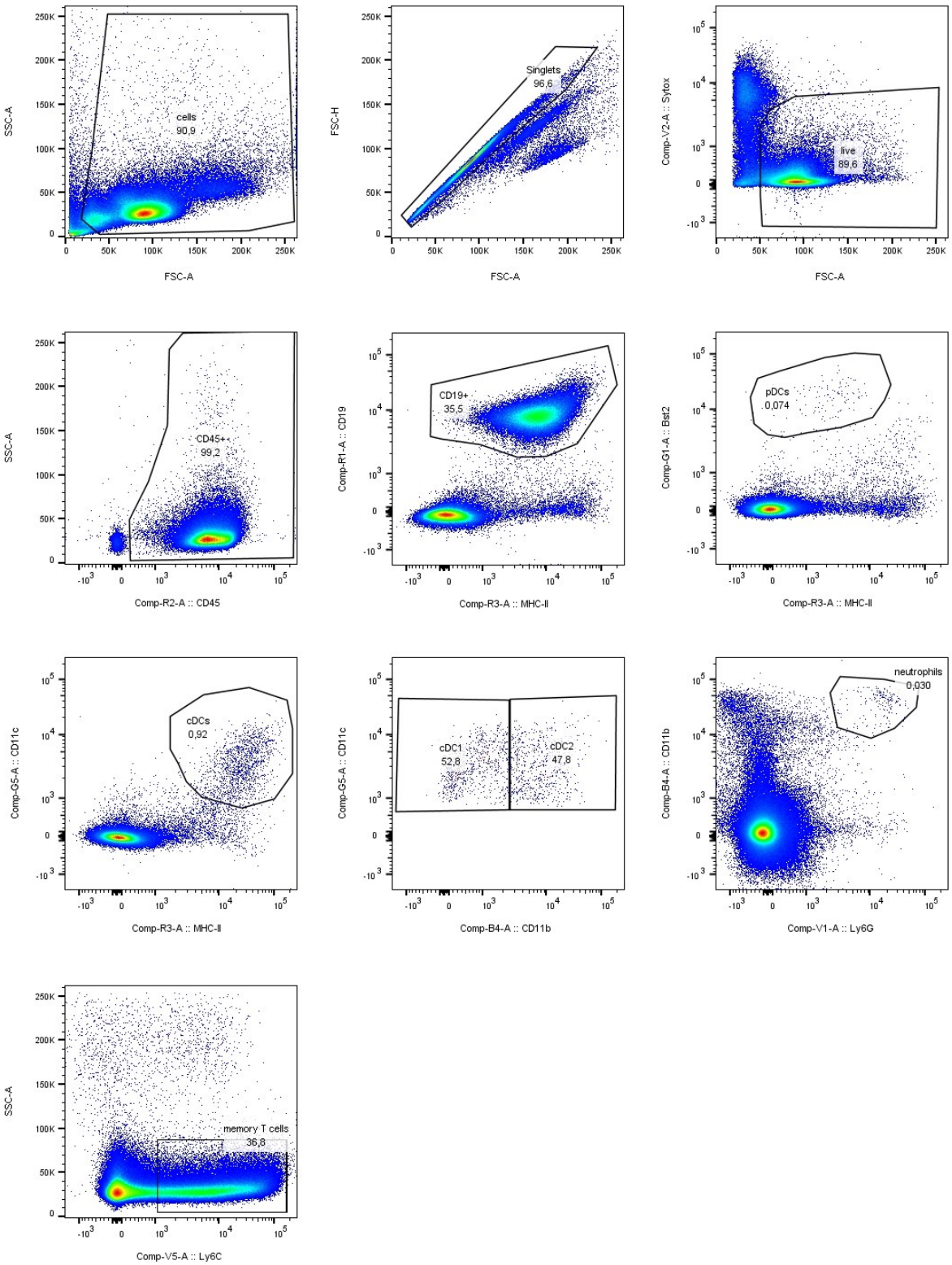

S_Figure 3: Gating strategy: myeloid panel MLNs.

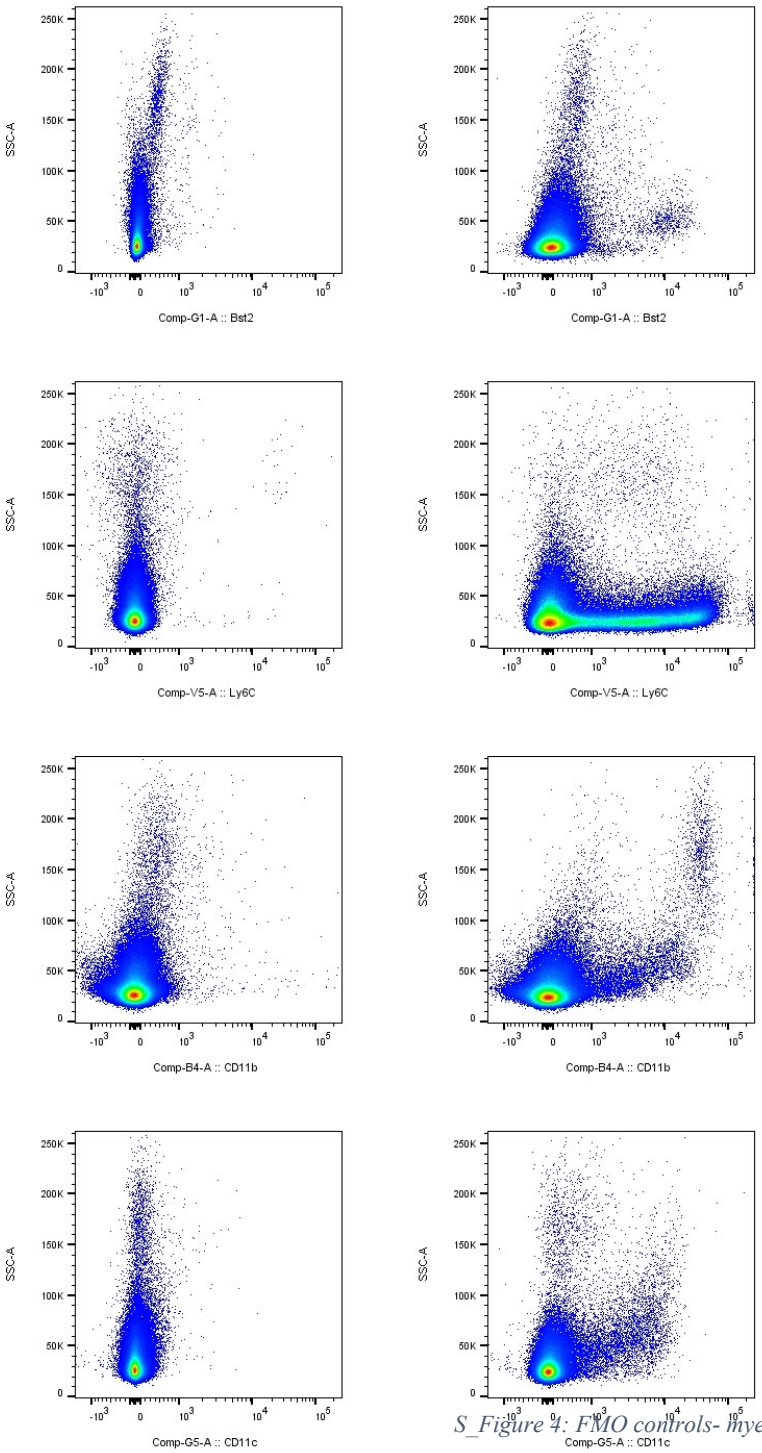

S_Figure 4: FMO controls- myeloid panel.

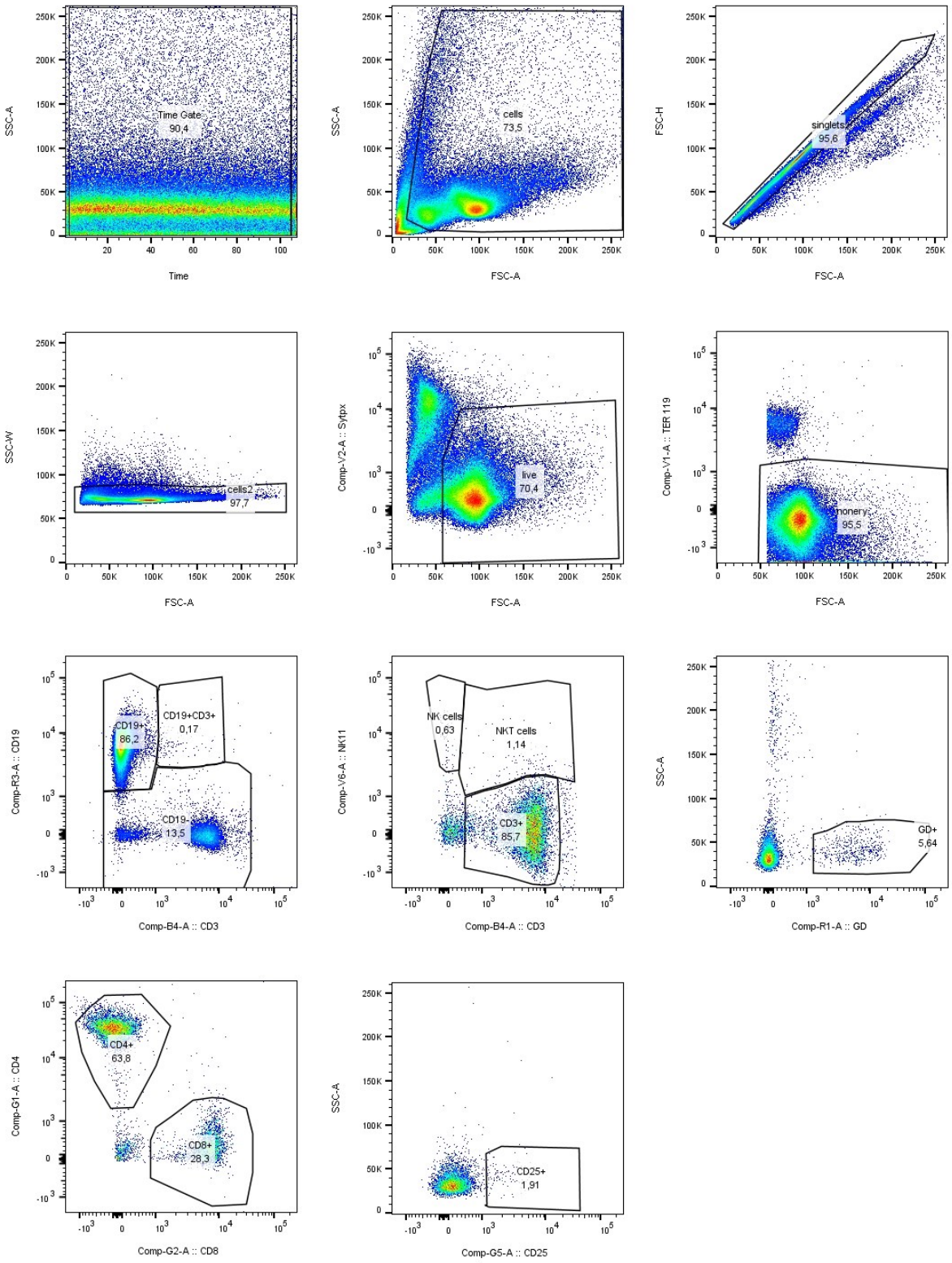

S_Figure 5: Gating strategy: lymphoid panel - PPs.

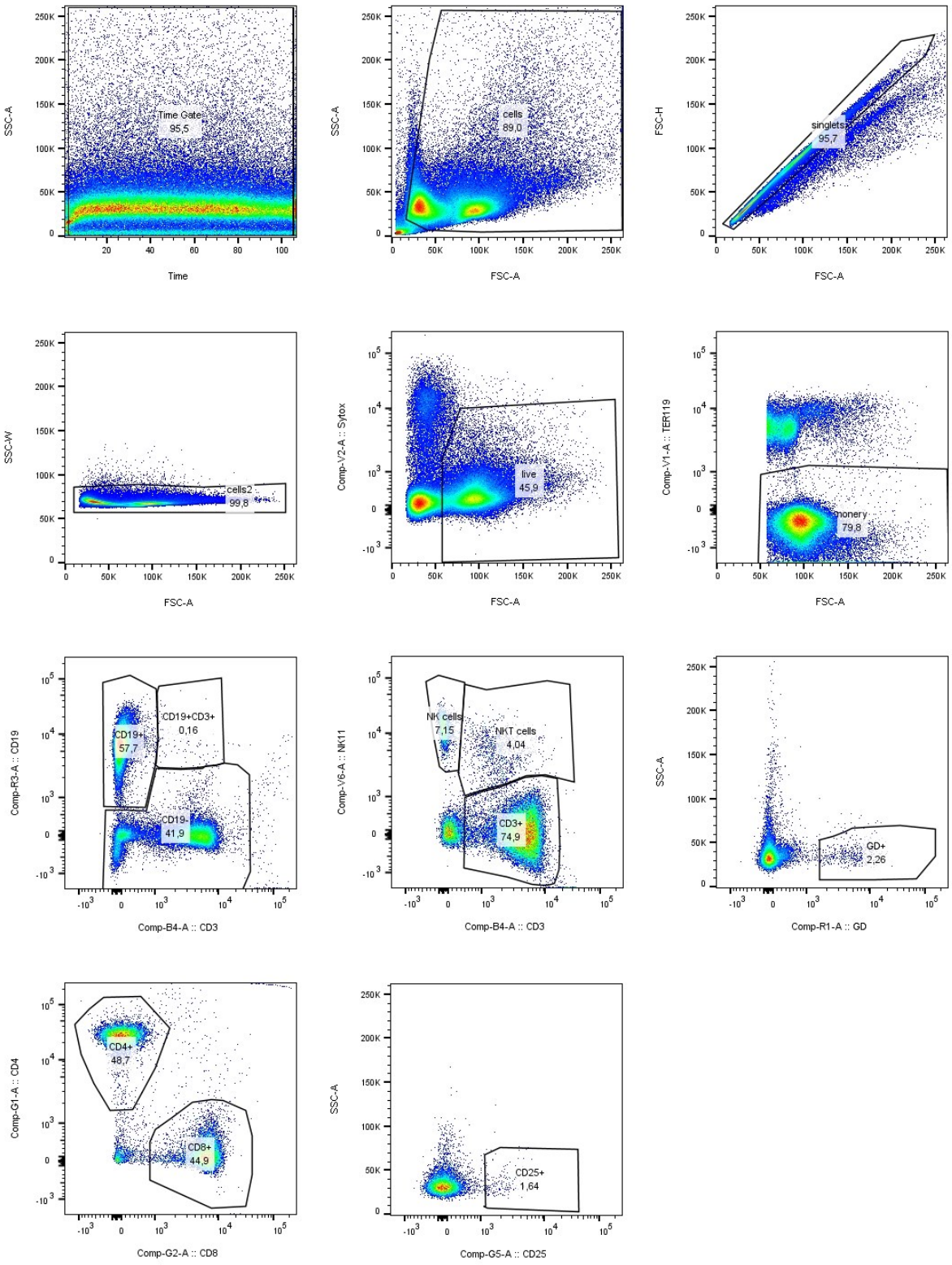

S_Figure 6: Gating stratey - lymphoid panel – spleen.

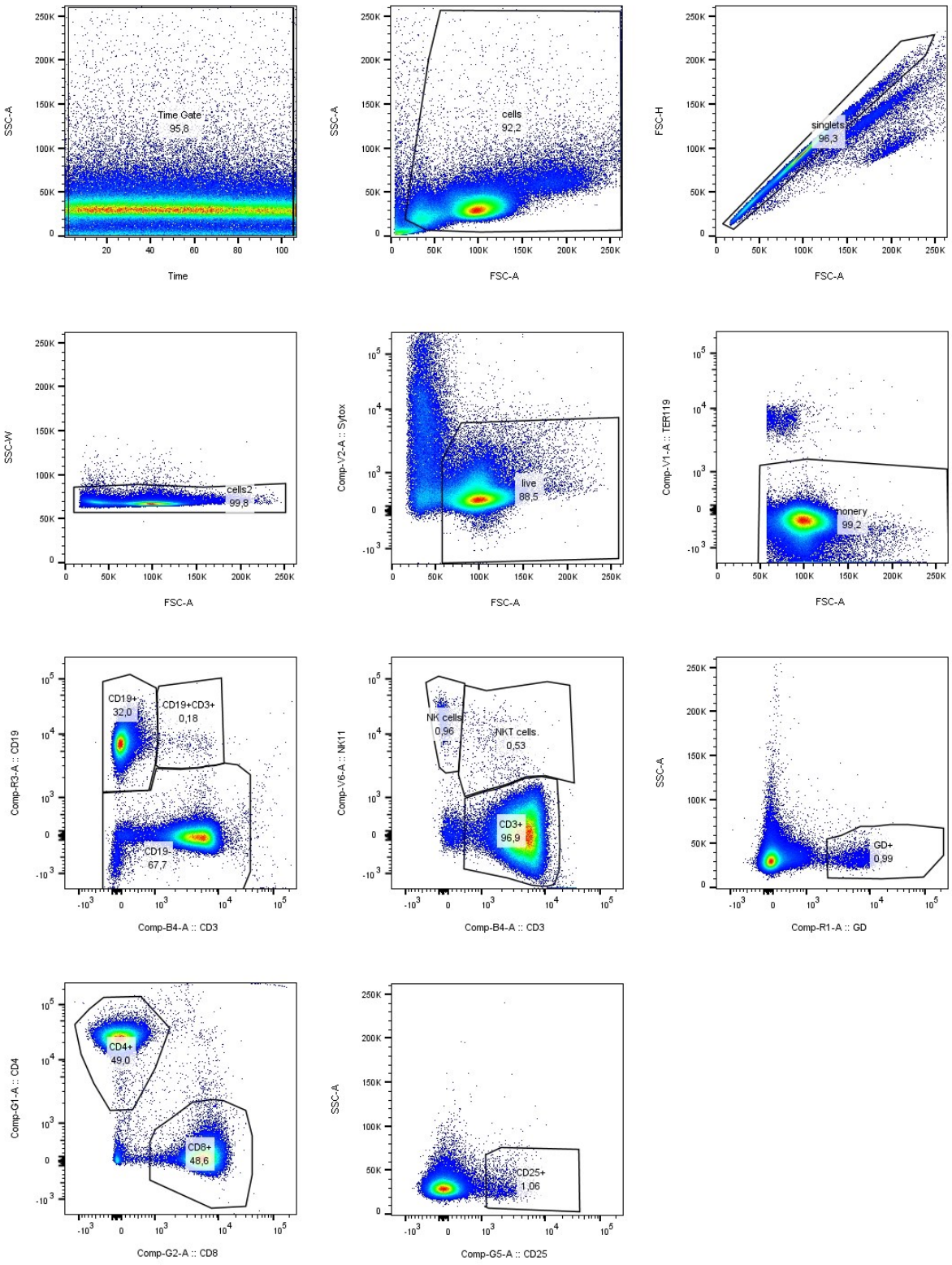

S_Figure 7: Gating strategy: lymphoid panel MLNs.

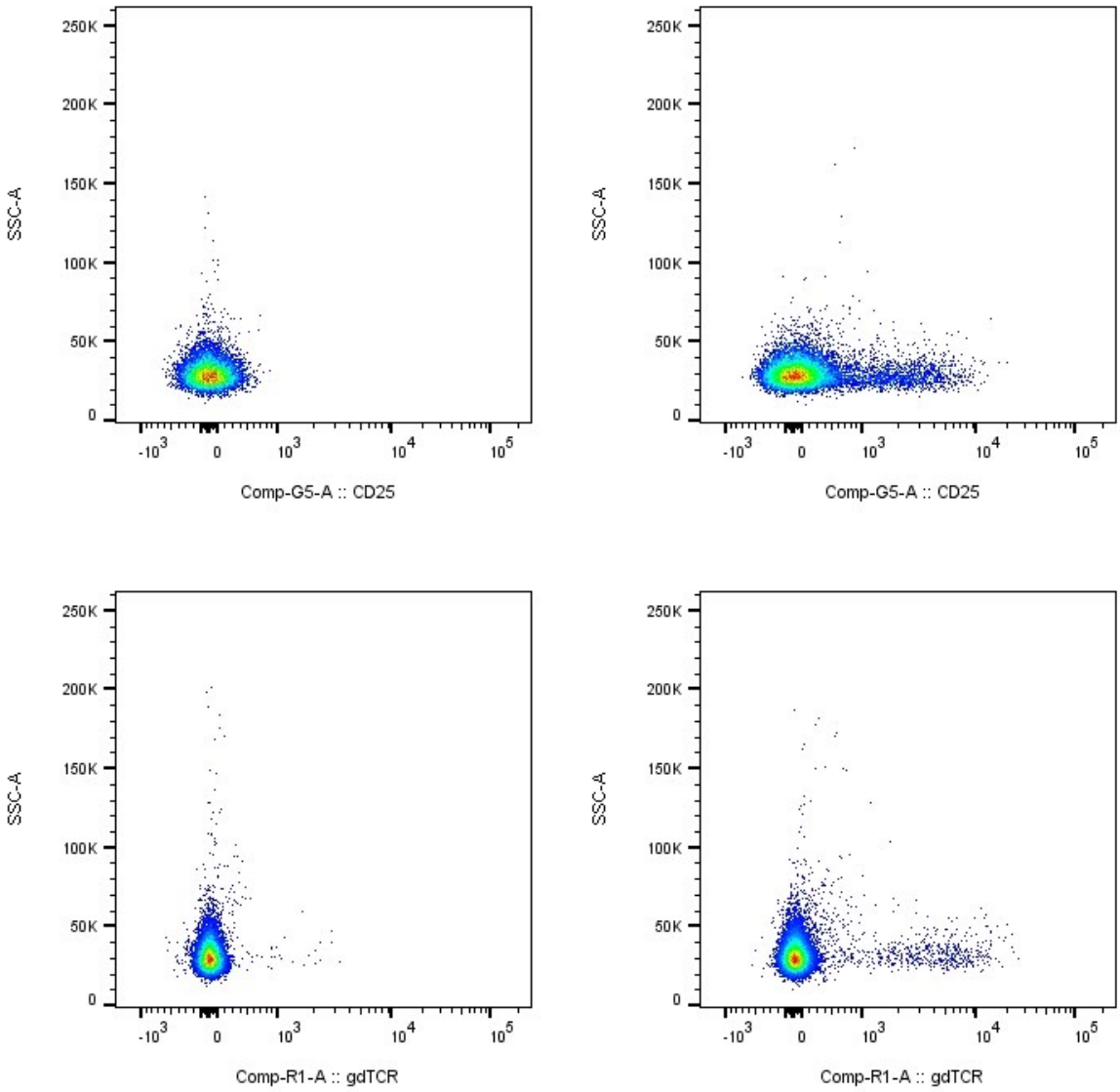

S_Figure 8: FMO control – lymphoid panel.